

NUMERICAL SIMULATION OF THE PHOTOISOMERIZATION OF RETINAL
FROM THE *CIS* TO THE *TRANS* FORM

A Dissertation

by

INDRANI SINHA

Submitted to the Office of Graduate Studies of
Texas A&M University
in partial fulfillment of the requirements for the degree of

DOCTOR OF PHILOSOPHY

December 2007

Major Subject: Physics

NUMERICAL SIMULATION OF THE PHOTOISOMERIZATION OF RETINAL
FROM THE *CIS* TO THE *TRANS* FORM

A Dissertation

by

INDRANI SINHA

Submitted to the Office of Graduate Studies of
Texas A&M University
in partial fulfillment of the requirements for the degree of

DOCTOR OF PHILOSOPHY

Approved by:

Co-Chairs of Committee, Robert R. Lucchese

A. Lewis Ford

Committee Members, Joseph H. Ross, Jr.

Bhaskar Dutta

Head of Department, Edward S. Fry

December 2007

Major Subject: Physics

ABSTRACT

Numerical Simulation of the Photoisomerization of Retinal
from the *cis* to the *trans* Form. (December 2007)

Indrani Sinha, B.Sc., Jadavpur University, Calcutta, India;

M.S., The University of Kansas

Co-Chairs of Advisory Committee: Dr. Robert R. Lucchese
Dr. A. Lewis Ford

This dissertation describes a tight-binding technique that treats the dynamics of electrons and ions simultaneously. The main features are a generalized Hellmann-Feynman theorem, a standard, time-dependent, self-consistent-field description and the interaction picture. The time-dependence is incorporated by using Peierls Substitution. We also apply the velocity-Verlet algorithm to predict the motion of the ions.

We first test the validity of this semi-empirical tight-binding approach on several smaller systems including ethylene, 2-butene, and stilbene. The *cis-trans* isomerization is modeled and in each case the results agree well with those obtained from other computational and empirical methods. Next, we use the tight-binding model to simulate the photoisomerization of the retinal molecule from its *cis* to *trans* form. The results are comparable to those obtained from experiments. The vibrational frequencies for retinal obtained using the force-constant techniques in this model agree well with those obtained from Fourier transform methods and a standard software. The *cis-trans* isomerization takes 217.91 fs to complete with a field strength of 1.0 gauss·cm, which is comparable to 200 fs reported from experiments. The isomerization depends on the strength of the vector potential, the time-step of the simulation

and also the wavelength of the light. Using different parameters the isomerization takes place in 1-2 ps which is within the range reported from experimentation.

The present semi-empirical technique provides an excellent compromise between computationally-prohibitive first principles methods and approximate empirical methods to model the motion of electrons and ions in a large molecule like retinal.

To my parents

ACKNOWLEDGMENTS

I would like to begin my acknowledgments by first thanking my parents for believing in me and guiding me along the right course in my journey through life. They are my pillars of hope and confidence. I would also like to thank my brother for his continued support and encouragement. He has always ventured out in the unknown and charted a path, and most of the time that is the course I followed.

My husband Darren is the wind beneath my wings, and for that I am very grateful. He has always believed in me, and I truly appreciate his unwavering enthusiasm for my work.

This research would not have been possible without Dr. Robert Lucchese's unselfish support and guidance. He provided invaluable advice on a topic which was unfamiliar to him and did his utmost to see me through to the completion of my work. I would also like to thank Dr. Lewis Ford for being pragmatic and for being involved in my project from the beginning to the end. I am thankful for Dr. Joseph Ross' genuine interest in my work and his useful suggestions to my dissertation. Dr. Bhaskar Dutta's generosity by being part of my committee is greatly appreciated. I would also like to take this opportunity to thank Dr. Robert Kenefick who reminds me that there are some great people in this world.

And finally, I would like to express my love and appreciation for our cats Mishti, Princess and Forest and my niece Radhika for the kind of joy and gratification that only pets and children can bring.

TABLE OF CONTENTS

CHAPTER		Page
I	INTRODUCTION	1
	A. Photo-reception in the Eye	4
	B. Theoretical Motivation of the Current Work	7
II	THE TIGHT-BINDING MODEL	10
	A. Time-dependent Schrödinger Equation	13
	B. Tight-Binding with s - p Orbitals	17
	C. Peierls Substitution	18
	1. The vector potential and the electro-magnetic field . .	19
	2. Effect of the vector potential on the Hamiltonian . . .	20
	D. Hellmann-Feynman theorem	21
	E. Cayley Algorithm to Solve the Schrödinger Equation . . .	24
	F. Hellmann-Feynman Theorem for Non-Adiabatic Processes	25
III	NUMERICAL METHODS	27
	A. Geometry Optimization	27
	B. Calculating the Hessian Matrix and the Vibrational Frequencies	29
	1. Obtaining vibrational frequencies using force-constant techniques	30
	2. Obtaining vibrational frequencies using Fourier-transform techniques	32
	C. Velocity-Verlet Algorithm	33
	D. Determining the Constants for the Repulsive Potential . .	34
	E. Population Analysis to Determine the Highest Occu- pied Molecular Orbital (HOMO) and the Lowest Unoc- cupied Molecular Orbital (LUMO)	36
IV	RESULTS FOR TEST MOLECULES	40
	A. Results for the Ethylene Molecule	40
	1. Molecular dynamics study of <i>cis-trans</i> isomeriza- tion of ethylene by switching the highest-occupied and lowest-unoccupied molecular orbitals	40

CHAPTER	Page
2. Results for the dynamics of the ethylene molecule without the application of an external field	45
3. Results for the photo-isomerization of the ethylene molecule with the application of an electro-magnetic field	47
B. Results for the 2-Butene Molecule	58
1. Molecular dynamics study of <i>cis-trans</i> isomerization of 2-butene by switching the highest-occupied and lowest-unoccupied molecular orbitals	59
2. Results for the dynamics of 2-butene without the application of an external field	61
3. Results for the photo-isomerization of 2-butene with the application of an electro-magnetic field	63
C. Results for the Stilbene Molecule	72
1. Molecular dynamics study of <i>cis-trans</i> isomerization of stilbene by switching the highest-occupied and lowest-unoccupied molecular orbitals	73
2. Results for the dynamics of stilbene without the application of an external field	75
3. Results for the photo-isomerization of stilbene with the application of an electro-magnetic field	77
D. Frequency Calculations Using Force-Constant Technique	88
E. Frequency Calculations Using Fourier Transforms	98
V RESULTS FOR THE MODEL MOLECULE RETINAL	101
A. Results for the Retinal Molecule	102
1. Molecular dynamics study of <i>cis-trans</i> isomerization of retinal by switching the highest-occupied and lowest-unoccupied molecular orbitals	102
2. Results for the dynamics of retinal without the application of an external field	104
3. Results for the photo-isomerization of retinal with the application of an electro-magnetic field	116
VI CONCLUSIONS	123
REFERENCES	126
APPENDIX A	131

CHAPTER	Page
APPENDIX B	134
VITA	147

LIST OF TABLES

TABLE		Page
I	Tight-binding parameters for an s - p model according to Harrison[26]. ($\eta_{ps\sigma} = -\eta_{sp\sigma}$).	18
II	Values of the constant C in the form of the potential: $U_{\text{rep}} = C/R^4$. . .	36
III	Eigenvalues of the second-derivative matrix of the potential and the corresponding vibrational frequencies for ethylene.	88
IV	Eigenvalues of the second-derivative matrix of the potential and the corresponding vibrational frequencies for 2-butene.	90
V	Eigenvalues of the second-derivative matrix of the potential and the corresponding vibrational frequencies for stilbene.	92
VI	Eigenvalues of the second-derivative matrix of the potential and the corresponding vibrational frequencies for retinal.	107
VII	Tight-binding parameters for as s - p model according to Harrison[40]. ($\eta_{ps\sigma} = -\eta_{sp\sigma}$).	133
VIII	Molecular orbital energy eigenvalues of ethylene without an ex- ternal field.	134
IX	Molecular orbital energy eigenvalues of 2-butene without an ex- ternal field.	135
X	Molecular orbital energy eigenvalues of stilbene without an exter- nal field.	137
XI	Molecular orbital energy eigenvalues of retinal without an external field.	141

LIST OF FIGURES

FIGURE		Page
1	The retinal molecule in its 11- <i>cis</i> form.	3
2	Isomerization of the <i>cis</i> retinal molecule to the <i>trans</i> form upon interaction with light.	5
3	The ethylene molecule.	41
4	The H2-C1=C2-H4 dihedral angle on the excited electronic state and the expectation value of the C1=C2 bond distance is plotted as a function of time[43]. The initial motion on the excited state is a stretching of the C1=C2 bond and the <i>cis-trans</i> torsional motion begins ~ 70 fs after the excitation. The quenching to the ground electronic state begins only after the energy is transferred out of the twisted coordinate.	43
5	Excited state-ground state simulation for ethylene. The dihedral angle measurements are from H2-C1=C2-H4 plane. The HOMO and the LUMO are switched and the dynamics of the dihedral angle is measured with respect to time. The isomerization of ethylene from <i>cis-trans</i> form starts ~ 70 fs after the beginning of the excitation.	44
6	Excited state-ground state simulation for ethylene. The bond distance measurements between the carbon atoms are plotted. The HOMO and the LUMO are switched and the dynamics of the C1=C2 bond distance is measured with respect to time without any external field.	45
7	The histogram shows a distribution of the molecular orbital energy eigenvalues of ethylene without the application of an electromagnetic field.	46
8	The C1=C2 bond distance is plotted over time for ethylene molecule with no external field applied. The time step $\Delta t = 0.005$ fs.	47

FIGURE	Page
9	The energy eigenvalues for ethylene molecule are plotted over time. The time step is $\Delta t = 0.005$ fs, the amplitude of the vector potential is $A = 0.5$ gauss·cm and the wavelength of the light is $\lambda = 228.094$ nm. 49
10	The total energy for ethylene molecule is plotted over time. The time step is $\Delta t = 0.005$ fs, amplitude of the vector potential is $A = 0.5$ gauss·cm and the wavelength of the light is $\lambda = 228.094$ nm. 50
11	The dihedral angle H2-C1=C2-H4 for ethylene molecule is plotted over time. The time step is $\Delta t = 0.005$ fs, amplitude of the vector potential is $A = 0.5$ gauss·cm and the wavelength of the light is $\lambda = 228.094$ nm. 51
12	The C1=C2 bond distance is plotted over time for ethylene molecule with amplitude of the vector potential is $A = 0.5$ gauss·cm and the wavelength of the light is $\lambda = 228.094$ nm The time step $\Delta t = 0.005$ fs. 52
13	The dihedral angle is plotted over time for ethylene molecule with amplitude of the vector potential is $A = 0.5, 1.0$ and 2.0 gauss·cm and the wavelength of the light is $\lambda = 228.094$ nm. The time step $\Delta t = 0.005$ fs. 53
14	The C1=C2 bond distance is plotted over time for ethylene molecule with amplitude of the vector potential is $A = 0.5, 1.0$ and 2.0 gauss·cm and the wavelength of the light is $\lambda = 228.094$ nm. The time step $\Delta t = 0.005$ fs. 54
15	The dihedral angle is plotted over time for ethylene. The vector potential $A=0.5$ gauss·cm, wavelength $\lambda = 114.047$ nm, 228.094 nm and 456.188 nm and the time step $\Delta t = 0.005$ fs. 55
16	The dihedral angle is plotted over time for ethylene. The vector potential $A=0.5$ gauss·cm, wavelength $\lambda = 228.094$ nm and the time steps are $\Delta t = 0.005, 0.010$ and 0.050 fs. 56

FIGURE	Page
17	The C1=C2 bond distance is plotted over time for ethylene molecule with amplitude of the vector potential is $A = 0.5$ gauss·cm and the wavelength of the light is $\lambda = 228.094$ nm. The time step $\Delta t = 0.005, 0.010$ and 0.050 fs. 57
18	The 2-butene molecule in its <i>cis</i> form. 58
19	Excited state-ground state simulation for 2-butene. The dihedral angle measurements are from H4-C2=C3-H5 plane. The HOMO and the LUMO are switched and the dynamics of the dihedral angle is measured with respect to time. The isomerization of butene from <i>cis-trans</i> form starts ~ 175.0 fs after the beginning of the excitation. 59
20	Excited state-ground state simulation for 2-butene. The HOMO and the LUMO are switched and the dynamics of the C2=C3 bondlength is measured with respect to time. The isomerization of butene from <i>cis-trans</i> form starts ~ 175.0 fs after the beginning of the excitation. 60
21	The histogram shows a distribution of the molecular orbital energy eigenvalues of 2-butene without the application of an electromagnetic field. 61
22	The C2=C3 bond distance is plotted over time for 2-butene with no external field applied. The time step $\Delta t = 0.005$ fs. 62
23	The <i>cis-trans</i> isomerization of the 2-butene molecule. 64
24	The energy eigenvalues for 2-butene molecule are plotted over time. The time step is $\Delta t = 0.005$ fs, amplitude of the vector potential is $A = 1.0$ gauss·cm and the wavelength of the light is $\lambda = 244.0$ nm. 65
25	The total energy for 2-butene molecule is plotted over time. The time step is $\Delta t = 0.005$ fs, amplitude of the vector potential is $A = 1.0$ gauss·cm and the wavelength of the light is $\lambda = 244.0$ nm. 66

FIGURE	Page
26	The dihedral angle H4-C2=C3-H5 for 2-butene molecule is plotted over time. The time step is $\Delta t = 0.005$ fs, amplitude of the vector potential is $A = 1.0$ gauss·cm and the wavelength of the light is $\lambda = 244.0$ nm. 67
27	The C2=C3 bond distance is plotted over time for 2-butene molecule with amplitude of the vector potential is $A = 1.0$ gauss·cm and the wavelength of the light is $\lambda = 244.0$ nm. The time step $\Delta t = 0.005$ fs. 68
28	The dihedral angle is plotted over time for 2-butene molecule with amplitude of the vector potential is $A = 0.5, 1.0$ and 2.0 gauss·cm and the wavelength of the light is $\lambda = 244.0$ nm. The time step $\Delta t = 0.005$ fs. 69
29	The dihedral angle is plotted over time for 2-butene. The vector potential $A=1.0$ gauss·cm, wavelength $\lambda = 122.0$ nm, 244.0 nm and 488.0 nm and the time step $\Delta t = 0.005$ fs. 70
30	The dihedral angle is plotted over time for 2-butene. The vector potential $A=1.0$ gauss·cm, wavelength $\lambda = 244.0$ nm and the time steps are $\Delta t = 0.005, 0.010$ and 0.050 fs. 71
31	The stilbene molecule in its <i>cis</i> form. 72
32	Excited state-ground state simulation for stilbene. The dihedral angle measurements are from H6-C7=C8-H7 plane. The HOMO and the LUMO are switched and the dynamics of the dihedral angle is measured with respect to time. The isomerization of stilbene from <i>cis-trans</i> form starts ~ 325 fs after the beginning of the excitation. 74
33	Excited state-ground state simulation for stilbene. The bond distance measurements between the carbon atoms are plotted. The HOMO and the LUMO are switched and the dynamics of the C7=C8 bond distance is measured with respect to time without any external field. 75

FIGURE	Page
34	The histogram shows a distribution of the molecular orbital energy eigenvalues of stilbene without the application of an electromagnetic field. 76
35	The C7=C8 bond distance is plotted over time for stilbene molecule with no external field applied. The time step $\Delta t = 0.005$ fs. 77
36	The <i>cis-trans</i> isomerization of the stilbene molecule. 78
37	The energy eigenvalues for stilbene molecule are plotted over time. The time step is $\Delta t = 0.005$ fs, amplitude of the vector potential is $A = 1.2$ gauss·cm and the wavelength of the light is $\lambda = 458.0$ nm. 79
38	This plot is a subsection of Figure 37. The energy eigenvalues near the HOMO and the LUMO are plotted over time. The time step is $\Delta t = 0.005$ fs, amplitude of the vector potential is $A = 1.2$ gauss·cm and the wavelength of the light is $\lambda = 458.0$ nm. 80
39	The total energy for stilbene molecule is plotted over time. The time step is $\Delta t = 0.005$ fs, amplitude of the vector potential is $A = 1.2$ gauss·cm and the wavelength of the light is $\lambda = 458.0$ nm. 81
40	The dihedral angle H6-C7=C8-H7 for stilbene molecule is plotted over time. The time step is $\Delta t = 0.005$ fs, amplitude of the vector potential is $A = 1.2$ gauss·cm and the wavelength of the light is $\lambda = 458.0$ nm. 82
41	The C7=C8 bond distance is plotted over time for stilbene molecule with amplitude of the vector potential is $A = 1.2$ gauss·cm and the wavelength of the light is $\lambda = 458.0$ nm. The time step $\Delta t = 0.005$ fs. 82
42	The dihedral angle is plotted over time for stilbene molecule with amplitude of the vector potential is $A = 0.5, 1.2$ and 2.0 gauss·cm and the wavelength of the light is $\lambda = 458.0$ nm. The time step $\Delta t = 0.005$ fs. 83

FIGURE	Page
43	The C7=C8 bond distance is plotted over time for stilbene molecule with amplitude of the vector potential is $A = 0.5, 1.2$ and 2.0 gauss·cm and the wavelength of the light is $\lambda = 458.0$ nm. The time step $\Delta t = 0.005$ fs. 84
44	The dihedral angle is plotted over time for stilbene. The vector potential $A=1.2$ gauss·cm, wavelength $\lambda = 229.0$ nm, 458.0 nm and 916.0 nm and the time step $\Delta t = 0.005$ fs. 85
45	The C7=C8 bond length is plotted over time for stilbene. The vector potential $A=1.2$ gauss·cm, wavelength $\lambda = 229.0$ nm, 458.0 nm and 916.0 nm and the time step $\Delta t = 0.005$ fs. 86
46	The dihedral angle is plotted over time for stilbene. The vector potential $A=1.2$ gauss·cm, wavelength $\lambda = 458.0$ nm and the time steps are $\Delta t = 0.005, 0.010$ and 0.050 fs. 87
47	Frequency measurements for the ethylene molecule from Fourier-Transform techniques. The C1=C2 bondlengths were measured over time and transformed to get vibrational frequencies. The graph represents the Fourier amplitudes plotted with respect to the corresponding frequencies. The time step $\Delta t = 0.005$ fs and the total time is 400 fs. 98
48	Frequency measurements for the 2-butene molecule from Fourier-Transform techniques. The C2=C3 bondlengths were measured over time and transformed to get vibrational frequencies. The graph represents the fourier amplitudes plotted with respect to the corresponding frequencies. The time step $\Delta t = 0.005$ fs and the total time is 400 fs. 99
49	Frequency measurements for the stilbene molecule from Fourier-Transform techniques. The C7=C8 bondlengths were measured over time and transformed to get vibrational frequencies. The graph represents the fourier amplitudes plotted with respect to the corresponding frequencies. The time step $\Delta t = 0.005$ fs and the total time is 400 fs. 100
50	The retinal molecule in its 11- <i>cis</i> form. 101

FIGURE	Page
51	Excited state-ground state simulation for retinal. The dihedral angle measurements are from H10-C11=C12-H11 plane. The 52 nd and the 62 nd are switched and the dynamics of the dihedral angle is measured with respect to time. 103
52	Excited state-ground state simulation for retinal. The dihedral angle measurements are from H10-C11=C12-H11 plane. The 55 th and the 62 nd are switched and the dynamics of the dihedral angle is measured with respect to time. 104
53	The histogram shows a distribution of the molecular orbital energy eigenvalues of retinal without the application of an electromagnetic field. 105
54	The C11=C12 bond distance is plotted over time for the retinal molecule with no external field applied. The time step $\Delta t = 0.005$ fs. 106
55	Frequency measurements for the retinal molecule from Fourier-Transform techniques. The C11=C12 bondlengths were measured over time and transformed to get vibrational frequencies. The graph represents the fourier amplitudes plotted with respect to the corresponding frequencies. The time step $\Delta t = 0.005$ fs and the total time is 400 fs. 115
56	The energy eigenvalues for the retinal molecule are plotted over time. The time step is $\Delta t = 0.005$ fs, amplitude of the vector potential is $A = 1.0$ gauss·cm and the wavelength of the light is $\lambda = 568.0$ nm. 117
57	The total energy for the retinal molecule is plotted over time. The time step is $\Delta t = 0.005$ fs, amplitude of the vector potential is $A = 1.0$ gauss·cm and the wavelength of the light is $\lambda = 568.0$ nm. . . 117
58	The dihedral angle H10-C11=C12-H11 for the retinal molecule is plotted over time. The time step is $\Delta t = 0.005$ fs, amplitude of the vector potential is $A = 1.0$ gauss·cm and the wavelength of the light is $\lambda = 568.0$ nm. 118

FIGURE	Page
59	The C11=C12 bond distance is plotted over time for the retinal molecule with amplitude of the vector potential is $A = 1.0$ gauss·cm and the wavelength of the light is $\lambda = 568.0$ nm. The time step $\Delta t = 0.005$ fs. 119
60	The energy eigenvalues for the retinal molecule are plotted over time. The time step is $\Delta t = 0.005$ fs, amplitude of the vector potential is $A = 0.8$ gauss·cm and the wavelength of the light is $\lambda = 568.0$ nm. 120
61	The total energy for the retinal molecule is plotted over time. The time step is $\Delta t = 0.005$ fs, amplitude of the vector potential is $A = 0.8$ gauss·cm and the wavelength of the light is $\lambda = 568.0$ nm. . . 121
62	The dihedral angle H10-C11=C12-H11 for the retinal molecule is plotted over time. The time step is $\Delta t = 0.005$ fs, amplitude of the vector potential is $A = 0.8$ gauss·cm and the wavelength of the light is $\lambda = 568.0$ nm. 121
63	The C11=C12 bond distance is plotted over time for the retinal molecule with amplitude of the vector potential is $A = 0.8$ gauss·cm and the wavelength of the light is $\lambda = 568.0$ nm. The time step $\Delta t = 0.005$ fs. 122

CHAPTER I

INTRODUCTION

Molecules that undergo rapid excited-state photochemical reactions in the condensed phase present important problems in chemical reaction dynamics[1, 2].

Recent progress in the field of short laser pulse generation in picosecond and femtosecond range makes it possible to obtain detailed information on the structural dynamics of different organic molecules[3]. Molecular dynamics simulations enables one to interpret the experimental observations and to deepen and broaden the understanding of the physics of the processes taking place in the molecules upon interaction with light. In this work, we study the simulation of the molecular dynamics in various organic molecules undergoing photoisomerization.

The simplest of the molecules we will study is ethylene which has only two carbon and four hydrogen atoms and is a prototype for other more complex ethenes. The absorption of light by the ethylene molecule results in an increase of its internal energy. If the light is in the ultraviolet or visible regions of the electromagnetic spectrum, the initial excess energy takes the form of electronic excitation. The nature of this excited state depends on the wavelength of the light absorbed and the electronic structure of the molecule. The excess electronic energy can become distributed to vibrational and rotational degrees of freedom of the molecule. This can subsequently lead to the isomerization of the molecule through the twisting of one CH_2 group by 180° about the carbon-carbon double bond.

Two other test molecules that were used as examples for the photo-isomerization simulation in this work were 2-butene and stilbene. There are several experiments

This dissertation follows the style of Physical Review A.

that have been conducted with these simple molecules and the results are compared with the current method to further enforce the validity of the model.

In recent years, stilbene photochemistry has been the focus of several experimental and theoretical works[4, 5]. A detailed analysis of photo-stimulated structural transitions of benzene-type structures plays an important role in studying of organic molecules. This problem can be successfully solved by using photo-isomerization since both linear and non-linear properties of organic molecules strongly depend on their structure.

The main objective of the current work is to study the photo-isomerization of the retinal pigment in the eye, rhodopsin. The human eye captures light and transmits the neurological signals to the visual centers of the brain where sight is perceived. The retina in the human eye is populated by two types of photoreceptors which have a frequency dependent response: rods which are very sensitive to light and function in black-and-white vision at night; and cones which are less sensitive to light and account for color vision during the day.

The visual pigment in the eye consists of a light-absorbing molecule called retinal, bonded to a protein known as opsin. Each type of photoreceptor in the eye has a characteristic kind of opsin which affects the absorption spectrum of the retinal. In the case of rods, the whole pigment complex, retinal plus the specific type of opsin, is called rhodopsin. The membrane protein in rhodopsin, called bacteriorhodopsin[6], contains an 11-*cis*-retinal in a binding site lined by amino acid groups and water molecules that guide the photodynamics of retinal. Vision begins with the 11-*cis*-to-all-*trans* photoisomerization of the retinal[7]. This isomerization drives conformational changes in the surrounding protein that results in the excitation of the retinal rod cell. Light absorption by rhodopsin produces an early photoproduct called bathorhodopsin that stores a large amount of energy (~ 30 kcal/mole). The 11-*cis*-

retinal is shown in Figure 1.

The process of photoreception involves the conversion of a light signal to the electrical response of the optical photoreceptor cells. This is accomplished by the retinal pigment which is an excellent molecular switch. Upon interaction with light, the chromophore of the visual pigment, 11-*cis* retinal, isomerizes to a highly twisted all *trans* form in the restricted cavity in the visual pigment. The highly twisted chromophore then induces stepwise changes of the protein and finally leads to the formation of the enzymatically active state responsible for the G protein activation.

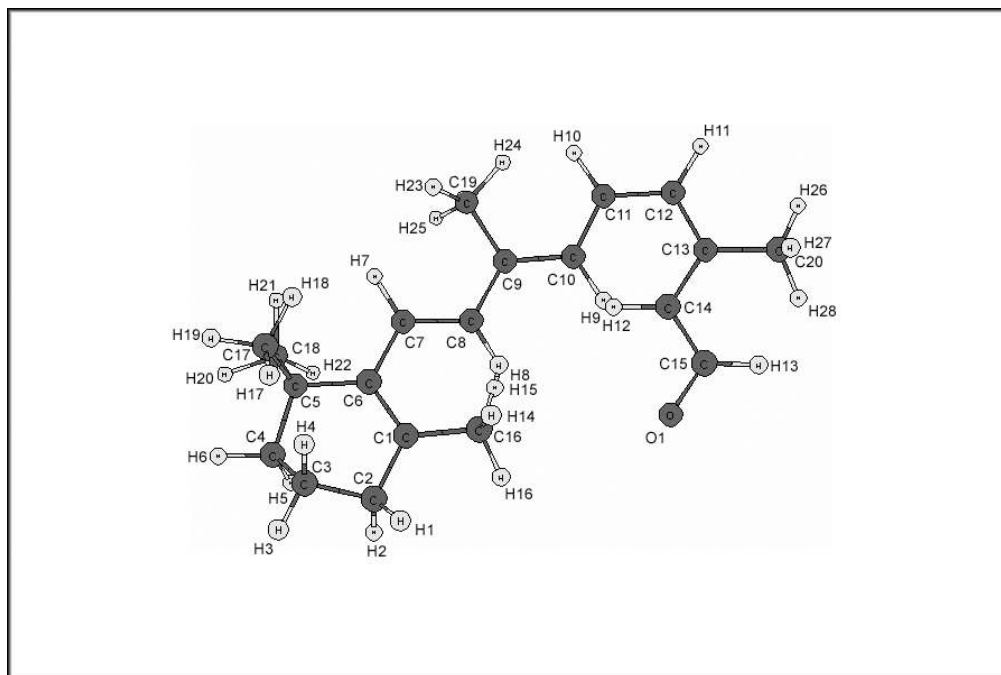


Fig. 1. The retinal molecule in its 11-*cis* form.

A. Photo-reception in the Eye

The first 200 femtoseconds in the life of the photoexcited rhodopsin molecule are extremely important for the development of visual sensation[8]. Immediately upon excitation, a dramatic change in the charge distribution in the cationic 11-*cis* retinal protonated Schiff base chromophore occurs that is quantitated by the change in electronic dipole moment of ~ 15 Debye. The protein opsin, then tunes the absorption maximum of the pigment to the blue or to the red enabling color vision. This is manifested by placing dipolar rather than charged residues in the chromophore binding site to differentially stabilize either the ground or the excited state. Resonance Raman intensity analysis points out that the 11-*cis* retinal chromophore then distorts violently about the double bond between the 11th and the 12th carbon atoms reaching a torsional angle of up to 50 degrees in only 30 fs[9].

Raman intensity analysis is used to determine how photochemically active molecules change structure upon electronic excitation. The analysis of resonance Raman intensities with time-dependent wavepacket techniques provides a multi-mode picture of their femtosecond excited-state reaction dynamics. Time-dependent wavepacket techniques also provide a powerful approach for the analysis of femtosecond transient absorption experiments as well as spontaneous and time-resolved emission.

The isomerization of the retinal molecule from its *cis* to *trans* form is shown in Figure 2.

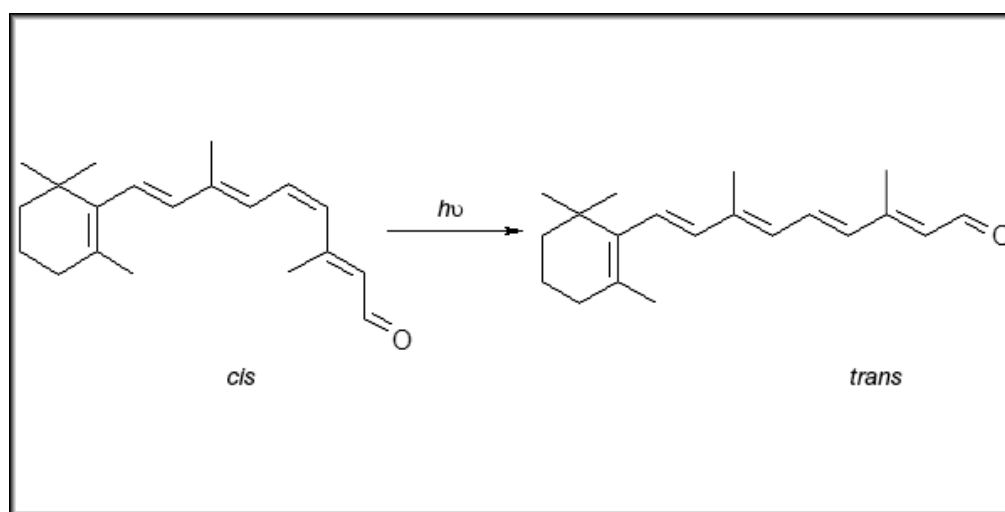


Fig. 2. Isomerization of the *cis* retinal molecule to the *trans* form upon interaction with light.

Since the discovery of the visual pigments in the 1870s[10], molecular mechanisms of photoreception and phototransduction in visual pigments have been the focus of numerous studies. The protein in the eye, rhodopsin, absorbs light and fades in color from red to pale yellow. This process is known as “photobleaching”. The photobleaching phenomenon comprises both photochemical and thermal reactions. Upon absorbing a photon, rhodopsin goes up to an excited state. This transition is a photophysical process which only takes a few femtoseconds for completion. In the absence of light, the relaxation process of the singlet excited state to the ground state can occur through four possible different processes: radiationless internal conversion, fluorescence, intersystem crossing and photochemical reaction[11]. The first three processes generate a ground state identical to the original state before photon absorption and therefore, the light signal is not trapped in the rhodopsin molecule. Thus, the fourth process, namely, the photochemical *cis-trans* isomerization is the only process which is involved in the trapping mechanism of the light signal and must be more efficient than the other processes in order to activate the vision process. The efficiency, however, depends on how fast the process occurs and, therefore, the *cis-trans* isomerization should occur as fast as the other processes. Ultra fast spectroscopy using femtosecond laser pulse shows that the isomerization is complete within 200 fs[12]. Theoretical computations involving absorption spectroscopy have found that the isomerization starts at about 50-60 fs after the photon absorption. Thus, the isomerization occurs as fast as vibrational motions of the chromophore, which causes a coherent production of the primary intermediate, photorhodopsin[13, 14].

After photon absorption by rhodopsin, the formation of an intermediate product, photorhodopsin, takes only about 200 fs[15]. This means that only minor rearrangement of the amino acid residues constituting the chromophore binding site can occur. Since the *cis* to *trans* isomerization causes an extension of the longitudinal length of

the chromophore, the chromophore should be in a highly twisted conformation in the restricted chromophore binding site. This causes an elevation of the potential energy. In fact, calorimetric studies showed that about 60% of the photon energy (~ 30 kcal) is stored as an increase in enthalpy[16] mainly due to the distortion of the chromophore in the restricted chromophore binding site[17]. Thus, in essence, the primary role of the chromophore isomerization is to trap a photon signal in such a manner that the absorbed light energy is converted into chemical free energy, stored in a highly twisted conformation of the chromophore, which then induces conformational changes of the protein to its active state.

The photoisomerization from the *trans* to the *cis* form of retinal has also been studied[18, 19] but is not the focus in this work.

B. Theoretical Motivation of the Current Work

The motivation behind this work came from using a relatively simple method to explain some rather complex molecular dynamics in large organic molecules. The process of vision has long been an enigma to the physical and chemical worlds. There have been several experiments conducted to try to explain the vision phenomenon. Unfortunately, due to the large size of the retinal molecule and prohibitive computational requirements, not much theoretical work has been done to explain the isomerization of the retinal molecule from its *cis* to *trans* form under the influence of laser pulse. The current work has been devised to test the tight-binding method on organic molecules based on the fact that the same model has been very successfully proven for semiconductors[20] and complex biological molecules[21].

Our work entails calculations at the molecular physics level, in terms of the time evolution in a quantum mechanical description of the molecule as it interacts

with an external electromagnetic field such as visible light. We employ tight-binding techniques and apply Peierls substitution and Hellmann-Feynman methods in our model to simulate the behavior of the molecule upon interaction with light.

In our present calculations, we consider only nearest-neighbor interactions which are the interactions between a particular atom and the ones to which it is attached via a chemical bond. We ignore all distant-neighbor and non-bonded interactions. One of the shortcomings of this semiempirical tight-binding model is that the tight-binding parameters are only fitted to nearest neighbors. In order to incorporate interactions with second nearest neighbors, one has to introduce a new set of parameters in the Hamiltonian. This makes the calculation more complicated thereby losing the essence of this simple semi-empirical model.

The primary intent of the current work is to successfully explain the photochemical phenomenon of vision via the isomerization of the retinal molecule. We also test some simpler molecules, e.g., ethylene, 2-butene and stilbene. There have been numerous experiments conducted with these smaller molecules and hence we were able to compare these results with the ones obtained from the current tight-binding model. In all the cases, they seem to agree reasonably well, thereby proving the validity of our model.

The calculations involve using a Born-Oppenheimer type of approximation where the electrons are treated quantum-mechanically and the time-dependent Schrödinger equation is used to solve for the motion of the electrons. The nuclei are treated classically using Lorentz-force calculations. The motion of the atoms is solved using a form of Ehrenfest's theorem which calculates the forces on the individual atoms. This information is used in the velocity-Verlet algorithm to yield the new positions of the atoms which constitutes the molecular dynamics under photo-isomerization.

We use the tight-binding model which involves these tools and has been success-

ful in explaining electronic and structural responses of semiconductors, e.g., gallium arsenide and silicon[22] and biological molecules, e.g. chlorophyll[21] to laser pulses. In earlier studies, the authors successfully used the tight-binding method to determine the isomerization in gallium-arsenide and arsenic and correctly predict many electronic properties such as the density of states, band structure and Fermi energy and the isomerization of chlorophyll under the influence of light.

In the cases mentioned above, the authors show that the results obtained from the tight-binding model closely follow experimental results. In order to test the validity of the model for our work we first employ small molecules like ethylene and 2-butene which have been extensively studied and therefore allow us to compare with available results. Based on satisfactory results for these small molecules, we proceeded with calculations for more complex molecules such as retinal which has 49 atoms and hope to gain valuable insight into the vision process. Tests were also done with stilbene which consists of 26 atoms and is a very interesting molecule and heavily researched in current years.

CHAPTER II

THE TIGHT-BINDING MODEL

During the simulation of the molecular dynamics of organic molecules, both the geometrical and electronic properties of these molecules are affected by the introduction of light in the system. This is due to the fact that under the influence of intense sub-picosecond laser pulse, the chemical bondings of the atoms are altered which in turn affects both the geometry of the molecule and the electronic structure.

The change in the structural and electronic properties can be addressed by monitoring the dynamics of the molecule during photoisomerization. Molecular dynamics can be obtained by one of three techniques, namely, empirical, first principles and semi-empirical tight-binding methods[23].

An empirical model consists of a function that fits the data. If data exists, we can often use this data as the sole basis for an empirical model. In this case of photochemistry, empirical methods simulate very well the geometrical structural changes under the influence of light but do not address any effect on the electronic properties. This is a major deficiency of these methods, although one could modify the empirical potential after the interaction with light, but that seems to generate approximate results[20]. In addition, empirical methods use classical potentials to determine the forces on each atom, which requires an empirical fit of the parameters in the potential. Although these methods have been used in a variety of semiconductor systems successfully, in our current study of organic molecules, it was important to correctly interpret the behavior of the electronic structure under the influence of light. Therefore, empirical models were deemed not suitable for the current scope of work.

The first-principles method involve solving the Schrödinger equation for the real-space wavefunctions. The first-principles method gives an excellent view of the elec-

tronic structure of the atoms upon interaction with light. These methods have successfully contributed to studying the molecular dynamics of various solid state and chemical systems. For current purposes these exact calculations would have very heavy computational requirements which wasn't feasible for our molecules, especially for retinal which has 49 atoms.

The method of choice for this work was the semi-empirical tight-binding technique. It addresses the dynamics of the geometrical as well as the electronic structure under photoisomerization while not being computationally restrictive. In this method, the matrix elements in the Hamiltonian are represented by simple analytical expressions and are obtained from experimental and theoretical calculations. The accuracy of a tight-binding model largely depends on the correct choice of the basis functions and proper fitting of the parameters. In the context of the present work, we were able to obtain good results in explaining the molecule's electronic structure and the molecular dynamics based on a reasonable choice of input parameters.

In order to simulate the photoreception in the eye quantum-mechanically, we begin with the time-independent Hamiltonian for the electrons and the nuclei. The electronic time-independent Hamiltonian operator is given by,

$$H_e = T_e + V_{ee} + V_{en}. \quad (2.1)$$

In the above equation, T_e , V_{ee} and V_{en} are the operators for the electronic kinetic energy, electron-electron repulsion energy, and electron-nuclear attraction energy respectively. We make a Born-Oppenheimer type of approximation to represent the molecular wave function as:

$$\Psi = \Psi_e(\mathbf{r}, \mathbf{R})\Psi_n(\mathbf{R}) \quad (2.2)$$

where Ψ_e is the electronic wave function, which depends on the electronic and nuclear

coordinates \mathbf{r} and \mathbf{R} respectively and Ψ_n is the nuclear wave function which solely depends on the nuclear coordinates. This approximation is valid since $(m_e/m_n)^{1/4} \ll 1$. Using this type of Born-Oppenheimer approximation we find that minimal error is introduced in the computation of the ground electronic states of many-electron molecules. Corrections for the excited states are typically larger than the ground states. However, this is small compared to the approximations used to solve the electronic Schrödinger equation, e. g., Cayley algorithm[20] used in the present calculations.

For isolated systems, one could solve for the electronic and the nuclear wave functions using the time-independent Schrödinger equation:

$$\mathbf{H}\Psi = E\Psi. \quad (2.3)$$

The electronic Schrödinger equation for the molecule becomes,

$$(T_e + V_{ee} + V_{en})\Psi_e = E_e(\mathbf{R})\Psi_e. \quad (2.4)$$

At a particular nuclear configuration \mathbf{R} , the solution to the above equation gives the electronic energy E_e for that configuration. The sum of E_e and the nuclear-nuclear repulsion energy V_{nn} is the total potential energy in which the nuclei move with kinetic energy T_n . By performing the calculation at many different nuclear configurations a complete potential energy surface may be determined. The nuclear wavefunction may be found by solution of the nuclear Schrödinger equation. The nuclear time-independent Hamiltonian can be described by the following:

$$H_n = T_n + V_{nn} + E_e \quad (2.5)$$

where T_n is the kinetic energy operator for the nuclei, V_{nn} denotes the nuclear-nuclear repulsion and E_e is the energy of the electrons. Using the above nuclear Hamiltonian

we can write the form of the nuclear Schrödinger equation for the system as follows:

$$(T_n + V_{nn} + E_e)\Psi_n = E\Psi_n \quad (2.6)$$

where E is the total energy of the system, since the Hamiltonian in equation (2.5) includes operators for both nuclear and electronic energies. E is simply a number and does not depend on any coordinates. However, for each electronic state of a molecule we must solve a different nuclear Schrödinger equation, since the potential energy differs from state to state.

A. Time-dependent Schrödinger Equation

The Schrödinger equations for the nuclei and the electrons described earlier are all time-independent. However, when we apply the electromagnetic field in the form of light to simulate the photoisomerization of the molecule, we introduce an explicit time-dependence in our system. In order to introduce time-dependence in our calculations, we write the time-dependent Schrödinger equation as,

$$i\hbar \frac{\partial \Psi_{\mathbf{k}}(\mathbf{r}, \mathbf{t})}{\partial t} = \mathbf{H}(t) \Psi_{\mathbf{k}}(\mathbf{r}, \mathbf{t}) \quad (2.7)$$

where $\Psi_{\mathbf{k}}$ represent the one-electron wave functions which are the same as the electronic wave functions $\Psi_{\mathbf{e}}$ in equation (2.4). This describes the equation of motion for a time-dependent self-consistent-field approximation.

The one-electron wave functions can be written as a set of localized basis functions $\psi_k(r, t)$:

$$\Psi_k(\mathbf{r}, t) = \sum_l c_l \psi_l(\mathbf{r}, t). \quad (2.8)$$

In the above equation (2.8), c_l is a fermion operator.

The Hamiltonian of the system can be expressed as:

$$\begin{aligned}
\mathbf{H} &= \sum_l \frac{\mathbf{P}_l^2}{2M_l} + \sum_k \frac{\mathbf{p}_k^2}{2m_k} + \mathbf{H}_{ii} + \mathbf{H}_{ee} + \mathbf{H}_{ei} + \mathbf{H}_{ext}, \\
\mathbf{H}_{ii} &= \sum_{l>l'} v_{ll'}(\mathbf{R}_l - \mathbf{R}_{l'}), \\
\mathbf{H}_{ee} &= \sum_{k>k'} v_{kk'}(\mathbf{r}_k - \mathbf{r}_{k'}), \\
\mathbf{H}_{ei} &= \sum_{k,l} v_{kl}(\mathbf{r}_k - \mathbf{R}_l). \tag{2.9}
\end{aligned}$$

In equation (2.9), l and k respectively label the ions and the electrons. \mathbf{H}_{ii} denotes the ion-ion interaction, \mathbf{H}_{ee} is the electron-electron interaction term and \mathbf{H}_{ei} represents the electron-ion interaction. The last term \mathbf{H}_{ext} stands for the Hamiltonian term due to the interaction of the ions and the electrons with external fields, which in our case is the electro-magnetic field.

We denote the electronic charge as e and the atomic number as Z_l . The terms $v_{ll'}$, $v_{kk'}$ and v_{kl} can be expressed as the following:

$$\begin{aligned}
\sum_{l>l'} v_{ll'} &= \sum_{l>l'} \frac{Z_l Z_{l'} e^2}{(R_l - R_{l'})}, \\
\sum_{k>k'} v_{kk'} &= \sum_{k>k'} \frac{e^2}{(r_k - r_{k'})}, \\
\sum_{k,l} v_{kl} &= \sum_{k,l} \frac{Z_l e^2}{(r_k - r_{k'})}. \tag{2.10}
\end{aligned}$$

We now consider a simplifying assumption, that the nuclei occupy fixed positions in space. This is the Born-Oppenheimer approximation which has been discussed earlier. The electrons in a molecule are much lighter than the nuclei and move much faster. Essentially, we can consider the nuclei as “frozen” and the electrons are moving in the field created by the nuclei. Our problem then reduces to that of calculating the

wave functions and energies of the electrons.

For the electronic motion alone, we can write the Hamiltonian in the following form[20]:

$$\mathbf{H} = \sum_k -\frac{\hbar^2}{2m} \nabla_k^2 + \sum_{kl} v_{kl}(\mathbf{r}_k - \mathbf{R}_l) + \frac{1}{2} \int d^3(r_k - r_{k'}) n(\mathbf{r}_k - \mathbf{r}_{k'}, t) v(\mathbf{r}_k - \mathbf{r}_{k'}) + \mathbf{H}_{ext} \quad (2.11)$$

where

$$n(\mathbf{r}, t) = \sum_k n_k \Psi_k^*(\mathbf{r}, t) \Psi_k(\mathbf{r}, t), \quad (2.12)$$

and

$$n_k = \langle c_k^\dagger c_k \rangle. \quad (2.13)$$

n_k in the above equation stands for the occupation number of the state. Thus,

$$n_k = 0 \text{ or } 2 \quad (2.14)$$

depending on whether the state is empty or singly-occupied by an electron.

The first sum in equation (2.11) represents the kinetic energy of the electrons, the second term is due to the attraction of the electrons and the nuclei and the third term stands for the mutual repulsion between the electrons.

In our formulation of the Hamiltonian, we have not included the requirement that the total wave function $\Psi(\mathbf{r}, \mathbf{t})$ be antisymmetric upon interchange of two electrons:

$$\Psi(\cdots \mathbf{r}_j, \mathbf{r}_k \cdots) = -\Psi(\cdots \mathbf{r}_k, \mathbf{r}_j \cdots). \quad (2.15)$$

In order to solve the time-dependent Schrödinger equation, one could postulate a semiempirical tight-binding Lagrangian[23] of the form,

$$L = \sum_{\ell, \alpha} \frac{1}{2} M \dot{X}_{\ell, \alpha}^2 - U_{rep} + \sum_k \Psi_k^\dagger \cdot \left(i\hbar \frac{\partial}{\partial t} - \mathbf{H} \right) \cdot \Psi_k. \quad (2.16)$$

In the above equation, each of the electrons is denoted by the symbol k and is represented by its own time-dependent state vector Ψ_k . The first term in equation (2.16) is the kinetic energy of the ions, with coordinates $X_{\ell,\alpha}$, which are treated classically. The subscript l represents the ions and $\alpha = x, y, z$. The second is a summation over repulsive potentials which model the ion-ion repulsion, together with the negative of the electron-electron repulsion which is doubly counted in the third term[24].

$$U_{rep} = U_{ii} - U_{ee}. \quad (2.17)$$

The last term is the tight-binding version of the standard Lagrangian in a time-dependent self-consistent-field approximation. We can adopt the point of view that each electron is labeled by k and has its own time-dependent state vector Ψ_k . If there are N tight-binding basis functions in the system, Ψ_k is N -dimensional.

We next follow the derivations following the lagrangian in equation (2.16) as done in [22]. In their paper Graves *et al.* first show the equations explaining the motion of the molecules for the non-orthogonal case. And finally they assume an orthogonal tight-binding model which is also the case considered in the present context. This simplifies the final form of the equation of motion for the molecules which are stated as follows:

$$i\hbar\partial\Psi_k/\partial t = H(t)\Psi_k, \quad (2.18)$$

and

$$M\ddot{X} = -\sum_k \Psi_k^\dagger \cdot \frac{\partial H}{\partial X} \cdot \Psi_k - \frac{\partial U_{rep}}{\partial X} \quad (2.19)$$

where M is the mass and X the coordinate of any ion. These are respectively the time-dependent Schrödinger equation and the Hellmann-Feynman theorem (or Ehrenfest's theorem), with the electrons treated in a tight-binding picture and the ions treated

classically.

B. Tight-Binding with s - p Orbitals

In order to find the eigenstates of the electronic system, we begin with the Hamiltonian $H_{i\alpha,j\beta}$ of the form[20]:

$$H_{i\alpha,j\beta} = t_{i\alpha,j\beta}^0(\mathbf{r}_i - \mathbf{r}_j). \quad (2.20)$$

The off-diagonal matrix elements $t_{i\alpha,j\beta}^0$ give the interaction between neighboring atoms i and j . These matrix elements give the interaction between the wave function at the site \mathbf{r}_j with orbital symmetry β and at the site \mathbf{r}_i with orbital symmetry α . The diagonal elements of the Hamiltonian matrix are simply the atomic energies within the molecule.

The wave function of an electron can be represented by a sum over basis functions which have the symmetry of atomic orbitals. We use an s - p atomic orbital model, where there are four independent primitive matrix elements $t_{i\alpha,j\beta}^0$ for the pair of states represented by $ss\sigma$, $sp\sigma$, $pp\sigma$ and $pp\pi$. Tight-binding provides a better chemical description when d -functions and f -functions are included, but for present purposes modeling the Hamiltonian with only s and p proved sufficient. The matrix elements can be written as follows:

$$t_{is,js}^0(\mathbf{r}_i - \mathbf{r}_j) = \eta_{ss\sigma} \frac{\hbar^2}{md^2}, \quad (2.21)$$

$$t_{is,jp_\mu}^0(\mathbf{r}_i - \mathbf{r}_j) = l_\mu \eta_{sp\sigma} \frac{\hbar^2}{md^2} = -t_{ip_\mu,js}(\mathbf{r}_i - \mathbf{r}_j), \quad (2.22)$$

$$t_{ip_\mu,jp_\nu}^0(\mathbf{r}_i - \mathbf{r}_j) = [l_\mu l_\nu (\eta_{pp\sigma} - \eta_{pp\pi}) + \delta_{\mu\nu} \eta_{pp\pi}] \frac{\hbar^2}{md^2} = t_{ip_\nu,jp_\mu}. \quad (2.23)$$

In the above equations, m represents the electronic mass, \mathbf{r}_i stands for the position of the i^{th} atom and \mathbf{r}_j stands for the position of the j^{th} atom, which is i^{th} atom's nearest neighbor. The term $l_\mu = d_\mu/d$ is a directional cosine between sites i and j separated by a distance d , i.e., if the vector from i to j is $\mathbf{d} = x, y, z$ with components x, y and z (indexed by μ and ν), then $l_x = x/d$ and similarly for l_y and l_z . The subscripts π and σ denote the relative orientation of the orbitals, namely, σ when the lobes of the p-orbitals on the two interacting sites are pointing directly towards each other and π when the lobes are parallel to each other.

In our calculations for the force on the individual atoms, we find that for the electronic part, we need to find the derivative of the Hamiltonian. In order to calculate the values of the Hamiltonian and its derivatives, we use the formulation of Slater and Koster[25].

Table I. Tight-binding parameters for an s - p model according to Harrison[26].

$$(\eta_{ps\sigma} = -\eta_{sp\sigma}).$$

Tight-Binding parameter	Value (eV)
$\eta_{ss\sigma}$	-1.32
$\eta_{sp\sigma}$	1.42
$\eta_{ps\sigma}$	-1.42
$\eta_{pp\sigma}$	2.22
$\eta_{pp\pi}$	-0.63

C. Peierls Substitution

We have so far discussed the Hamiltonian matrix in a time-independent form. When we introduce an electromagnetic field in our problem in the form of light, we have to

consider the time-dependence of the Hamiltonian. Peierls substitution[27] is used to incorporate time-dependence into our otherwise time-independent Hamiltonian. We apply a time-dependent electromagnetic field and observe the interaction of the atoms with the field. Peierls substitution shows that this involves simply multiplying each element of the original tight-binding Hamiltonian by a phase factor. We can then use the Hamiltonian in the time-dependent Schrödinger equation.

1. The vector potential and the electro-magnetic field

We consider a vector potential of the form

$$\mathbf{A}(t) = A_0 \hat{\mathbf{e}} \cos(\omega t) \quad (2.24)$$

where A_0 is the amplitude of the electromagnetic wave and ω is the angular frequency of the light. $\hat{\mathbf{e}}$ gives the direction of polarization of the light. We consider the wave in the Coulomb or radiation gauge[28] where

$$\nabla \cdot \mathbf{A} = 0. \quad (2.25)$$

Also, in the Coulomb gauge, the polarization direction (which is also the direction of the electric field), the magnetic field direction and the propagation direction must be mutually perpendicular. This condition is expressed as,

$$\hat{\mathbf{e}} \cdot \mathbf{k} = 0. \quad (2.26)$$

The name “radiation gauge” arises from the fact that the transverse radiation fields are given by only the vector potential. This gauge is useful in quantum mechanical calculations, since a quantum-mechanical description of photons requires quantization of the vector potential.

We can then describe the associated electric $\mathbf{E}(t)$ and magnetic $\mathbf{B}(t)$ fields as the

following:

$$\begin{aligned}\mathbf{E}(t) &= -\frac{\partial \mathbf{A}}{\partial t} \\ &= A_0 \hat{\mathbf{e}} \omega \sin(\omega t)\end{aligned}\tag{2.27}$$

and

$$\begin{aligned}\mathbf{B}(t) &= \frac{1}{c}(\hat{k} \times \mathbf{E}) \\ &= \frac{\omega}{c}(\hat{k} \times \hat{\mathbf{e}}) A_0 \sin(\omega t).\end{aligned}\tag{2.28}$$

In the above set of equations, we have only considered time-dependence of the vector potential and the electric and the magnetic fields and ignored the spatial dependence. The reason for this approximation is that the wavelength of the pulse is much longer than the interatomic distances.

2. Effect of the vector potential on the Hamiltonian

To include the effect of the electromagnetic field we make the transformation,

$$\begin{aligned}\mathbf{H}(\mathbf{r}, \mathbf{p} - \frac{e}{c}\mathbf{A}(\mathbf{r}, t)) \\ = \exp[-\frac{ie}{\hbar c} \int \mathbf{A}(\mathbf{s}, t) \cdot d\mathbf{s}] \mathbf{H}(\mathbf{r}, \mathbf{p}) \exp[\frac{ie}{\hbar c} \int \mathbf{A}(\mathbf{s}, t) \cdot d\mathbf{s}].\end{aligned}\tag{2.29}$$

In equation (2.29) above, \mathbf{A} denotes the external, time-dependent electromagnetic field which varies slowly over distance and hence can be replaced by a summation instead of the integral. $H(\mathbf{r}, \mathbf{p})$ represents the Hamiltonian as a function of the canonical variables \mathbf{r} and \mathbf{p} and $d\mathbf{s}$ is a line element. The result is that the new interatomic matrix element $t_{i\alpha,j\beta}(\mathbf{r}_i - \mathbf{r}_j)$ of the Hamiltonian is given by the old matrix element $t_{i\alpha,j\beta}^0(\mathbf{r}_i - \mathbf{r}_j)$ times a multiplicative factor:

$$t_{i\alpha,j\beta}(\mathbf{r}_i - \mathbf{r}_j) = t_{i\alpha,j\beta}^0(\mathbf{r}_i - \mathbf{r}_j) \exp[-\frac{ie}{\hbar c}(r_i - r_j) \cdot \mathbf{A}(t)].\tag{2.30}$$

In our calculations, we treat the electrons and the nuclei as coupled since the forces on the nuclei are influenced by the electronic states. We add the effect of the field to the electronic motion using the Peierl's substitution. In order to incorporate the influence of the field in the nuclear motion, we first calculate the electric and magnetic fields as described in equations (2.27) and (2.28) above, and then find the additional force on the nuclei due to the electromagnetic field in the form of a Lorentz force:

$$\mathbf{F}_{nuclei} = q(\mathbf{E}(t) + \mathbf{v} \times \mathbf{B}(t)) \quad (2.31)$$

where q represents the charge of the ion core, namely 1 for hydrogen, 4 for carbon and 6 for oxygen.

D. Hellmann-Feynman theorem

A generalized Hellmann-Feynman[29, 30] theorem states[23]:

$$M\partial_t^2\langle\mathbf{X}\rangle = -\left\langle\frac{\partial\mathbf{H}}{\partial X}\right\rangle \quad (2.32)$$

where X and M are any ion's coordinate and mass respectively. In our tight-binding model, we apply the Hellmann-Feynman theorem to simulate the isomerization of the retinal molecule.

The total energy consists of contributions from the one-electron Hamiltonian and the repulsive potential. The electronic energy is

$$E_{electron} = \sum_k n_k \Psi_k^\dagger \cdot \mathbf{H} \cdot \Psi_k \quad (2.33)$$

where n_k represents the occupancy of state k . Applying the classical equations of

motion to the electronic energy we have,

$$\begin{aligned}
M_i \ddot{\mathbf{R}}_i &= - \sum_k n_k \Psi_k^\dagger \cdot \frac{\partial \mathbf{H}(k)}{\partial \mathbf{R}_i} \cdot \Psi_k \\
&\quad - \sum_k n_k \frac{\partial \Psi_k^\dagger}{\partial \mathbf{R}_i} \cdot \mathbf{H}(k) \cdot \Psi_k \\
&\quad - \sum_k n_k \Psi_k^\dagger \cdot \mathbf{H}(k) \cdot \frac{\partial \Psi_k}{\partial \mathbf{R}_i}.
\end{aligned} \tag{2.34}$$

The position of the i^{th} atom is represented by \mathbf{R}_i and its mass by M_i . The above equation can be simplified in the special case that the one-electron states Ψ_k are eigenstates of the Hamiltonian:

$$\mathbf{H} \Psi_k = \varepsilon_k \Psi_k. \tag{2.35}$$

We then follow the usual proof of the Hellmann-Feynman theorem and obtain the following:

$$\begin{aligned}
M_i \ddot{\mathbf{R}}_i &= - \sum_k n_k \Psi_k^\dagger \cdot \frac{\partial \mathbf{H}(k)}{\partial \mathbf{R}_i} \cdot \Psi_k \\
&\quad - \sum_k n_k \frac{\partial \Psi_k^\dagger}{\partial \mathbf{R}_i} \cdot \mathbf{R}_i \cdot \varepsilon_k \Psi_k \\
&\quad - \sum_k n_k \Psi_k^\dagger \cdot \varepsilon_k \cdot \frac{\partial \Psi_k}{\partial \mathbf{R}_i} \\
&= - \sum_k n_k \Psi_k^\dagger \cdot \frac{\partial \mathbf{H}(k)}{\partial \mathbf{R}_i} \cdot \Psi_k \\
&\quad - \sum_k n_k \varepsilon_k \frac{\partial (\Psi_k^\dagger \cdot \Psi_k)}{\partial \mathbf{R}_i}.
\end{aligned} \tag{2.36}$$

The atomic orbitals in our tight-binding scheme are considered to be Löwdin-like or Wannier-like orbitals which are orthogonalized, so there is no overlap matrix. The eigenvectors of the Hermitian matrix H can be taken to be orthonormal:

$$\Psi_k^\dagger \cdot \Psi_{k'} = \delta_{k,k'}. \tag{2.37}$$

The second term in equation(2.36) is then zero, because of the constant normalization as expressed above and the total force on an ion i including the repulsive potential becomes,

$$M_i \ddot{\mathbf{R}}_i = - \sum_k n_k \Psi_k^\dagger \cdot \frac{\partial \mathbf{H}(k)}{\partial \mathbf{R}_i} \cdot \Psi_k - \frac{\partial U_{\text{rep}}}{\partial \mathbf{R}_i}. \quad (2.38)$$

The factor $\partial \mathbf{H}(k)/\partial \mathbf{R}_i$ implies that the derivative of each element in the Hamiltonian matrix must be found with respect to the coordinates of each ion in the molecule. This is called directional cosines, described earlier in section B, and we calculate these according to the position of the element in an orbital, namely s or p . The repulsive potential U_{rep} is of the form,

$$U_{\text{rep}} = \sum_i \sum_{j(j>i)} f(R_{ij}). \quad (2.39)$$

The above repulsive potential can be fitted to the repulsive potential of Harrison[31] and co-workers[32] and Sankey[33] as follows:

$$U_{\text{rep}} = \frac{C}{R^4}. \quad (2.40)$$

In the above equation, C is a constant for a particular pair of ions which has to be determined. The determination of the constant C is discussed in Chapter III. Thus using Hellmann-Feynman equations we should be able to find out the electronic forces on the individual ions and from there, we use velocity Verlet algorithm, to find the position of the atoms as a function of time. The new configuration gives the new positions of the individual atoms and after the appropriate time, we find that the original molecule has isomerized to the new form.

E. Cayley Algorithm to Solve the Schrödinger Equation

We next use the effective Hamiltonian, as described in equation (2.29), in the time-dependent Schrödinger equation and solve for the response of the system to the radiation field:

$$i\hbar \frac{\partial \Psi_k}{\partial t} = \mathbf{H}(t) \Psi_k. \quad (2.41)$$

The time step Δt in the simulation must be considerably smaller than the characteristic time scale for the dynamics, which is about 200 fs.

In order to solve the above equation, if we use the conventional solution we get,

$$\Psi_k(t + \Delta t) = \left(1 - \frac{i}{\hbar} \mathbf{H}(t) \Delta t\right) \Psi_k(t) \quad (2.42)$$

which does not conserve probability. Hence, we need a solution which will conserve the norm of the eigenvectors:

$$\Psi_k^\dagger \cdot \Psi_{k'} = \delta_{k,k'}. \quad (2.43)$$

We consider a solution of the form:

$$\Psi_k(t + \Delta t) = \exp^{-i\mathbf{H}(t)\Delta t/\hbar} \Psi_k(t). \quad (2.44)$$

We apply a Cayley algorithm technique[22], where we split the exponential term,

$$\begin{aligned} \exp^{-i\Delta} &= \exp^{-i\Delta/2} \exp^{-i\Delta/2} \\ &= \frac{\exp^{-i\Delta/2}}{\exp^{i\Delta/2}} \\ &\simeq \frac{1 - i\Delta/2}{1 + i\Delta/2} \end{aligned} \quad (2.45)$$

where we have approximated the exponential by keeping only its first two terms. We

apply similar splitting technique to the solution of the Schrödinger equation to get,

$$\begin{aligned}
\Psi_k(t + \Delta t) &= \exp\left(\frac{-i\mathbf{H}\Delta t}{\hbar}\right) \Psi_k(t) \\
&= \exp\left(\frac{-i\mathbf{H}\Delta t}{2\hbar}\right) \exp\left(\frac{-i\mathbf{H}\Delta t}{2\hbar}\right) \Psi_k(t) \\
&= \frac{\exp\left(\frac{-i\mathbf{H}\Delta t}{2\hbar}\right)}{\exp\left(\frac{i\mathbf{H}\Delta t}{2\hbar}\right)} \Psi_k(t) \\
&= \frac{(\mathbf{1} - \frac{i\mathbf{H}\Delta t}{2\hbar})}{(\mathbf{1} + \frac{i\mathbf{H}\Delta t}{2\hbar})} \cdot \Psi_k(t).
\end{aligned} \tag{2.46}$$

This gives the final form of the solution as,

$$\Psi_k(t + \Delta t) = (\mathbf{1} + \frac{i\mathbf{H}\Delta t}{2\hbar})^{-1} \cdot (\mathbf{1} - \frac{i\mathbf{H}\Delta t}{2\hbar}) \cdot \Psi_k(t). \tag{2.47}$$

Thus, using a form of the solution as in equation(2.47), we find that both probability and orthogonality are preserved. The algorithm described above is good to $O(\Delta t)^2$. Higher order precision in the time step Δt were deemed not necessary in the current calculations since it would have been more expensive computationally.

F. Hellmann-Feynman Theorem for Non-Adiabatic Processes

The equations we have described so far, have been considered in an adiabatic system. We have assumed that the force calculations from the Hellmann-Feynman theorem is valid for both ground and excited states. Initially, we consider the state vector of the system to be an eigenstate of the Hamiltonian. However, when we propagate the state vector over time, it does not remain an eigenstate of the Hamiltonian.

Even though the state vector is not an eigenstate of the Hamiltonian, Hellmann-Feynman theorem is still applicable. We employ the Ehrenfest's theorem[34],

$$\frac{d}{dt}\langle \mathbf{p} \rangle = -\langle \nabla V \rangle \tag{2.48}$$

which describes the relation between classical and quantum dynamics. The above

equation expressed as expectation values in quantum mechanical form becomes classical without the brackets. The classical form then simply gives the equation for the force on the nuclei. Thus we see that we can apply our general method in non-adiabatic systems as well.

Therefore, we find that using an orthogonal tight-binding electron-ion dynamics approach, we can effectively describe the isomerization of the retinal molecule. The method has been successfully used in semiconductors, e.g., silicon and gallium arsenide[22] and in some biological molecules like chlorophyll[21].

CHAPTER III

NUMERICAL METHODS

In order to employ the tight-binding technique described in the previous chapter, we employ various numerical methods, the first of which was to do the modeling starting from the equilibrium geometry for the molecule. We describe in the following section how we obtained the optimized geometry for each molecule.

A. Geometry Optimization

The first step in creating the tight-binding model is to start with a stationary point for the molecules. The objective therefore is to find a local minimum in the total energy U of the system in the neighborhood of an initially assumed geometry. The process of finding the minimum in the energy is known as geometry optimization. For our current work, we started with an initial coordinate structure for all the molecules, namely, ethylene, 2-butene, stilbene and retinal[35]. Thereafter, the task was to obtain the equilibrium geometry which would stabilize the molecule in the context of the current tight-binding model. In the beginning, a brute-force method was applied where the atoms in the molecule were initially at rest and they were allowed to propagate over time. The atoms moved randomly and at each time step their velocities were cut down by about 1-2%. The process was carried on until the global minimum in the energy was attained. This method was quite efficient for the test molecules ethylene and 2-butene. However for the 26-atom stilbene and 49-atom retinal molecule, this was a time-consuming effort and we needed to find a more efficient numerical method to get the equilibrium coordinate geometry for the larger molecules.

In order to stabilize the molecules, the conjugate gradient method was found to

be the most appropriate to reach the global minimum[36]. In this method, we first calculated the total energy U_1 and the derivative of the energy ∇U_1 at the initially assumed geometry. The vector ∇U_1 points in the direction of greatest rate of increase in U_1 . In the conjugate gradient method each search step is in the direction of $-\nabla U_1$. This direction is perpendicular to the contour surface of constant U_1 that goes through point 1. The size of the step is determined by a line search. We can summarize the conjugate gradient steps as follows:

$$q_2 = q_1 - \lambda_1 \nabla U_1. \quad (3.1)$$

In the above equation, λ_1 is found from a line search. The direction of each subsequent step k is defined by a vector d_k (where $k = 1, 2, 3, \dots$) that is a linear combination of the negative gradient $-\nabla U_k$ and the preceding direction. We can summarize the method in the following set of equations:

$$\begin{aligned} q_{k+1} &= q_k + \lambda_k d_k, \\ d_1 &= -\nabla U_1, \\ d_k &= -\nabla U_k + \beta_k d_{k-1} \quad k > 1. \end{aligned} \quad (3.2)$$

The constant λ_k is found by a line search that minimizes U in the direction of d_k . In the Fletcher-Reeves version of the conjugate-gradient method, β_k is calculated from the formula:

$$\beta_k = \frac{\nabla U_k \cdot \nabla U_k}{\nabla U_{k-1} \cdot \nabla U_{k-1}}. \quad (3.3)$$

For the present purposes, the conjugate gradient method worked quite well and it took only a few iterations to stabilize all the molecules. However, to ensure that we have found the minimum in the energy and not a saddle point, it was necessary to test the nature of the stationary point found by the geometry optimization. This

was accomplished by performing vibrational frequency calculations at the minimum geometry. For a true minimum stationary point, all the frequencies would be real, whereas at the saddle point, one calculated frequency would be imaginary.

We assume an N -atom molecule and use internal coordinates with a fixed center of mass. This gives us $3N-6$ degrees of freedom since the energy of the system is invariant with respect to translation of the center of mass and rotation of the molecule. In order to calculate these frequencies, we first calculate the Hessian matrix which is described in the next section.

B. Calculating the Hessian Matrix and the Vibrational Frequencies

The quantity U' represents the first-order value of the energy which is simply the force within the molecule. The calculation of the second-order U'' which is known as the Hessian matrix, is a little more complicated. Using a treatment from force considerations, it is calculated as follows:

$$\begin{aligned} U''(\mathbf{r}) &= \frac{\partial U'(\mathbf{r})}{\partial \mathbf{r}} \\ &= \frac{U'(\mathbf{r} + \Delta \mathbf{r}) - U'(\mathbf{r})}{\Delta \mathbf{r}} \end{aligned} \quad (3.4)$$

where $U'(\mathbf{r} + \Delta \mathbf{r})$ is the value of the force calculated by incrementing each of the coordinates of every atom by a value of $\Delta \mathbf{r} = 0.0000001$ au. For instance, in the case of test molecule ethylene, there are six atoms each with three coordinates. These were treated as generalized coordinates and each independently incremented in order to obtain an (18×18) U' matrix. The value of each of the $U'(\mathbf{r}_i + \Delta \mathbf{r}_i)$ terms were calculated by incrementing the 18 elements of the argument one at a time and calculating U' at every instant. In the case of retinal, this is a (147×147) -dimensional matrix.

We next used the Hessian matrix to find the vibrational energies in the system to ensure that we have the true minimum in energy at the optimized geometry which we describe in the following section.

1. Obtaining vibrational frequencies using force-constant techniques

We use geometry optimization to obtain a quantum-mechanical estimate of the molecular energy U evaluated at a local minimum, and a conformational search[36] yields an estimate of the global energy minimum.

The Schrödinger equation for nuclear motion in a molecule is,

$$H_n \Psi_n = (T_n + V_{nn} + E_e) \Psi_n = E \Psi_n. \quad (3.5)$$

The energy U can be written as $U = V_{nn} + E_e$.

The total molecular energy E is approximately the sum of translational, rotational, vibrational and electronic energies. In the harmonic-oscillator approximation, the vibrational energy of an N -atom molecule is the sum of $3N-6$ normal-mode vibrational energies ($3N-5$ for a linear molecule, e. g., hydrogen):

$$E_{\text{vib}} \sim \sum_{k=1}^{3N-6} \left(n_k + \frac{1}{2} \right) h\nu_k \quad (3.6)$$

where ν_k is the harmonic (or equilibrium) vibrational frequency for the k th normal mode and each vibrational quantum number n has the possible values of 0, 1, 2, ..., independent of the values of the other vibrational quantum numbers. For the ground vibrational state, each of the $3N-6$ vibrational quantum numbers equals zero, and the zero-point energy in the harmonic-oscillator approximation is,

$$E_{ZPE} = \sum_{k=1}^{3N-6} \frac{h\nu_k}{2}. \quad (3.7)$$

The electronic Schrödinger equation is solved for several molecular geometries to find the equilibrium geometry of the molecule. Then, the set of second derivatives ($\partial^2 U / \partial X_i \partial X_j$) of the molecular electronic energy U with respect to the $3N$ nuclear Cartesian coordinates of a coordinate system with the origin at the center of mass, where these derivatives are evaluated at the equilibrium geometry. From the mass-weighted force-constant (or mass-weighted Hessian) matrix elements,

$$F_{ij} = \frac{1}{(m_i m_j)^{1/2}} \frac{\partial^2 U}{\partial X_i \partial X_j} \quad (3.8)$$

where i and j each go from 1 to $3N$ and m_i is the mass of the atom corresponding to coordinate X_i . Solution of the $3N$ linear equations in $3N$ unknowns yields

$$\sum_{j=1}^{3N} (F_{ij} - \delta_{ij} \lambda_k) l_{jk} = 0, \quad i = 1, 2, \dots, 3N. \quad (3.9)$$

In this set of equations (3.9), δ_{ij} is the Kronecker delta. In order that this set of homogeneous equations have a nontrivial solution, the coefficient determinant must vanish,

$$\det(F_{ij} - \delta_{ij} \lambda_k) = 0. \quad (3.10)$$

This determinant is of order $3N$ and when expanded gives a polynomial whose highest power of λ_k is λ_k^{3N} , so the determinant (secular) equation will yield $3N$ roots for λ_k .

The molecular harmonic vibrational frequencies are then calculated from

$$\nu_k = \frac{\lambda_k^{1/2}}{2\pi}. \quad (3.11)$$

Six of the λ_k values found should be zero, yielding six frequencies with value zero, corresponding to the three translational and three rotational degrees of freedom of the molecule. However, since the equilibrium geometry cannot be found with infinite accuracy, the six vibrational frequencies found had values close to zero. The

remaining $3N-6$ vibrational frequencies are the molecular vibrational frequencies.

The accuracies of the calculated vibrational frequencies were estimated by computing the frequencies independently using a standard Chemistry software package Gaussian[37]. The results are discussed in the following chapter. For ethylene we were able to compare the frequencies with those obtained from experimental measurements.

2. Obtaining vibrational frequencies using Fourier-transform techniques

We also employed the Fourier-transform method in order to find the vibrational frequencies within the molecule. We looked at the bondlengths between two neighboring pairs of atoms at the stable geometry. From the dynamics of the bondlengths over time, we were able to extract the vibrational frequencies.

A physical process[38] can be either described in the *time domain*, by the value of some quantity h (in this case, bondlength) as a function of time t , e. g., $h(t)$, or else in the *frequency domain*, where the process is specified by giving its amplitude H as a function of frequency f , that is $H(f)$, with $-\infty < f < \infty$. We can then represent the *Fourier Transform* equations as,

$$\begin{aligned} H(f) &= \int_{-\infty}^{\infty} h(t) \exp^{2\pi i f t} dt \\ h(t) &= \int_{-\infty}^{\infty} H(f) \exp^{-2\pi i f t} df. \end{aligned} \quad (3.12)$$

In our calculations, t was measured in fs and the frequencies are in units of cm^{-1} . The bondlengths were measured in units of Å.

C. Velocity-Verlet Algorithm

In this section we discuss the different techniques we used in order to perform numerical calculations in our model. One such method is the velocity-Verlet algorithm, which is a classical method involving simple equations to propagate the atoms forward in time.

The finite difference method for Newton's equations of motion with continuous force functions was used in the calculations. We consider the motion of the particles in three dimensions and write Newton's equations of motion in the form[20]:

$$\frac{\partial \mathbf{v}}{\partial t} = \mathbf{a}, \quad (3.13)$$

and

$$\frac{\partial \mathbf{r}}{\partial t} = \mathbf{v}. \quad (3.14)$$

The object of all finite difference methods is to determine the values of \mathbf{r}_{n+1} , \mathbf{v}_{n+1} at time $t_{n+1} = t_n + \Delta t$. The value of Δt should be chosen such that the integration method generates a stable solution. A value of Δt which is too large will result in nonconservation of total energy and unstable solutions for \mathbf{r}_{n+1} and \mathbf{v}_{n+1} , i.e., numerical solutions whose departure from the true solution increases with time. On the other hand, if we use small values for Δt , the calculations become excessively long due to the many steps required to integrate a given final time.

The velocity-Verlet algorithm[39] is described in the following equations:

$$\begin{aligned} \mathbf{r}_i(t + \Delta t) &= \mathbf{r}_i(t) + \dot{\mathbf{r}}_i(t)\Delta t + \frac{1}{2}\ddot{\mathbf{r}}_i(t)\Delta t^2, \\ \dot{\mathbf{r}}_i(t + \Delta t) &= \dot{\mathbf{r}}_i(t) + \frac{1}{2}[\ddot{\mathbf{r}}_i(t + \Delta t) + \ddot{\mathbf{r}}_i(t)]\Delta t. \end{aligned} \quad (3.15)$$

The time step is denoted by Δt . The atomic vibrations are on a time scale[40, 41] of approximately 100 fs, so a shorter time step is required. For the atomic motion, a

time step of about 2 fs was sufficient to conserve energy to one part in 10^6 during the simulation with the Hellmann-Feynman techniques. However, when the electronic dynamics and the effect of the time-dependent electromagnetic field are included, a much shorter time step of about 0.05 fs was required to conserve energy to one part in 10^5 . Hence, we used a time-step value of 0.05 fs for our calculations.

Another good option would have been to use the ordinary Verlet algorithm:

$$\mathbf{r}_i(t + \Delta t) = 2\mathbf{r}_i(t) - \mathbf{r}_i(t - \Delta t) + \ddot{\mathbf{r}}_i(t)\Delta t^2. \quad (3.16)$$

This has been used effectively in other calculations, but numerically the velocity-Verlet algorithm gives less round-off errors. The velocity-Verlet method is also self-starting as opposed to the ordinary-Verlet algorithm which requires another method to advance from $t=0$ to $t=0+\Delta t$. However, both the algorithms guarantee conservation of phase space.

D. Determining the Constants for the Repulsive Potential

As derived in Chapter II, the total force acting on an ion i due to its nearest neighbors is given by,

$$M_i \ddot{\mathbf{R}}_i = - \sum_k n_k \Psi_k^\dagger \cdot \frac{\partial \mathbf{H}(k)}{\partial \mathbf{R}_i} \cdot \Psi_k - \frac{\partial U_{\text{rep}}}{\partial \mathbf{R}_i}. \quad (3.17)$$

In the above equation, U_{rep} represents the repulsive potential term. In a one-electron picture, the total energy is given by a sum of three terms which the sum of the one-electron energy eigenvalues which are determined by the Hamiltonian of the problem, the ion-ion repulsion and the negative of the electron-electron interaction which is doubly counted in the sum of the one-electron energies as explained in

Chapter II. The first term denotes the attraction interaction between the participating atoms, because as the atoms come closer together, the occupied bonding states drop in energy while the unoccupied antibonding states rise. The sum of the last two terms, on the other hand, gives rise to a repulsive interaction. This is referred to as U_{rep} . We model U_{rep} as the sum over repulsive two-body potentials $U(R_{ij})$:

$$U_{\text{rep}} = \sum_{i < j} U(R_{ij}). \quad (3.18)$$

The distance between atoms i and j is denoted by R_{ij} . The above sum is over all the pairs of atoms.

The form of the potential that was used for our calculations is,

$$U(\mathbf{r}) = \frac{C}{R^4} \quad (3.19)$$

where $R = R_{ij}$ and C is an adjustable parameter. The fourth power of the distance was found reasonable in previous work[42] and hence was used in the present calculations.

To determine the constant C , we begin the calculations without any time-dependent electromagnetic field. The test molecule used first was hydrogen. Initially, using the value of C as 1, both the electronic and repulsive forces were calculated on each hydrogen atom. The form of the repulsive force is as follows:

$$F_{\text{rep}} = -\frac{\partial U_{\text{rep}}}{\partial R},$$

where,

$$U_{\text{rep}} = \frac{C}{R^4}.$$

Therefore,

$$F_{\text{rep}} = -\frac{4C}{R^5}. \quad (3.20)$$

In the absence of an external electromagnetic field and under equilibrium conditions, the electronic and the repulsive force components should be equal in magnitude. Hence, once the electronic part was calculated, the repulsive form of the force was equated to the value of the electronic part and the value of C was determined. This method was used for all other possible pairs and the values of the constant C for all of the pairs of bonds are listed in the following table.

In order to find the value of C , for Carbon-Carbon double bond and Carbon-Hydrogen single bond, the simplest molecule with such bonds was ethylene (C_2H_4). To calculate the value of C for Carbon-Oxygen double bond, carbon-dioxide (CO_2) was used.

Table II. Values of the constant C in the form of the potential: $U_{\text{rep}} = C/R^4$.

Type of Bond	Value of C (in units of $[eV][\text{\AA}]^4$)
Carbon-Carbon	52.399971
Carbon-Hydrogen	16.927891
Carbon-Oxygen	41.576265

E. Population Analysis to Determine the Highest Occupied Molecular Orbital (HOMO) and the Lowest Unoccupied Molecular Orbital (LUMO)

A widely used method to analyze SCF wave functions is the population analysis of the molecular orbitals[36], introduced by Mulliken. He proposed a technique whereby each electron in an n -electron system is assigned a net population n_r in the basis functions χ_r and overlap population of n_{r-s} for all possible pairs of basis functions.

Each molecular orbital ϕ_i comprises a set of basis functions $\chi_1, \chi_2, \dots, \chi_r$ as

follows:

$$\phi_i = \sum_s c_{si} \chi_s = c_{1i} \chi_1 + c_{2i} \chi_2 + \cdots + c_{ri} \chi_r. \quad (3.21)$$

In the above equation, we assume that the coefficients c_{ri} and the basis functions χ_r are real.

The probability density of electron i then becomes:

$$|\phi_i|^2 = c_{1i}^2 \chi_1^2 + c_{2i}^2 \chi_2^2 + \cdots + 2c_{1i}c_{2i} \chi_1 \chi_2 + 2c_{1i}c_{3i} \chi_1 \chi_3 + 2c_{2i}c_{3i} \chi_2 \chi_3 + \cdots \quad (3.22)$$

where ϕ_i and the χ_s are normalized. Integrating the above equation we get,

$$1 = c_{1i}^2 + c_{2i}^2 + \cdots + 2c_{1i}c_{2i}S_{12} + 2c_{1i}c_{3i}S_{13} + 2c_{2i}c_{3i}S_{23} + \cdots \quad (3.23)$$

In the above equation the S s are the overlap integrals:

$$S_{12} = \int \chi_1 \chi_2 dv_1 dv_2. \quad (3.24)$$

According to Mulliken, an electron contributes c_{1i}^2 to the net population in χ_1 , c_{2i}^2 to the net population in χ_2 etc., and $2c_{1i}c_{2i}S_{12}$ to the overlap between χ_1 and χ_2 .

Therefore, for n_i electrons in the molecular orbital ϕ_i ,

$$\begin{aligned} n_{r,i} &= n_i c_{ri}^2 \\ n_{r-s,i} &= n_i (2c_{ri}c_{si}S_{rs}) \end{aligned} \quad (3.25)$$

where, $n_{r,i}$ denotes the contributions of the electrons in the molecular orbital ϕ_i to the net population of the basis function χ_r and $n_{r-s,i}$ is the overlap population between χ_r and χ_s respectively. In the current application of this population analysis method, we have taken the overlap matrix S to be the unit matrix, which is consistent with the treatment of the overlap terms in the construction of the Hamiltonian.

Summing over all the orbitals we get the final form of the net population n_r in

χ_r and the overlap population $n_{r-s,i}$ between χ_r and χ_s as:

$$\begin{aligned} n_r &= \sum_i n_{r,i} \\ n_{r-s} &= \sum_i n_{r-s,i}. \end{aligned} \tag{3.26}$$

The population analysis technique was used to determine which orbitals corresponded to the π and π^* orbitals that were involved in the excitation of interest, which for the small systems corresponded to the highest occupied molecular orbital (HOMO) and the lowest unoccupied molecular orbital (LUMO). In the case of stilbene the calculation was more complicated since there was mixing between the σ and π states. However, from the population analysis, it was still possible to determine the localized occupied π and the unoccupied π^* based on the highest population value. For retinal however, the calculation seemed even more complex since retinal has 49 atoms and there were many combinations of the mixing between the σ and π states. In this case, we had to consider several states near in energy to the π and the π^* orbitals of interest and look at the individual atomic orbital population contributions to each of the π states.

We also used the concept of population analysis to plot the positions of the atoms and the orbitals to calculate in which direction to shine the light to break the double bond and make the molecule rotate from the *cis* to the *trans* form. For a small molecule like ethylene with six atoms, we examined the population density of the highest occupied molecular orbital (HOMO) and the lowest occupied molecular orbital (LUMO) to help determine π and the π^* orbitals. Examining the values of the orbital expansion coefficients, we know where the bonding becomes anti-bonding and hence we shine the photons in that direction. However, for a relatively larger molecule, like retinal, it is harder to determine in which direction to shine the light.

Instead of using a trial and error method to find which is the right direction, we find it by looking at the orbital coefficients.

CHAPTER IV

RESULTS FOR TEST MOLECULES

We conducted several tests of the tight-binding method with the smaller molecules ethylene, 2-butene and stilbene. These molecules were chosen since they have similar kind of carbon-carbon double bond as in retinal. These molecules gave us the opportunity to compare results using the current model with published experimental and theoretical results in order to prove the validity of our model.

A. Results for the Ethylene Molecule

The structure of the ethylene molecule is represented in the Figure 3.

1. Molecular dynamics study of *cis-trans* isomerization of ethylene by switching the highest-occupied and lowest-unoccupied molecular orbitals

In order to study the photoinduced rotation about the C1=C2 double bond of the ethylene molecule we performed several calculations. We also found comparable calculations from the study done by [43]. The authors studied the molecular dynamics of ethylene upon photo-isomerization using non-adiabatic nuclear dynamics known as the full multiple spawning (FMS) method. They observed that the initial motion on the excited state is a stretching of the C1=C2 bond and the photo-isomerization begins within ~ 70 fs of optical excitation.

The authors report that the quenching to the ground electronic state is found to be ultrafast and proceeds from an ionic state via a conical intersection. When ethylene absorbs a photon, an electron is promoted from a bonding π molecular orbital into an antibonding π^* molecular orbital. The ground electronic state of ethylene is planar and stable with respect to twisting of the double bond. However, it is not the case for

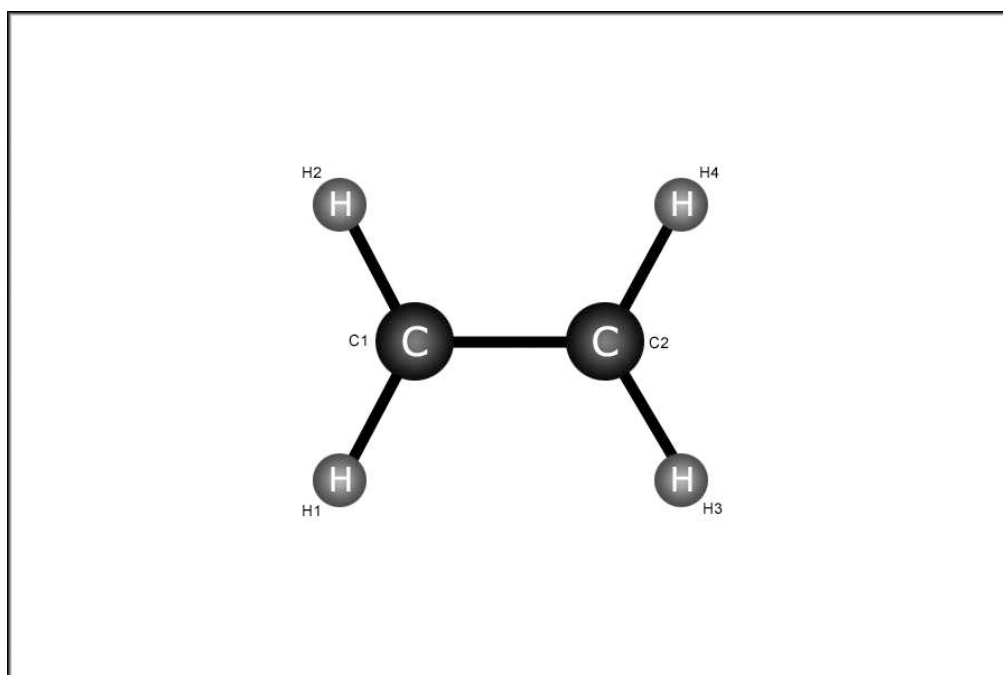


Fig. 3. The ethylene molecule.

the excited states. The electronic redistribution on the excited state favors a twisted geometry because there is no longer any π -bonding to offset the Coulomb repulsion between the p electrons of the two carbon atoms. Hence, the electronic excitation results in the relaxation of the molecule to a twisted geometry. The authors use a split operator procedure (with a time step of 0.25 fs) to propagate the set of coupled nuclear and electronic equations of motion. They report the expectation value of the C1=C2 bond distance over time. They also show results for the H2-C1=C2-H4 dihedral angle as a function of time for the excited electronic state. These results are shown in the following Figure 4.

We did similar calculations for the dihedral angle formed between the planes formed by the two carbons and one of the neighboring hydrogens of each. The authors started the computation with all the population on the singly excited state after the ultrafast excitation from the ground electronic state. They adjusted the initial conditions such that ethylene is instantaneously promoted to the singly excited state from its planar ground state equilibrium geometry. In our effort to obtain similar behavior, we began our calculations by switching the population of the highest occupied molecular orbital, also known as the HOMO (in this case the sixth orbital) and the lowest unoccupied molecular orbital, also known as the LUMO (in this case the seventh orbital). We artificially excited the electrons to a higher excited state and proceeded the calculations without any external electromagnetic field. Due to the limitations of the tight-binding model, we can only excite two electrons at a time since they are coupled together. Therefore, we can never do single excitation of an electron. We let the simulation run for ~ 400 fs and observed that the *cis-trans* torsional motion began ~ 70 fs after the molecule started relaxing from the higher state, which is comparable to the results reported by[43]. This is because the quenching to the ground electronic state occurs only after energy is transferred out of the twisting

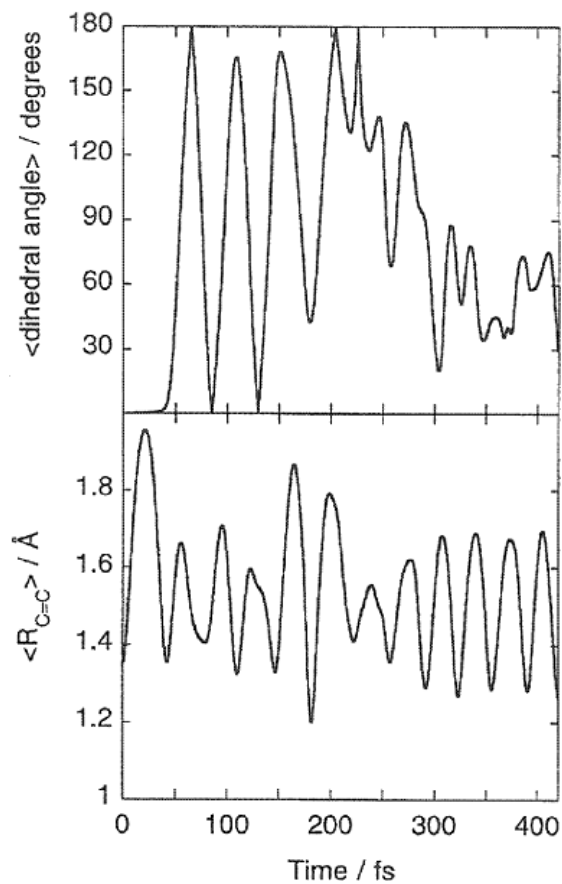


Fig. 4. The H2-C1=C2-H4 dihedral angle on the excited electronic state and the expectation value of the C1=C2 bond distance is plotted as a function of time[43]. The initial motion on the excited state is a stretching of the C1=C2 bond and the *cis-trans* torsional motion begins ~ 70 fs after the excitation. The quenching to the ground electronic state begins only after the energy is transferred out of the twisted coordinate.

coordinate. Results from the present calculations are shown in Figure 5.

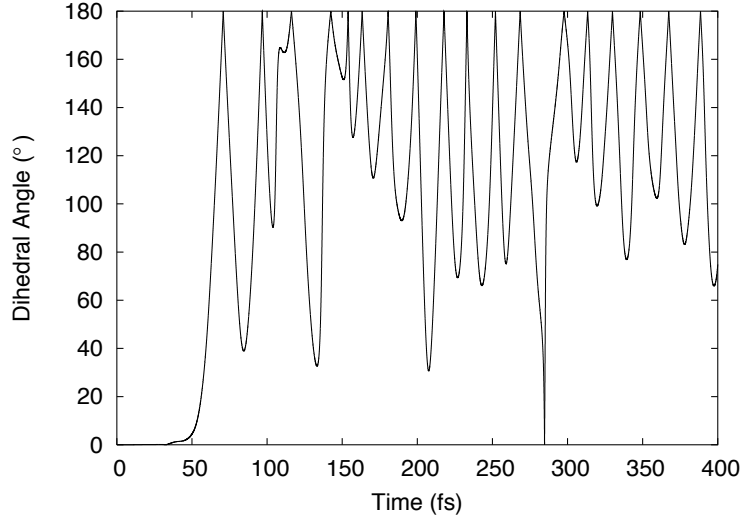


Fig. 5. Excited state-ground state simulation for ethylene. The dihedral angle measurements are from H2-C1=C2-H4 plane. The HOMO and the LUMO are switched and the dynamics of the dihedral angle is measured with respect to time. The isomerization of ethylene from *cis-trans* form starts ~ 70 fs after the beginning of the excitation.

We next look at the C1=C2 bond distance and observe how it changes over a period of 400 fs while the HOMO and the LUMO were switched. The results are reported in Figure 6.

From Figures 4, 5 and 6 we can conclude that the results from the work by Ben-Nun *et al.*[43] and our current method are comparable and therefore establish the validity of our model. We next look at the dynamics of the ethylene molecule, first without any application of an external field and then apply light to monitor the photo-isomerization. The results are reported in the following section.

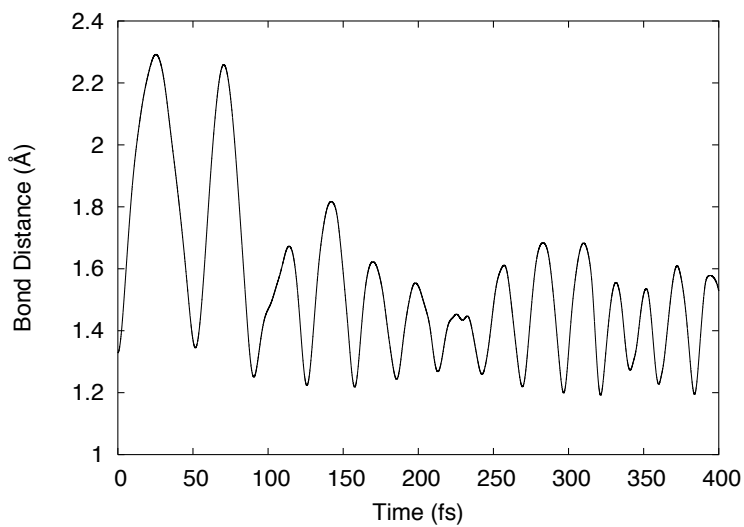


Fig. 6. Excited state-ground state simulation for ethylene. The bond distance measurements between the carbon atoms are plotted. The HOMO and the LUMO are switched and the dynamics of the C1=C2 bond distance is measured with respect to time without any external field.

2. Results for the dynamics of the ethylene molecule without the application of an external field

In the course of the dynamics in the ethylene molecule, we monitored several properties of the entire molecular system. Our first calculation involved testing the molecular dynamics without any field. This gave us an opportunity to investigate and compare the dynamics when the field was applied later. In addition, calculations involving no field were later used to determine some valuable properties like vibrational frequencies from the motion of the bond distance between the two carbon atoms. We also observed how the eigenvalues behaved over time. We monitored several other properties like velocities and dihedral angles but these didn't change without an external field and hence would not provide us with interesting information.

In the absence of an external field, (amplitude $A_0 = 0.00$ gauss-cm), the eigenvalues are listed in the following histogram plot given in Figure 7. The actual values are listed later in Appendix B.

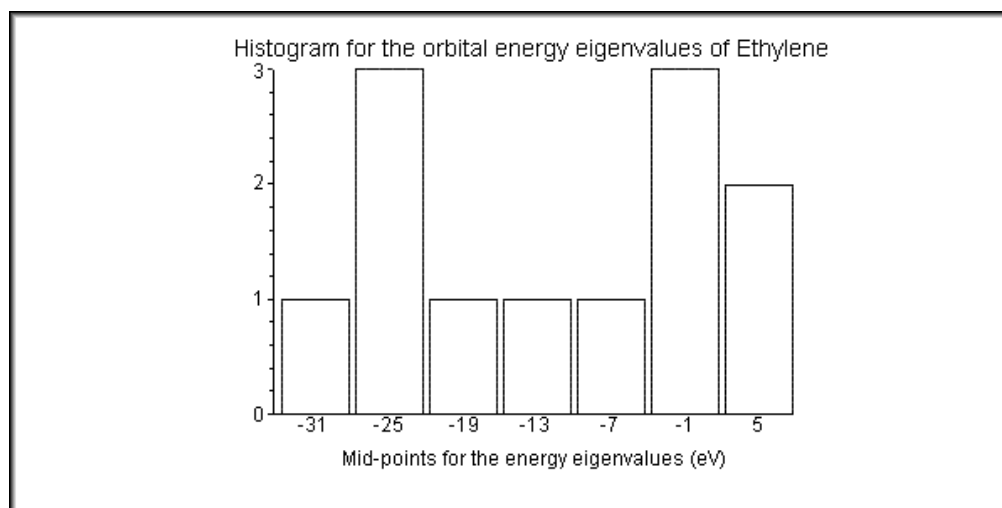


Fig. 7. The histogram shows a distribution of the molecular orbital energy eigenvalues of ethylene without the application of an electro-magnetic field.

We next looked at how the C=C bond distance develops over time in Figure 8. Since there is no external applied field, we expect the bond distance to be unchanged. We use this information to find the vibrational frequencies within the molecule. These results are reported later in Section E.

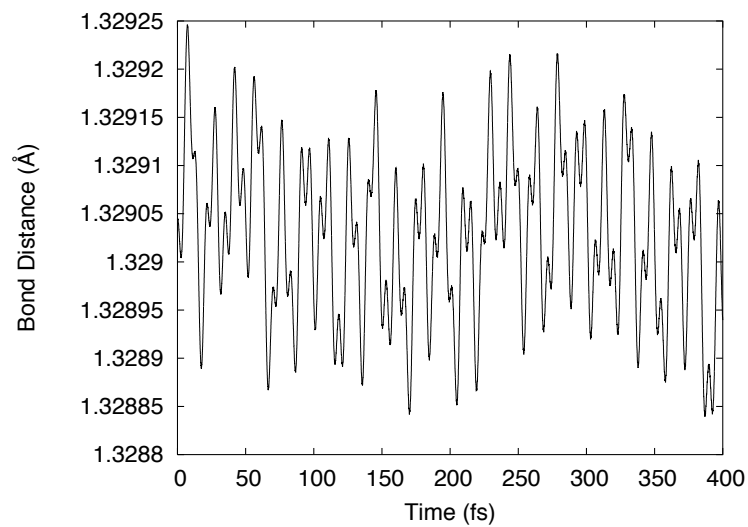


Fig. 8. The C1=C2 bond distance is plotted over time for ethylene molecule with no external field applied. The time step $\Delta t = 0.005$ fs.

3. Results for the photo-isomerization of the ethylene molecule with the application of an electro-magnetic field

We next applied an electro-magnetic field with a vector potential described in Chapter II. First, the wavelength of the light was determined from the energy eigenvalue of the highest occupied molecular orbital (HOMO) and the lowest unoccupied molecular orbital (LUMO). The difference between the energies of the HOMO and the LUMO is the minimum energy required for the electron to jump to the next highest orbital

during the isomerization. For ethylene,

$$\begin{aligned}\Delta E &= E_7 - E_6 \\ &= (-6.2522037064692 \text{ eV}) - (-11.687796386013 \text{ eV}) \\ &= 5.436 \text{ eV}\end{aligned}\tag{4.1}$$

$$\begin{aligned}\lambda &= \frac{hc}{\Delta E} \\ &= 228.094 \text{ nm}\end{aligned}\tag{4.2}$$

The strength of the field denoted by the amplitude A . The most common measure of pulse intensity used by experimental groups is the fluence[44],[45], [46]. Fluence is defined as the number of particles that intersect a unit area. In particular, it is used to describe the strength of a radiation field. From the calculations in Appendix A from Graves[20], the relationship between the fluence F and the amplitude of the field A is as follows:

$$F[\text{kJ/m}^2] = 0.815(A_0[\text{gauss} \cdot \text{cm}])^2.\tag{4.3}$$

Graves[20] also points out that for semiconductors, a fluence value more than 3.26 kJ/m² (corresponding $A=2.00$ gauss·cm) starts dissociating the crystalline structure. The sun's UV-B rays correspond to 7.5 kJ/m² at 300 nm, which makes A equal to 3.03 gauss·cm and a value of 8.0 kJ/m² for UV-R rays give a value of 3.13 gauss·cm for A . These are both harmful for the retina. In this case of organic molecules, we decided to use similar values for A as used for semiconductors[20] and found that in most cases if A was increased more than 2.00 gauss·cm, the molecule started to disintegrate.

In this current calculation, we begin with a value for A equal to 0.5 gauss·cm. The electro-magnetic field in the form of light was on for a period of 400 fs. The results are shown in the following figures. In Figure 9, the energy eigenvalues are plotted

over time. The plot shows a distinct avoided crossing region between the HOMO (the sixth eigenvalue) and the LUMO (the seventh eigenvalue). This is a region where the eigenvalues do not cross but intersect at one point only. This point is called the eigenvalue locus. In this region a drastic change of some characteristic occurs along the eigenvalue locus. In our case, this is where the electrons after absorbing enough energy jump from the HOMO to the LUMO thereby executing the π to the π^* excitation.

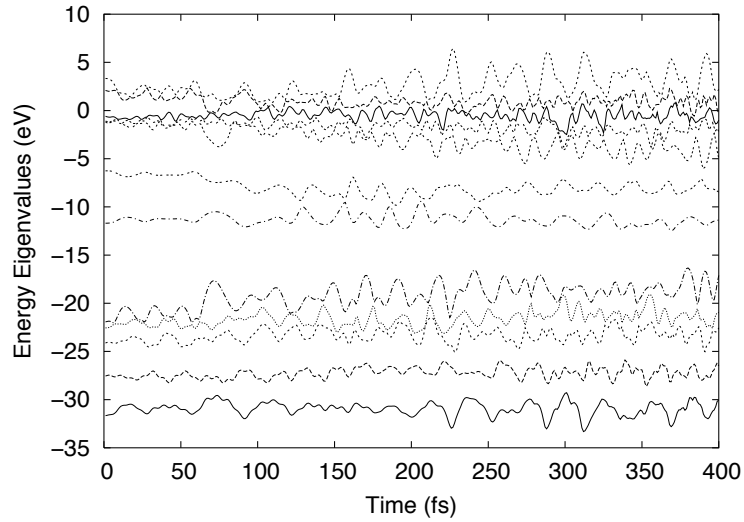


Fig. 9. The energy eigenvalues for ethylene molecule are plotted over time. The time step is $\Delta t = 0.005$ fs, the amplitude of the vector potential is $A = 0.5$ gauss-cm and the wavelength of the light is $\lambda = 228.094$ nm.

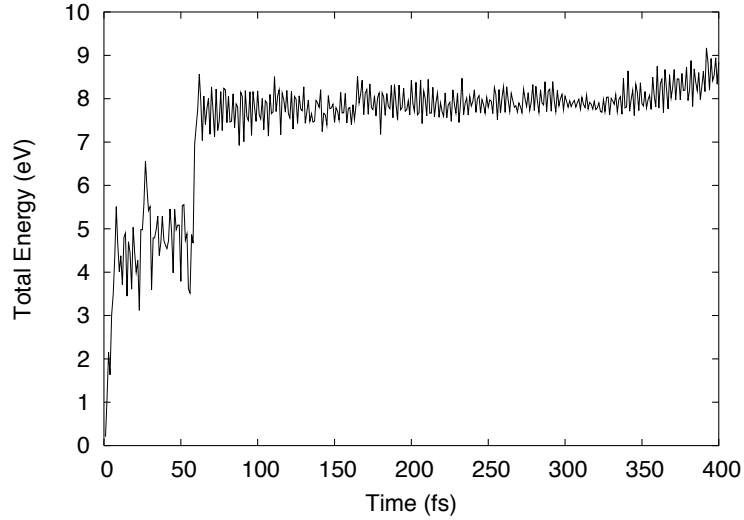


Fig. 10. The total energy for ethylene molecule is plotted over time. The time step is $\Delta t = 0.005$ fs, amplitude of the vector potential is $A = 0.5$ gauss·cm and the wavelength of the light is $\lambda = 228.094$ nm.

If we look at the energy and the dihedral angle plots in Figures 10 and 11, we find that the molecule absorbs energy very quickly and gets the energy of about 4 eV required to overcome the rotational barrier in about 10 fs. However, it does not actually rotate by 180° until about 140 fs. This result is in agreement with the statement reported in [5] that the entire excited state lifetime of ethylene is predicted to be less than 200 fs. This means that although the system absorbs the desired energy relatively quickly, it still takes longer to overcome the rotational barrier. After that, it continues to absorb energy while rotating back and forth, much like a free rotor. Finally, in the following Figure 12 we plot the Carbon-Carbon bond distance under the influence of light. We find the bondlength stretches up to 1.72\AA , vibrating vigorously about the mean length of 1.32\AA . However, with time the vibration slows down, showing that after an initial absorption of energy, the system starts to resonate

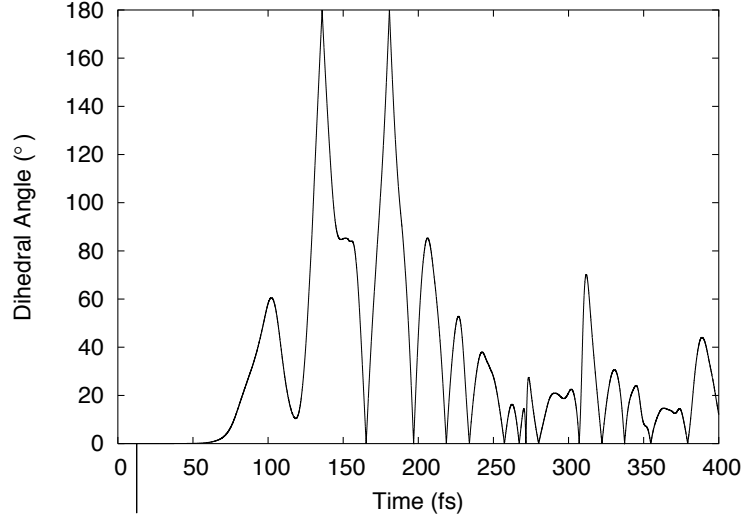


Fig. 11. The dihedral angle H2-C1=C2-H4 for ethylene molecule is plotted over time. The time step is $\Delta t = 0.005$ fs, amplitude of the vector potential is $A = 0.5$ gauss·cm and the wavelength of the light is $\lambda = 228.094$ nm.

with the frequency of the light.

In Figure 12 we find that the bond distance between the two carbon atoms gets bigger (~ 1.8 Å) around 60 fs, exactly at the time when the system absorbs enough energy of 4 eV to overcome the rotational barrier. After that time, the system stabilizes to about 8 eV of energy and the bond length also vibrates more uniformly about the 1.4 Å value. The energy of 4 eV required for the isomerization is in agreement with experimental results as reported in the paper by Quenneville *et al.*[47] which states a value of 4.59 eV[48]. The small discrepancy is due to the limitations of the current model.

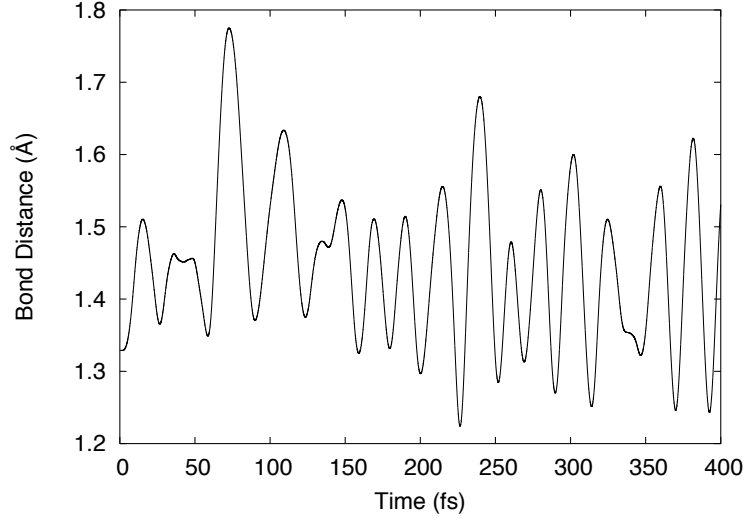


Fig. 12. The C1=C2 bond distance is plotted over time for ethylene molecule with amplitude of the vector potential is $A = 0.5$ gauss·cm and the wavelength of the light is $\lambda = 228.094$ nm The time step $\Delta t = 0.005$ fs.

Once we establish from the earlier plots that the dynamics of the molecule from the *cis* to the *trans* form occurs at a value of $A=0.5$ gauss·cm, wavelength $\lambda = 228.094$ nm and $\Delta t = 0.005$ fs, we next investigate how the dynamics depends on these three factors, namely, the field strength and the wavelength of the electro-magnetic field and the time step of the motion. Result of this study are shown in the following figures. In Figure 13 is shown a comparison of the behavior of the dihedral angle in ethylene as a function of the strength of the vector potential.

We find that the molecule rotates by 180° about the double bond from *cis* to *trans* in about 136 fs for $A = 0.5$ gauss·cm, 84 fs for $A = 1.0$ gauss·cm and 71 fs for $A = 2.0$ gauss·cm respectively. Now to determine which strength gives the correct dynamical behavior, we look at the behavior of the C1=C2 bondlength over time with the same field strengths. The results are shown in Figure 14.

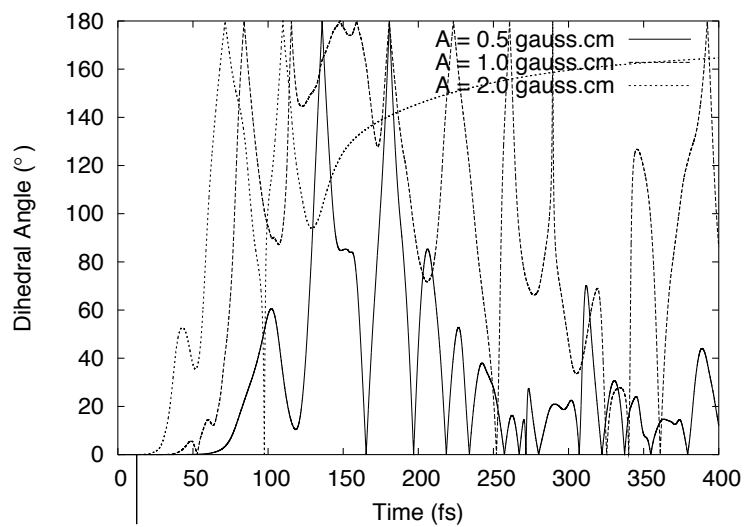


Fig. 13. The dihedral angle is plotted over time for ethylene molecule with amplitude of the vector potential is $A = 0.5, 1.0$ and 2.0 gauss·cm and the wavelength of the light is $\lambda = 228.094$ nm. The time step $\Delta t = 0.005$ fs.

From Figure 14 we clearly see that for $A = 1.0$ gauss·cm and $A = 2.0$ gauss·cm, the bond length becomes increasingly large very quickly and with time becomes 12-13 Å, which is unphysical and hence shows that the molecule has in fact disintegrated. Therefore, the conclusion is that the correct field strength is 0.5 gauss·cm which yields results that are comparable to one found from experiment and other forms of theoretical work.

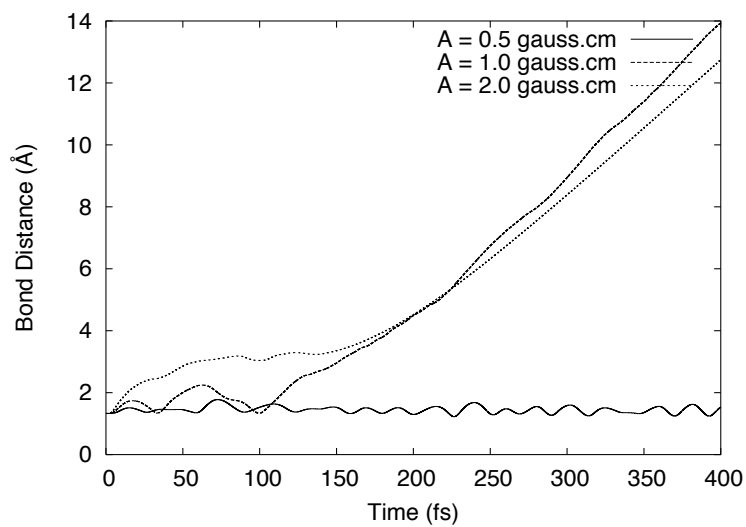


Fig. 14. The C1=C2 bond distance is plotted over time for ethylene molecule with amplitude of the vector potential is $A = 0.5, 1.0$ and 2.0 gauss·cm and the wavelength of the light is $\lambda = 228.094$ nm. The time step $\Delta t = 0.005$ fs.

Next we do some further comparison of the dihedral angle in ethylene for different wavelengths. The results are reported in Figure 15. In this case, a wavelength $\lambda = 228.094$ nm, which is the resonant wavelength allows the C1=C2 bond to turn thereby causing the isomerization under light. However, using half or twice the resonant wavelength doesn't rotate the dihedral angle.

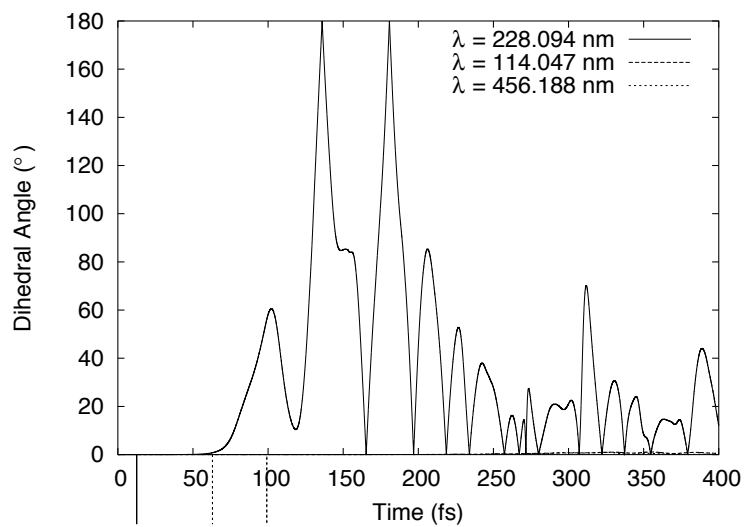


Fig. 15. The dihedral angle is plotted over time for ethylene. The vector potential $A=0.5$ gauss \cdot cm, wavelength $\lambda = 114.047$ nm, 228.094 nm and 456.188 nm and the time step $\Delta t = 0.005$ fs.

Finally, we do the comparison of various time steps in order to find the optimum value for the time step in the dynamics calculations. For smaller molecules like ethylene and 2-butene, a very small time step can be used since the photo-isomerization is obtained within a few minutes of computer time. However it is a matter of few hours of computation for stilbene and days for retinal which is discussed later. Therefore, it is very important to find a time step that is not too large because that will yield inaccurate results, whereas a small time step would make the computation unfeasible. Figures 16 and 17 show the results of different time steps and how the dihedral angle and the C1=C2 bond length behave for each time step. In the dihedral angle plot, we see that as the time step increases from 0.005 fs to 0.01 fs, the time it takes for the molecule to rotate from *cis* to *trans* increases from 136 fs to 173 fs, which is still within the range of < 200 fs as reported from experimental results. However, for a

time step $\Delta t = 0.05$ fs the molecule doesn't rotate by 180° , proving that it is too big for the dynamics. The C1=C2 bondlength seems to produce reasonable results, not going beyond 1.8 \AA . We shall see later that for molecules larger than ethylene, even 0.01 fs is too large to give accurate results.

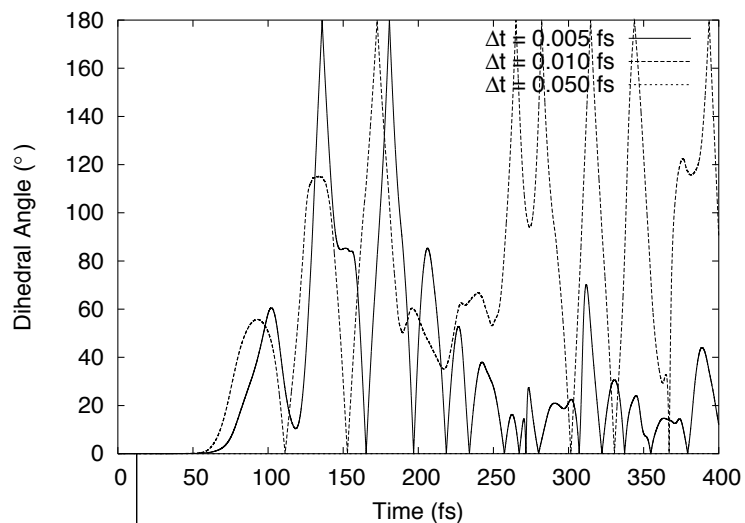


Fig. 16. The dihedral angle is plotted over time for ethylene. The vector potential $A=0.5$ gauss·cm, wavelength $\lambda = 228.094$ nm and the time steps are $\Delta t = 0.005, 0.010$ and 0.050 fs.

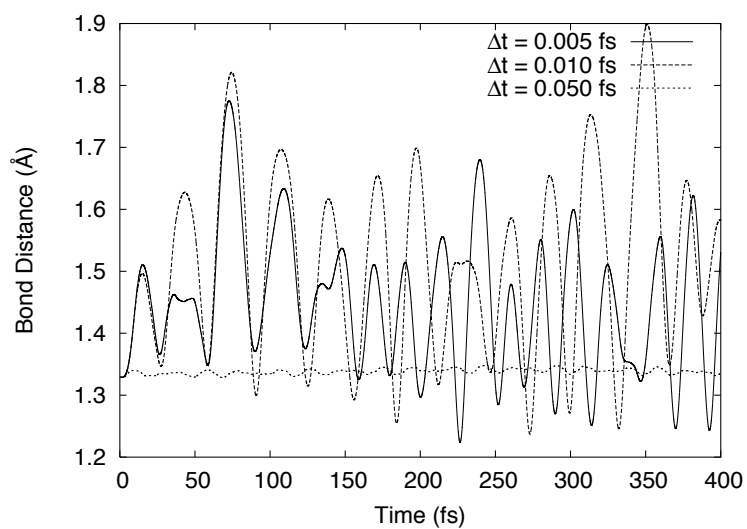


Fig. 17. The C1=C2 bond distance is plotted over time for ethylene molecule with amplitude of the vector potential is $A = 0.5$ gauss·cm and the wavelength of the light is $\lambda = 228.094$ nm. The time step $\Delta t = 0.005, 0.010$ and 0.050 fs.

B. Results for the 2-Butene Molecule

The 2-butene molecule in its *cis* form is represented in the following Figure 18:

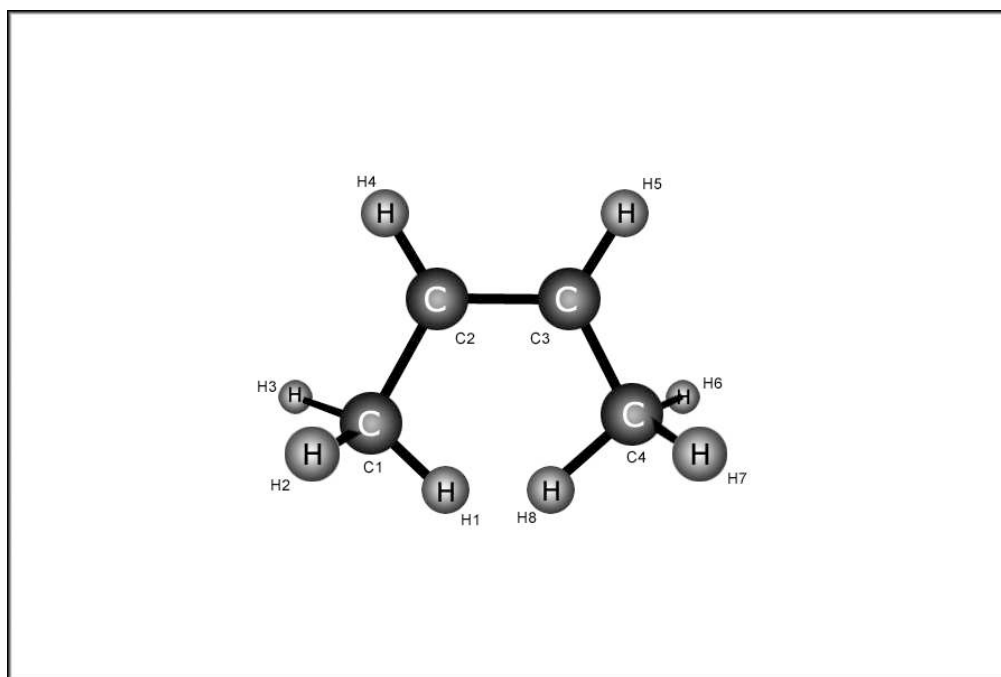


Fig. 18. The 2-butene molecule in its *cis* form.

We did similar tests for the butene molecule as we did for ethylene. The results are shown in the following three subsections.

1. Molecular dynamics study of *cis-trans* isomerization of 2-butene by switching the highest-occupied and lowest-unoccupied molecular orbitals

We studied the dynamics of the 2-butene molecule by switching the HOMO and the LUMO as was done for ethylene. In the case of 2-butene Figure 19 shows that the dihedral angle between H4-C2=C3-H5 takes about 175 fs to twist by 180° compared to 70 fs in ethylene. This is due to the fact that the 2-butene molecule is bigger than ethylene and therefore takes longer time to twist. Figure 20 shows that the C2=C3 bondlength only reaches 2.0 Å as opposed to 2.3 Å in ethylene.

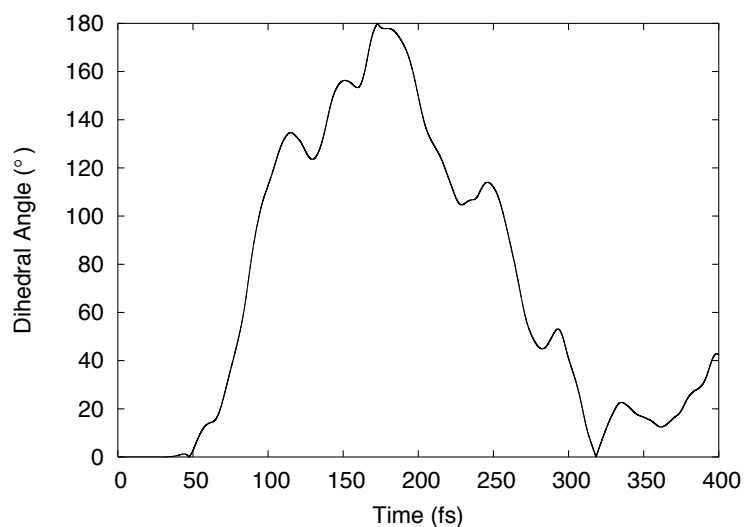


Fig. 19. Excited state-ground state simulation for 2-butene. The dihedral angle measurements are from H4-C2=C3-H5 plane. The HOMO and the LUMO are switched and the dynamics of the dihedral angle is measured with respect to time. The isomerization of butene from *cis-trans* form starts ~ 175.0 fs after the beginning of the excitation.

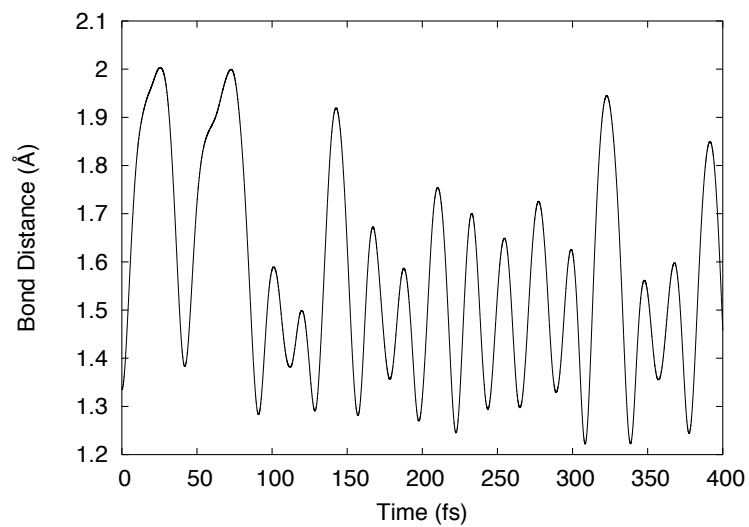


Fig. 20. Excited state-ground state simulation for 2-butene. The HOMO and the LUMO are switched and the dynamics of the C2=C3 bondlength is measured with respect to time. The isomerization of butene from *cis-trans* form starts ~ 175.0 fs after the beginning of the excitation.

2. Results for the dynamics of 2-butene without the application of an external field

We next investigate the dynamics of the 2-butene molecule without the application of the electro-magnetic field. In the histogram plot given in Figure 21 we show the stationary eigenvalues and their corresponding frequencies. Figure 22 shows the C2=C3 bond length over time. This information is used to extract the stationary vibrational frequencies by Fourier transform method. The results are reported in Section E.

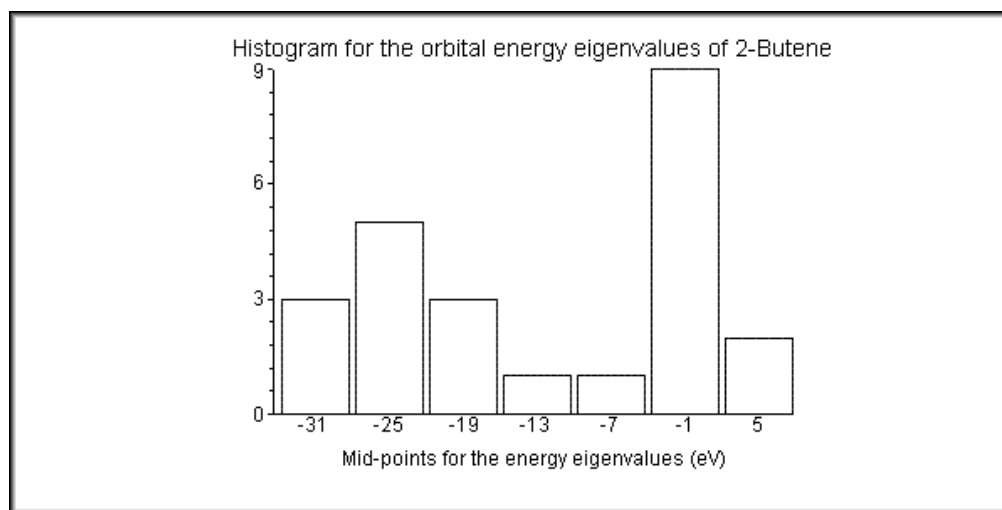


Fig. 21. The histogram shows a distribution of the molecular orbital energy eigenvalues of 2-butene without the application of an electro-magnetic field.

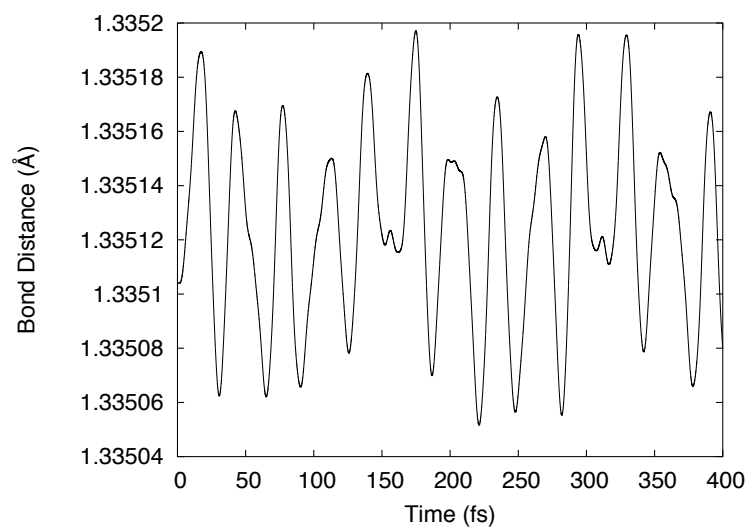


Fig. 22. The C2=C3 bond distance is plotted over time for 2-butene with no external field applied. The time step $\Delta t = 0.005$ fs.

3. Results for the photo-isomerization of 2-butene with the application of an electro-magnetic field

In this section, we study the photo-isomerization of the 2-butene molecule. We first calculate the resonant wavelength using the following equations:

$$\begin{aligned}\Delta E &= E_{13} - E_{12} \\ &= (-11.750036445955 \text{ eV}) - (-6.6753592796011 \text{ eV}) \\ &= 5.075 \text{ eV}\end{aligned}\tag{4.4}$$

$$\begin{aligned}\lambda &= \frac{hc}{\Delta E} \\ &= 244.0 \text{ nm}\end{aligned}\tag{4.5}$$

The isomerization mechanism is shown in Figure 23. We began the simulation by using a wavelength $\lambda = 244.0 \text{ nm}$ as derived from our calculations in equation 4.5. Similar values (254.0 nm) of the wavelength have been used for experimental studies of the isomerization of butene[49]. We used an initial vector field strength $A = 0.5 \text{ gauss}\cdot\text{cm}$ and time step $\Delta t = 0.005 \text{ fs}$. However, the molecule did not rotate by 180° along the C2=C3 double bond in a period of 400 fs. We next tried an intermediate value of $A = 0.8 \text{ gauss}\cdot\text{cm}$, but the molecule still did not rotate by 180° . Finally, a higher field strength value of $A = 1.0 \text{ gauss}\cdot\text{cm}$ was sufficient to accomplish the *cis-trans* transformation. The results are reported in the following figures.

Figure 24 shows the plot of the energy eigenvalues with time. The avoided crossing region between the HOMO (the eleventh eigenvalue) and the LUMO (the twelfth eigenvalue) as described earlier for ethylene is also shown in this plot, showing the $\pi-\pi^*$ excitation. In Figure 25, the total energy is plotted against time. We find that the system quickly absorbs energy in the first 4.86 fs and then stabilizes while the molecule rotates from the *cis* to the *trans* form. After which, since the light is

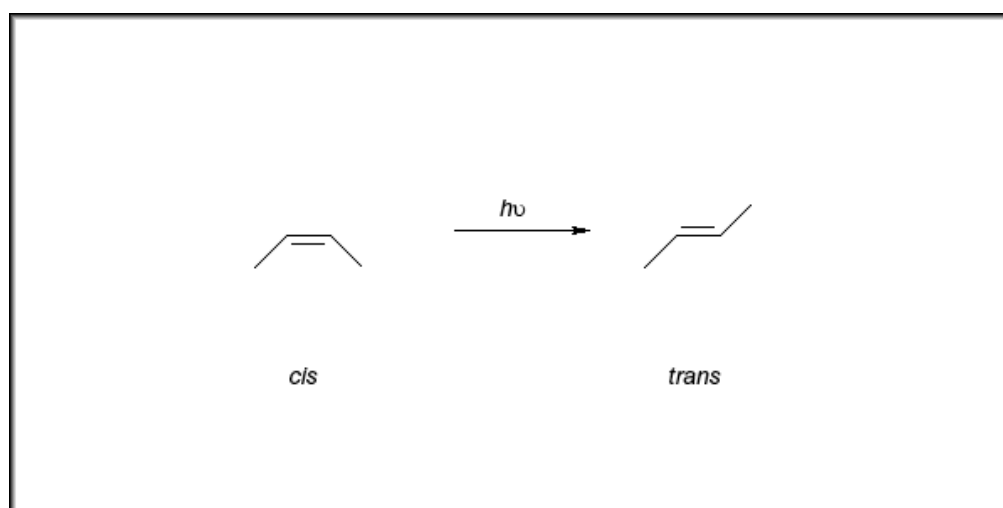


Fig. 23. The *cis-trans* isomerization of the 2-butene molecule.

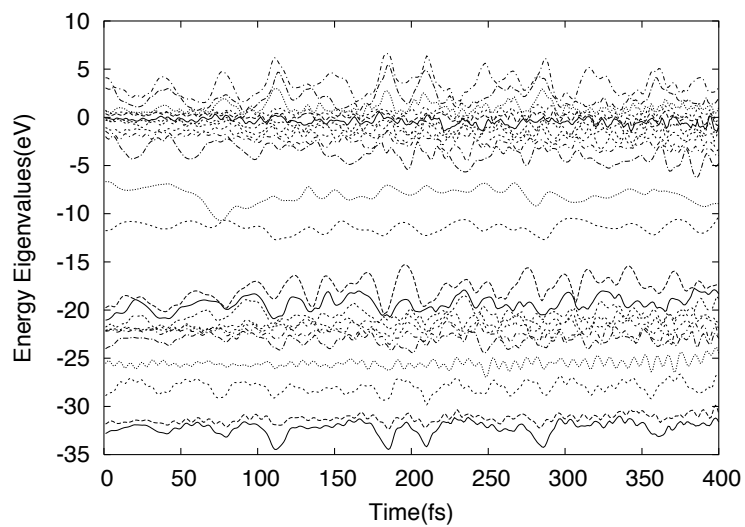


Fig. 24. The energy eigenvalues for 2-butene molecule are plotted over time. The time step is $\Delta t = 0.005$ fs, amplitude of the vector potential is $A = 1.0$ gauss·cm and the wavelength of the light is $\lambda = 244.0$ nm.

not turned off, the system continues to absorb energy and the value goes up to ~ 25 eV.

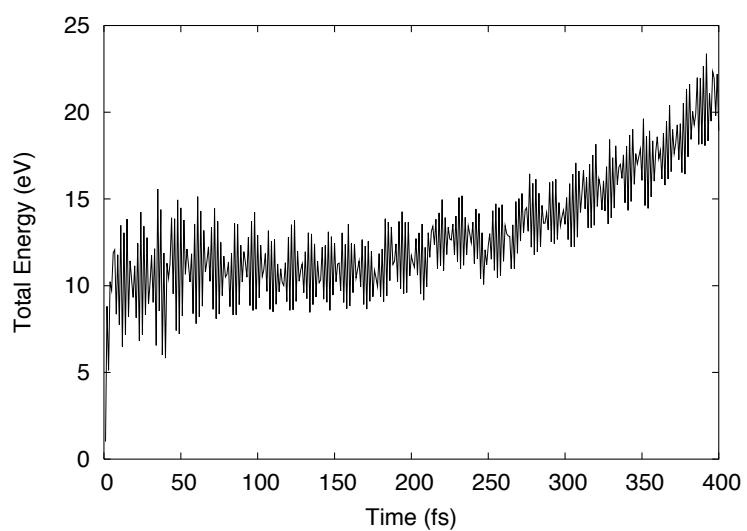


Fig. 25. The total energy for 2-butene molecule is plotted over time. The time step is $\Delta t = 0.005$ fs, amplitude of the vector potential is $A = 1.0$ gauss·cm and the wavelength of the light is $\lambda = 244.0$ nm.

In Figures 26 and 27 we plot the dihedral angle and the C2=C3 bond length respectively over time. The molecule twists by 180° in about 140 fs and the C2=C3 bond length vibrates from 1.22 to 1.7 Å.

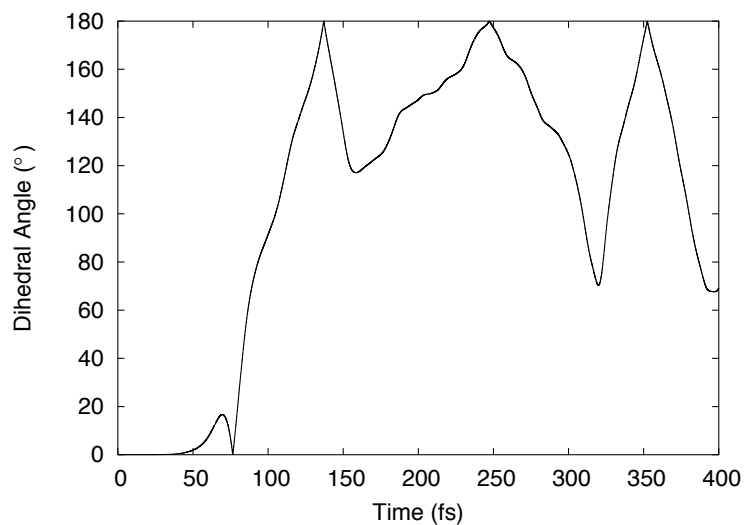


Fig. 26. The dihedral angle H4-C2=C3-H5 for 2-butene molecule is plotted over time. The time step is $\Delta t = 0.005$ fs, amplitude of the vector potential is $A = 1.0$ gauss·cm and the wavelength of the light is $\lambda = 244.0$ nm.

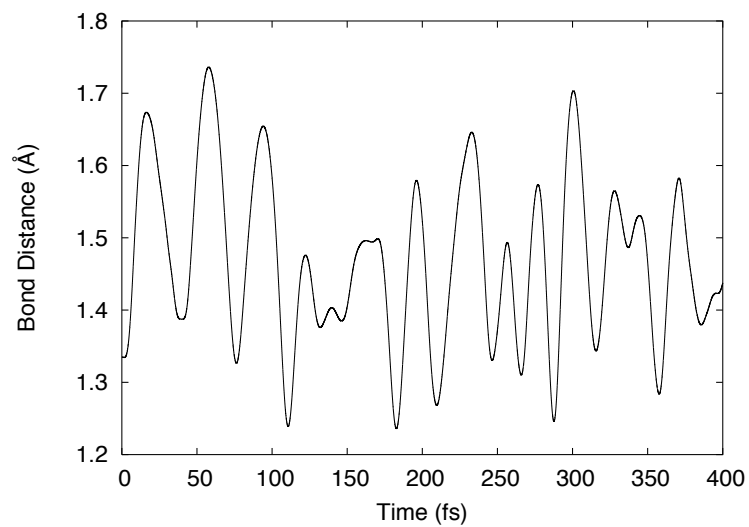


Fig. 27. The C2=C3 bond distance is plotted over time for 2-butene molecule with amplitude of the vector potential is $A = 1.0$ gauss-cm and the wavelength of the light is $\lambda = 244.0$ nm. The time step $\Delta t = 0.005$ fs.

The next three plots show comparison of different vector field strengths A , wavelengths λ and the time step Δt applied during the isomerization process. In Figure 28 we find how the dihedral angle behaves with time for different values of A . For a value of $A = 0.5$ gauss·cm, the dihedral angle rotates up to only 20° and for $A = 2.0$ gauss·cm the dihedral angle rotates by 160° but not enough to reach the *trans* configuration. Therefore the value of $A = 1.0$ gauss·cm is the most logical choice here.

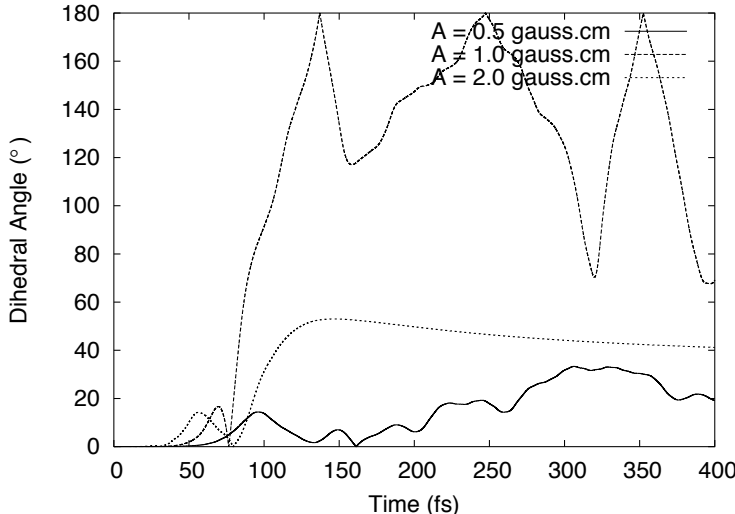


Fig. 28. The dihedral angle is plotted over time for 2-butene molecule with amplitude of the vector potential is $A = 0.5, 1.0$ and 2.0 gauss·cm and the wavelength of the light is $\lambda = 244.0$ nm. The time step $\Delta t = 0.005$ fs.

We next compare different values of the wavelength λ in Figure 29. We find the dihedral angle quickly reaches 180° in ~ 130 fs for the resonant wavelength of 244.0 nm, while for half the resonant wavelength of 122.0 nm the dihedral angle rotates by only 40° and for twice the wavelength value of 488.0 nm the dihedral angle doesn't rotate at all. This is because at 122.0 nm, it gets some energy to rotate but the energy corresponding to 488.0 nm is not sufficient to excite electrons from the highest

bound state to the nearest unbound state. Finally we look at the isomerization of

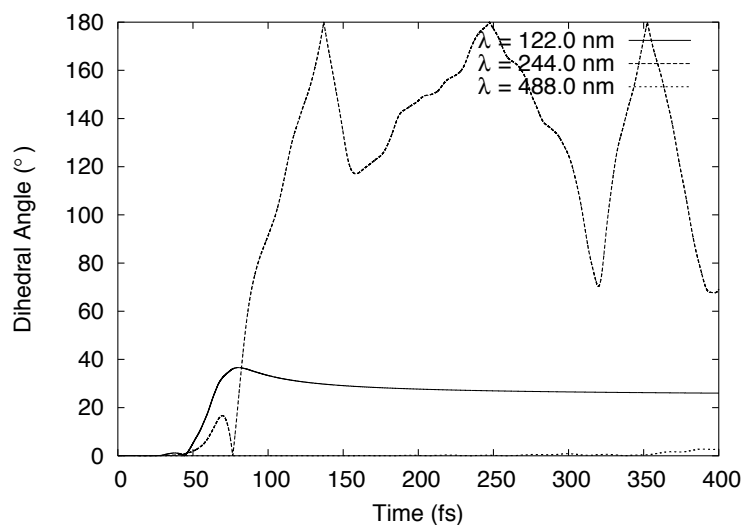


Fig. 29. The dihedral angle is plotted over time for 2-butene. The vector potential $A=1.0$ gauss \cdot cm, wavelength $\lambda = 122.0$ nm, 244.0 nm and 488.0 nm and the time step $\Delta t = 0.005$ fs.

2-butene at different time steps $\Delta t = 0.005$, 0.010 and 0.050 fs in Figure 30. We find that $\Delta t = 0.005$ fs yields results for the dynamics which are comparable to the ones obtained from experiments. A time step of $\Delta t = 0.010$ fs is also reasonable but the dihedral angle takes longer to rotate by 180° but for a time step of $\Delta t = 0.050$ fs the dihedral angle barely rotates. We therefore conclude that for this system, a bigger time step up to 0.010 fs will still generate accurate results but $\Delta t = 0.050$ fs although makes the computation faster proves to be too big for computation purposes.

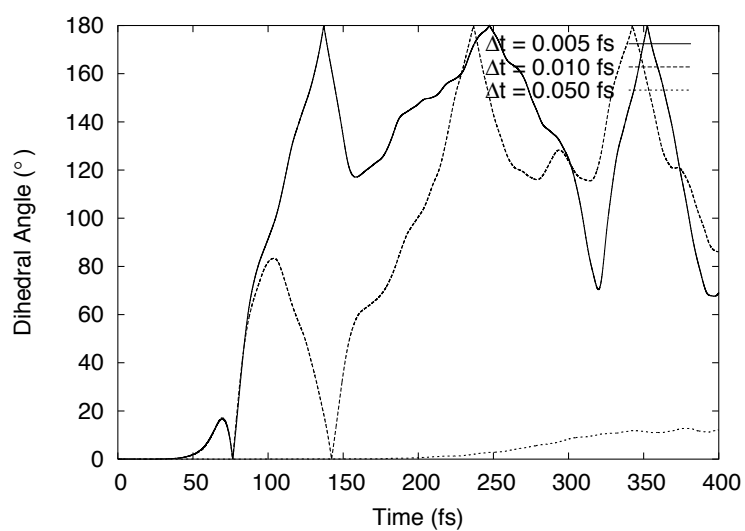


Fig. 30. The dihedral angle is plotted over time for 2-butene. The vector potential $A=1.0$ gauss·cm, wavelength $\lambda = 244.0$ nm and the time steps are $\Delta t = 0.005, 0.010$ and 0.050 fs.

C. Results for the Stilbene Molecule

The final molecule used to test the tight-binding techniques is stilbene. Stilbene in its *cis* form is represented in the Figure 31. The photophysics and photochemistry of

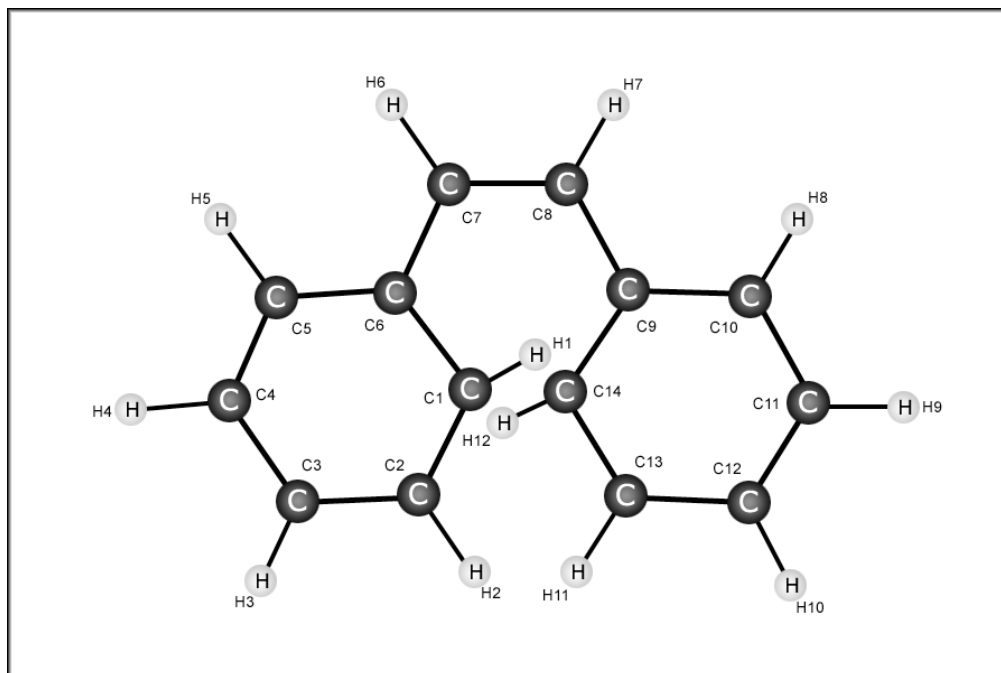


Fig. 31. The stilbene molecule in its *cis* form.

stilbene have been the subject of many investigations over the past 45 years. Interest in stilbene has primarily centered on its *cis-trans* photoisomerization[50, 51, 52], both as a model for natural *cis-trans* isomerization processes such as vision and as a model for testing solvent effects on isomerization reactions.

This reaction is believed to proceed adiabatically on the excited singlet surface from either the *cis* or the *trans* form through a common intermediate state at the perpendicular configuration before undergoing internal conversion back to the ground electronic state. Our results of the photo-isomerization of stilbene are given in the following three subsections.

1. Molecular dynamics study of *cis-trans* isomerization of stilbene by switching the highest-occupied and lowest-unoccupied molecular orbitals

In this section, we investigate the dynamics of the stilbene molecule by switching the π and the π^* , which in this case are the 34th and the 35th orbitals respectively. The identities of the π and the π^* orbitals were checked using the coefficients of the molecular orbitals which is discussed in Chapter III, Section E. Similar studies were done for ethylene and 2-butene which have been reported in earlier sections. In this case also we look at the behavior of the H6-C7=C8-H7 dihedral angle and the C7=C8 bond length over time for the stilbene molecule. Since stilbene is much larger than ethylene or 2-butene it takes longer to rotate to 180°, which is obtained in ~ 325 fs as shown in Figure 32. The C7=C8 bond distance plot shows that initially the bondlength vibrates to almost 1.55 Å but after about 150 fs it stabilizes and vibrates about the mean carbon-carbon double bond length of 1.35 Å as shown in Figure 33.

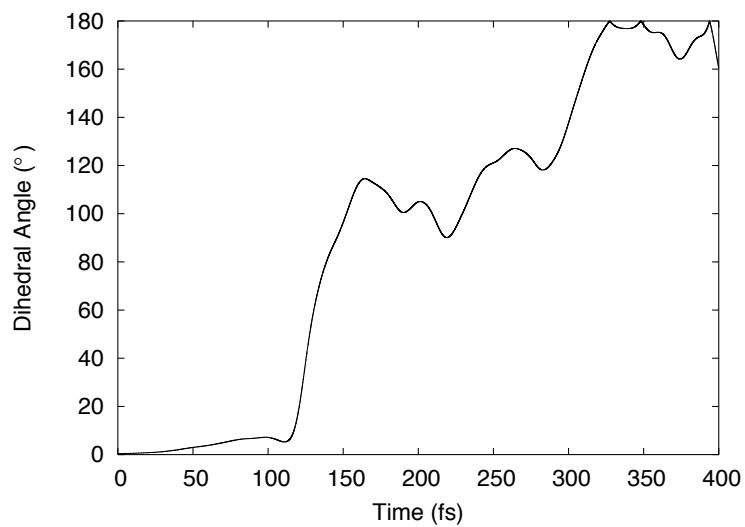


Fig. 32. Excited state-ground state simulation for stilbene. The dihedral angle measurements are from H6-C7=C8-H7 plane. The HOMO and the LUMO are switched and the dynamics of the dihedral angle is measured with respect to time. The isomerization of stilbene from *cis-trans* form starts ~ 325 fs after the beginning of the excitation.

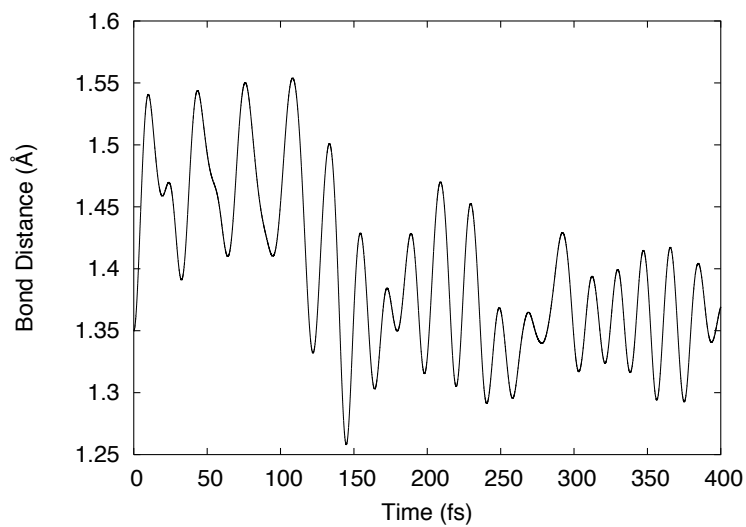


Fig. 33. Excited state-ground state simulation for stilbene. The bond distance measurements between the carbon atoms are plotted. The HOMO and the LUMO are switched and the dynamics of the C7=C8 bond distance is measured with respect to time without any external field.

2. Results for the dynamics of stilbene without the application of an external field

The following two figures show the results of the stilbene molecule without the electromagnetic field. First we look at the histogram plot of the eigenvalues to determine where the HOMO and the LUMO are located and use the corresponding energy eigenvalues difference to determine the resonant wavelength of the electro-magnetic field required to excite electrons from the HOMO to the LUMO. This is shown in Figure 34.

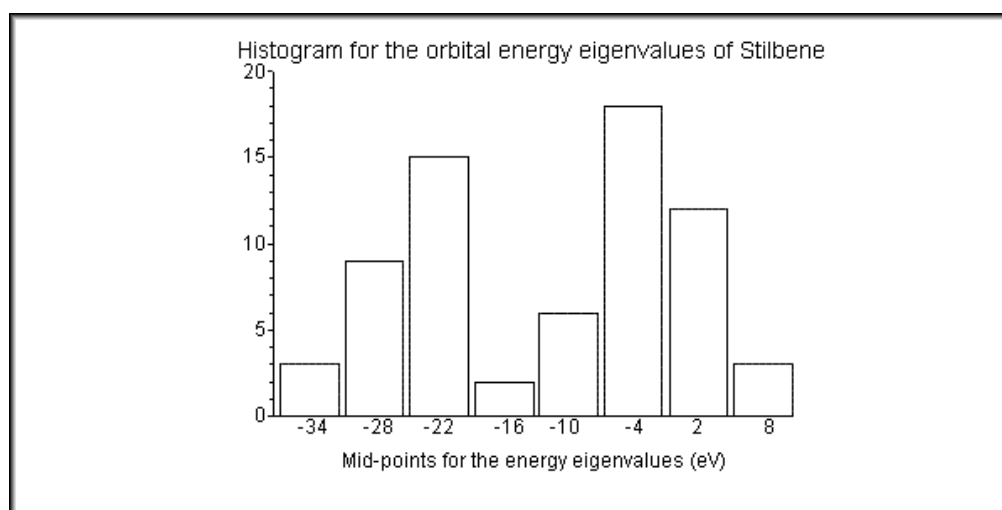


Fig. 34. The histogram shows a distribution of the molecular orbital energy eigenvalues of stilbene without the application of an electro-magnetic field.

The next plot of the C7=C8 bond distance in Figure 35 is used to extract fourier amplitudes using the fourier transform method (discussed in Chapter III, section B, subsection 2), from which we can get stationary vibrational frequencies.

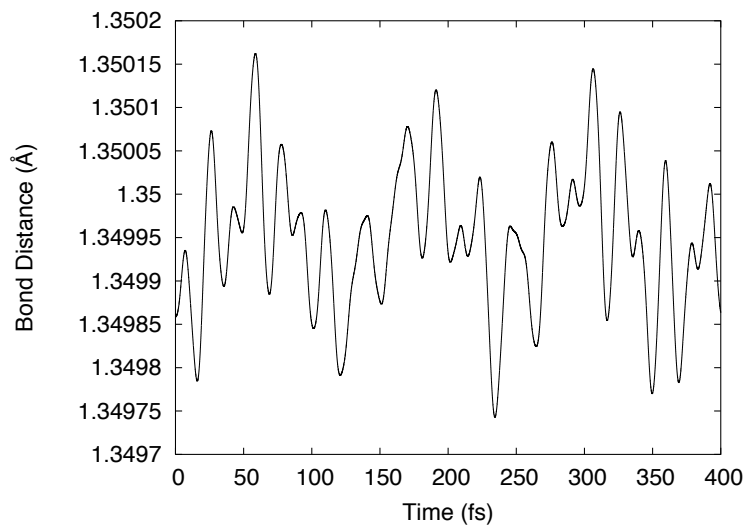


Fig. 35. The C7=C8 bond distance is plotted over time for stilbene molecule with no external field applied. The time step $\Delta t = 0.005$ fs.

3. Results for the photo-isomerization of stilbene with the application of an electro-magnetic field

$$\begin{aligned}
 \Delta E &= E_{35} - E_{34} \\
 &= (-10.321880237601 \text{ eV}) - (-7.6181353125286 \text{ eV}) \\
 &= 2.704 \text{ eV}
 \end{aligned} \tag{4.6}$$

$$\begin{aligned}
 \lambda &= \frac{hc}{\Delta E} \\
 &= 458.0 \text{ nm}
 \end{aligned} \tag{4.7}$$

In order to obtain the *cis-trans* transformation, the molecule needs a minimum of 2.704 eV of energy. The isomerization scheme is shown in Figure 36.

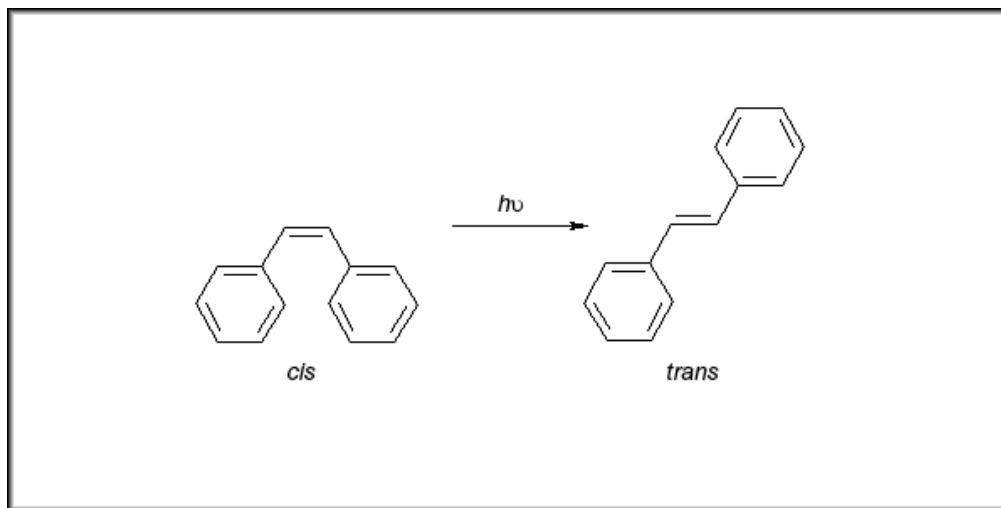


Fig. 36. The *cis-trans* isomerization of the stilbene molecule.

In the following Figures 37 and 38, we plot the energy eigenvalues versus time. Figure 38 is a subsection of Figure 37, and shows the energy eigenvalues near the π and the π^* orbitals. We detect the avoided crossing between molecular orbitals 34 (π orbital) and 35 (π^* orbital) that occurs at $t \sim 110.0$ fs.

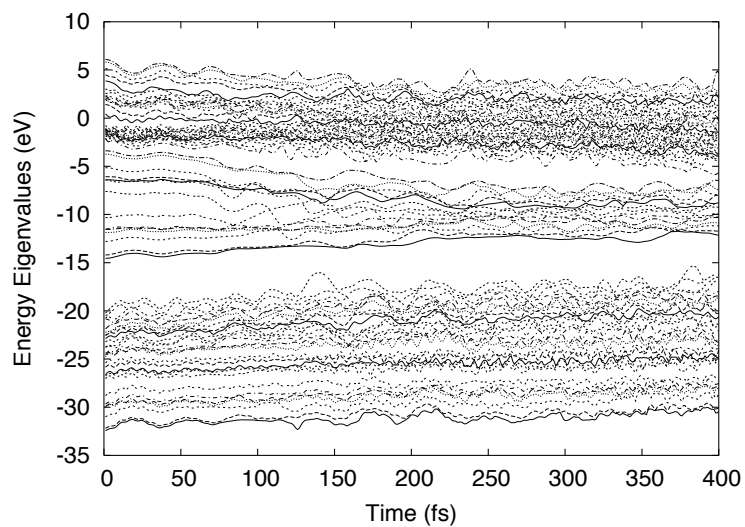


Fig. 37. The energy eigenvalues for stilbene molecule are plotted over time. The time step is $\Delta t = 0.005$ fs, amplitude of the vector potential is $A = 1.2$ gauss-cm and the wavelength of the light is $\lambda = 458.0$ nm.

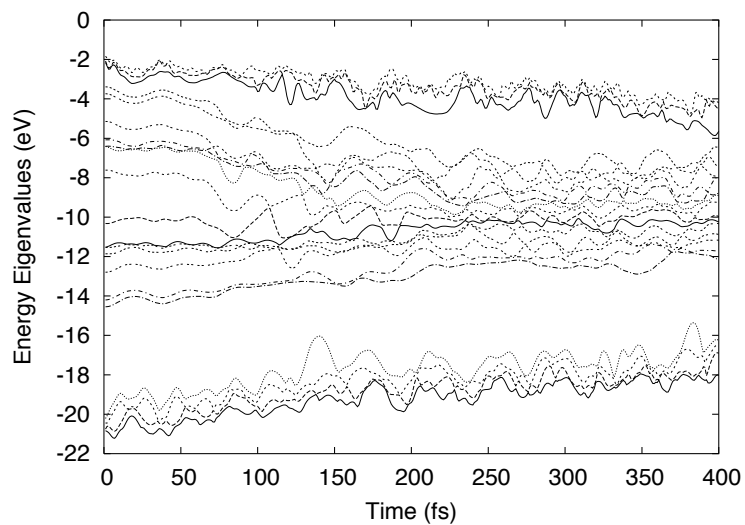


Fig. 38. This plot is a subsection of Figure 37. The energy eigenvalues near the HOMO and the LUMO are plotted over time. The time step is $\Delta t = 0.005$ fs, amplitude of the vector potential is $A = 1.2$ gauss·cm and the wavelength of the light is $\lambda = 458.0$ nm.

The next three Figures 39, 40 and 41 show the total energy, dihedral angle and bond distance respectively and how they change with time. Similar to ethylene and 2-butene, the stilbene molecule first absorbs enough energy to rotate from the *cis* to the *trans* form after which it continues to absorb energy from the electromagnetic field. The dihedral angle takes 487 fs to rotate by 180° , much longer than the ethylene or 2-butene molecules. This time value is consistent with the time range of the isomerization as reported by [57] to be 0.3-0.5 ps. The C7=C8 bondlength stays within reasonable range, showing that the results are within acceptable range. Initially, the bond length stays within the 1.35-1.6 Å up to 350 fs, as also reported in [57]. But afterwards in the current simulation the bond length increases to close to 2.0 Å since we continued to shine the light on the molecule, whereas Dou *et al.* applied a laser pulse that lasted only 150 fs.

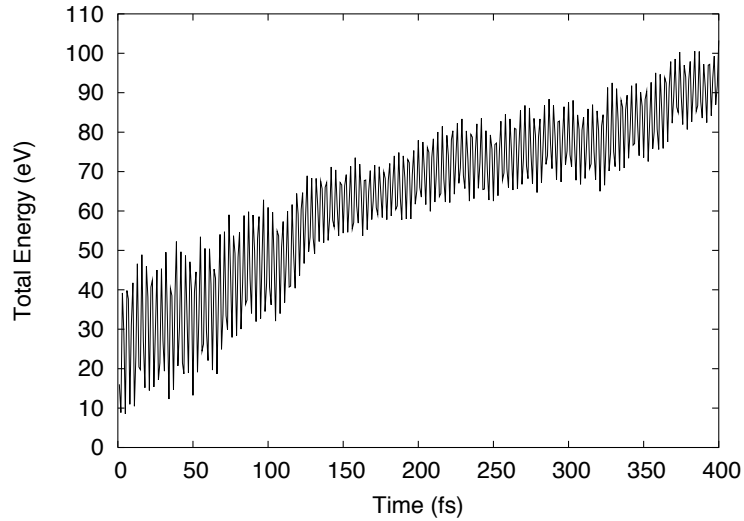


Fig. 39. The total energy for stilbene molecule is plotted over time. The time step is $\Delta t = 0.005$ fs, amplitude of the vector potential is $A = 1.2$ gauss·cm and the wavelength of the light is $\lambda = 458.0$ nm.

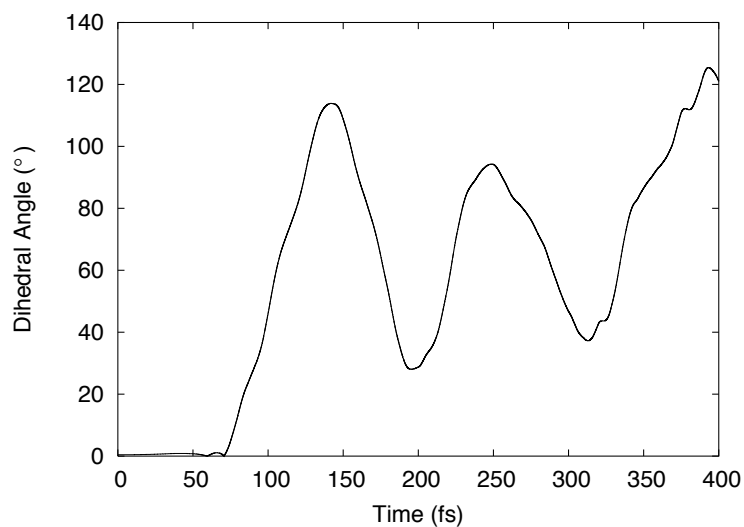


Fig. 40. The dihedral angle H6-C7=C8-H7 for stilbene molecule is plotted over time. The time step is $\Delta t = 0.005$ fs, amplitude of the vector potential is $A = 1.2$ gauss·cm and the wavelength of the light is $\lambda = 458.0$ nm.

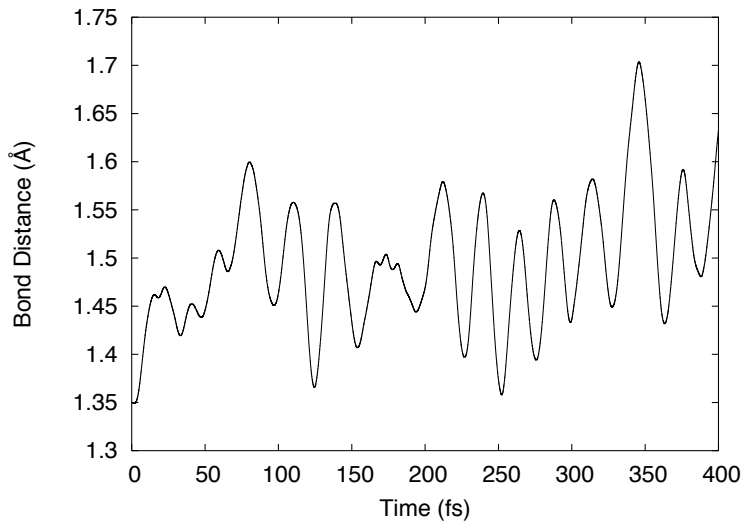


Fig. 41. The C7=C8 bond distance is plotted over time for stilbene molecule with amplitude of the vector potential is $A = 1.2$ gauss·cm and the wavelength of the light is $\lambda = 458.0$ nm. The time step $\Delta t = 0.005$ fs.

In the next few plots, we compare the field strength, wavelength and the time step in order to find the optimum values for each. Based on these findings, we can apply the appropriate values for retinal. This test is important with the test molecules since it gives us a good estimate on how to choose the parameters carefully for retinal where the dynamics calculation requires extensive computation time. In Figure 42,

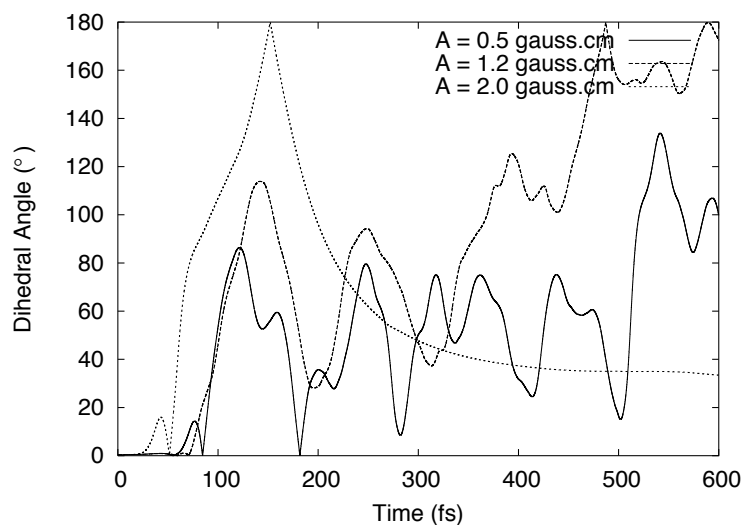


Fig. 42. The dihedral angle is plotted over time for stilbene molecule with amplitude of the vector potential is $A = 0.5, 1.2$ and 2.0 gauss \cdot cm and the wavelength of the light is $\lambda = 458.0$ nm. The time step $\Delta t = 0.005$ fs.

we find that any field strength smaller than 1.2 gauss \cdot cm is not sufficient to rotate the dihedral angle by 180° . The plot shows that $A = 2.0$ gauss \cdot cm achieves the 180° rotation quite quickly in 152 fs, but the next plot of the C7=C8 bondlength in Figure 43 shows that this is unphysical since the molecule essentially disintegrates at such high field strength.

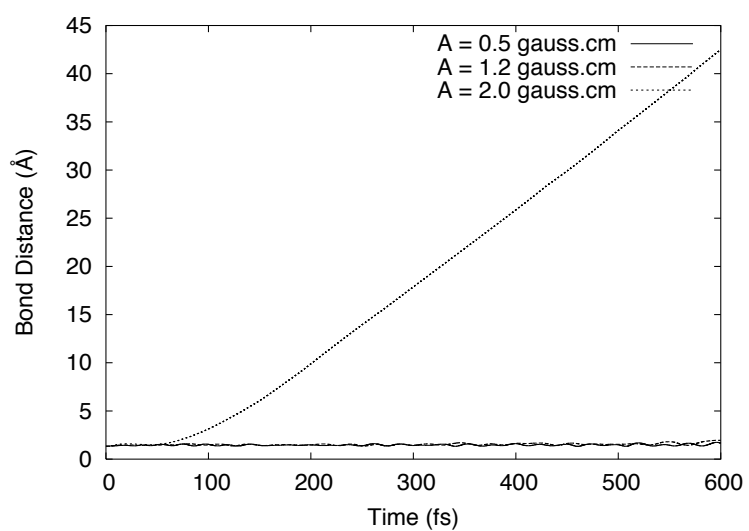


Fig. 43. The C7=C8 bond distance is plotted over time for stilbene molecule with amplitude of the vector potential is $A = 0.5, 1.2$ and 2.0 gauss-cm and the wavelength of the light is $\lambda = 458.0$ nm. The time step $\Delta t = 0.005$ fs.

In Figure 44 we show the dependence of the dihedral angle on the wavelength λ . For $\lambda = 458.0$ nm, which is the resonant wavelength, the molecule rotates by 180° in 487.155 fs, for $\lambda = 916$ nm, which is twice the resonant amplitude, the time required is 633 fs. However, for $\lambda = 229$ nm, which is half the resonant amplitude, the angle only goes up to about 60° . This is counter-intuitive, since smaller wavelength means larger energy and the molecule should have rotated for the smaller rather than the larger wavelength. However, when we interpret the next plot of C7=C8 bond distance versus time in Figure 45, we clearly see that only the resonant wavelength gives us the reasonable estimation.

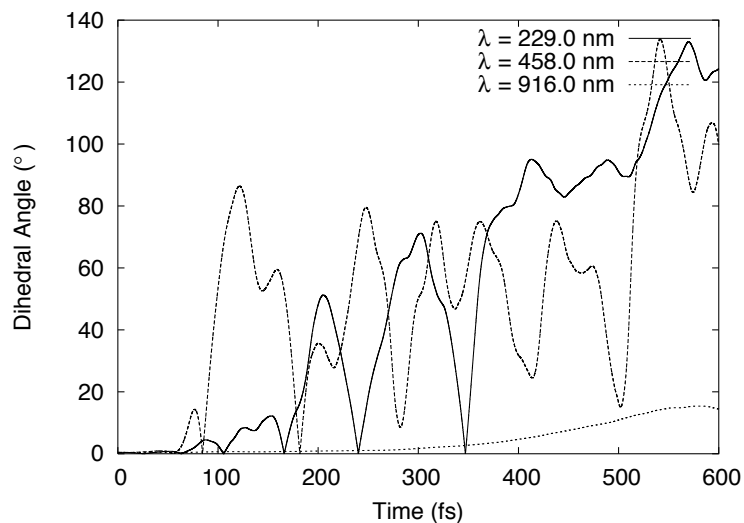


Fig. 44. The dihedral angle is plotted over time for stilbene. The vector potential $A=1.2$ gauss·cm, wavelength $\lambda = 229.0$ nm, 458.0 nm and 916.0 nm and the time step $\Delta t = 0.005$ fs.

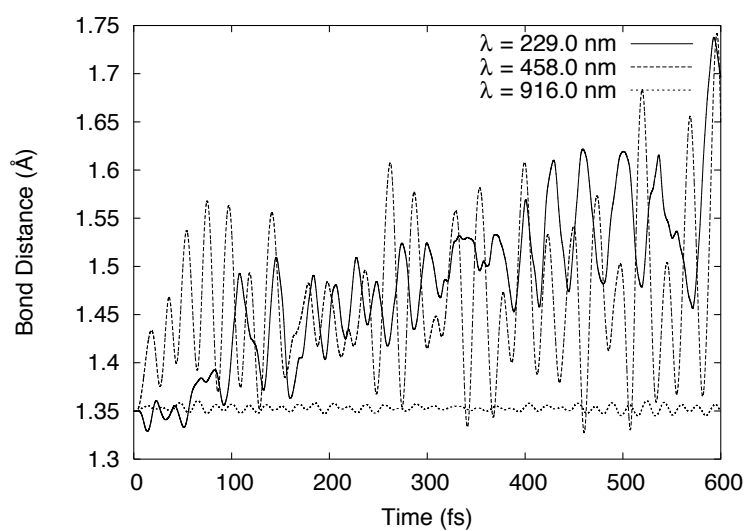


Fig. 45. The C7=C8 bond length is plotted over time for stilbene. The vector potential $A=1.2$ gauss \cdot cm, wavelength $\lambda = 229.0$ nm, 458.0 nm and 916.0 nm and the time step $\Delta t = 0.005$ fs.

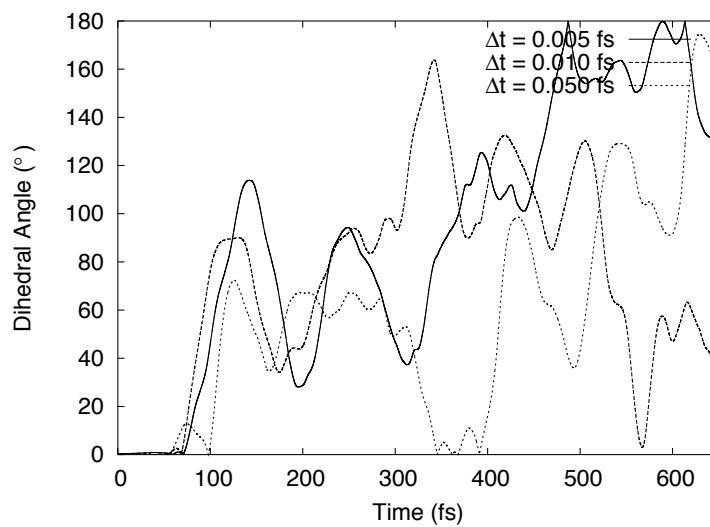


Fig. 46. The dihedral angle is plotted over time for stilbene. The vector potential $A=1.2$ gauss-cm, wavelength $\lambda = 458.0$ nm and the time steps are $\Delta t = 0.005, 0.010$ and 0.050 fs.

Finally a look at the dihedral angle versus time for different time steps in Figure 46 reveals that for a relatively large molecule like stilbene the only time step $\Delta t = 0.005$ fs produces comparable results, while both 0.010 and 0.050 fs are far too large to maintain accuracy in the computation. Therefore our conclusion is that for the retinal molecule we cannot use a time step that is larger than 0.005 fs.

D. Frequency Calculations Using Force-Constant Technique

The frequency calculations using the force constant method described in Chapter III Section B were performed on the test molecules ethylene, 2-butene and stilbene. The values for ethylene are listed in the following table:

Table III.: Eigenvalues of the second-derivative matrix of the potential and the corresponding vibrational frequencies for ethylene.

Vibrational Frequencies (cm^{-1}) Present Work	Vibrational Frequencies (cm^{-1}) Gaussian[37]	Vibrational Frequencies (cm^{-1}) Experiment
0.0975	0.0003	0
0.1362	0.0007	0
0.7198	0.7198	0
3.0091	16.7625	0
7.0801	19.5256	0
13.2072	29.4687	0
744.9418	889.4531	810
935.7514	1084.1163	949
1000.3888	1105.4359	950
1079.9204	1138.8397	1027
1383.5805	1342.7060	1236
1433.9292	1473.2826	1342
1674.1440	1588.9748	1443
1971.5036	1814.0646	1622

Table III.: *continued*

Vibrational Frequencies (cm^{-1}) Present Work	Vibrational Frequencies (cm^{-1}) Gaussian[37]	Vibrational Frequencies (cm^{-1}) Experiment
4797.2974	3270.3002	2988
4797.8561	3291.0196	3026
5003.2307	3342.4963	3102
5004.9688	3371.3486	3105

The frequency calculations using the force constant method yielded the following vibrational frequencies for 2-butene:

Table IV.: Eigenvalues of the second-derivative matrix of the potential and the corresponding vibrational frequencies for 2-butene.

Vibrational Frequencies (cm^{-1}) Present Work	Vibrational Frequencies (cm^{-1}) Gaussian[37]
0.1263	0.0002
0.2378	0.0004
0.5617	0.0007
2.2015	1.1103
5.8998	6.1729
7.46562	7.2091
10.9082	138.1114
11.7124	138.7045
209.3429	307.6122
356.4679	434.0497
515.6975	606.1539
569.9779	765.0649
955.1358	912.7622
1066.4677	1032.5425
1096.0819	1105.1251
1187.1524	1105.4683

Table IV.: *continued*

Vibrational Frequencies (cm^{-1}) Present Work	Vibrational Frequencies (cm^{-1}) Gaussian[37]
1199.1020	1164.9113
1222.4832	1175.1647
1276.2450	1252.8057
1331.1153	1390.5920
1584.1546	1508.6237
1714.0880	1543.5070
1736.7299	1563.5598
1743.6410	1598.8647
1747.9927	1604.4951
1748.1037	1606.4337
1775.3007	1612.4516
1990.2265	1869.3888
4546.7502	3152.5821
4548.6130	3155.2651
4664.4004	3189.5064
4664.5795	3190.0608
4741.4373	3237.5492
4742.0793	3259.9848
4912.4627	3264.1807
4916.7753	3291.5691

The following vibrational frequencies for the stilbene molecule were obtained using the force constant method.

Table V.: Eigenvalues of the second-derivative matrix of the potential and the corresponding vibrational frequencies for stilbene.

Vibrational Frequencies (cm^{-1}) Present Work	Vibrational Frequencies (cm^{-1}) Gaussian[37]
0.0531	0.0002
0.1732	0.0004
0.5461	0.0005
2.1588	0.4272
4.0438	1.1297
6.6550	1.6239
39.3496	65.7510
42.7906	111.3868
49.0873	184.4249
123.9514	189.4440
153.3807	226.8441
200.7392	393.8483
275.4759	406.1645
313.5832	423.1592

Table V.: *continued*

Vibrational Frequencies (cm^{-1}) Present Work	Vibrational Frequencies (cm^{-1}) Gaussian[37]
343.5183	463.9331
345.9354	465.9519
372.6559	517.8624
454.1055	529.8123
482.2336	548.8254
496.5784	605.7315
578.0878	625.2275
592.0749	675.1045
592.6386	686.6391
607.8353	769.2031
615.1062	775.2996
657.1289	800.0168
659.3969	827.7753
701.4804	850.7494
716.7085	864.9490
717.2227	875.6963
832.8710	954.2671
835.0426	970.2153

Table V.: *continued*

Vibrational Frequencies (cm^{-1}) Present Work	Vibrational Frequencies (cm^{-1}) Gaussian[37]
859.9605	1025.2523
917.6778	1032.2190
921.8059	1046.8732
951.0363	1082.0307
951.6801	1084.2895
982.7960	1097.0351
982.8681	1097.5627
1064.9340	1099.6493
1066.2821	1112.4769
1119.2220	1142.2752
1119.4297	1151.8820
1160.9651	1195.6389
1162.8331	1218.0743
1209.3301	1258.6665
1223.9858	1272.1211
1224.2839	1275.7402
1238.5032	1287.0498
1238.6899	1306.6481

Table V.: *continued*

Vibrational Frequencies (cm^{-1}) Present Work	Vibrational Frequencies (cm^{-1}) Gaussian[37]
1330.3829	1343.2534
1409.3882	1379.7709
1462.8956	1396.9204
1465.0256	1456.9657
1626.84016	1469.0369
1680.4408	1493.7324
1701.0790	1512.1728
1750.8779	1540.3216
1810.4905	1550.4932
1838.7875	1556.0861
1844.5475	1777.2761
1901.9451	1791.2815
1955.8910	1826.0664
1967.7942	1854.0808
1994.2835	1872.4538
1997.6954	1909.3412
4905.4266	3074.5007
4906.9026	3075.0662

Table V.: *continued*

Vibrational Frequencies (cm ⁻¹) Present Work	Vibrational Frequencies (cm ⁻¹) Gaussian[37]
4909.2015	3301.2973
4909.9258	3323.8379
4910.8049	3324.9323
4911.0737	3329.2538
4913.8277	3337.1697
4913.9557	3339.9154
4914.3814	3354.7880
4914.8117	3357.1030
4922.0852	3367.1369
4926.2854	3381.2527

In the tables above, the eigenvalues λ were obtained using the determinant,

$$\det(F_{ij} - \delta_{ij}\lambda_k) = 0 \quad (4.8)$$

which then gave the corresponding frequencies by using the following equation:

$$\nu_k = \frac{\lambda_k^{1/2}}{2\pi}. \quad (4.9)$$

The frequencies thus obtained had to be adjusted to the proper scaling factor.

$$\bar{\nu}_k = \frac{\nu_k}{c} \quad (4.10)$$

where c is the speed of light.

Now for a harmonic oscillator, the potential energy is defined to be,

$$U = \frac{1}{2}kx^2 \quad \omega = \sqrt{\frac{k}{m}} \quad (4.11)$$

where k is the force constant, m is in atomic mass units (amu) and x is the displacement in angstroms (\AA).

From the above equation we get,

$$\omega = \sqrt{\frac{2U}{x^2m}}. \quad (4.12)$$

To convert the angular frequencies to the appropriate units, we multiply them with the appropriate scaling factor.

$$\begin{aligned} \text{conversion factor} &= \frac{1}{c} \sqrt{\frac{2 \times 1.602177 \times 10^{-19} \text{J}}{(10^{-10} \text{m})^2 (1.6605402 \times 10^{-27} \text{kg})}} \\ &= 4.6305 \times 10^3 \text{cm}^{-1}. \end{aligned} \quad (4.13)$$

The above factor was multiplied to all the eigenvalues to obtain the next set of vibrational frequencies. As we see that although the frequencies are in the right order when compared to experimental values, they are all a little bit stiffer in the present calculations. The reason could be that we are using a semi-empirical method and the resulting frequencies seem to come from using a steep form of the repulsive potential.

E. Frequency Calculations Using Fourier Transforms

We performed a fourier transform analysis to check the accuracy of the vibrational frequencies within the molecules. We looked at the bondlength between the carbon atoms about which the rotation from the *cis* to the *trans* form for each molecule takes place and followed how it behaved over time. The fourier transform of the bondlength yielded the corresponding fourier amplitude. The plot of the fourier amplitude versus frequency for each of the molecules is shown in the following Figures 47, 48 and 49. These numbers seem to agree well with the results obtained from second-order energy calculations within the model.

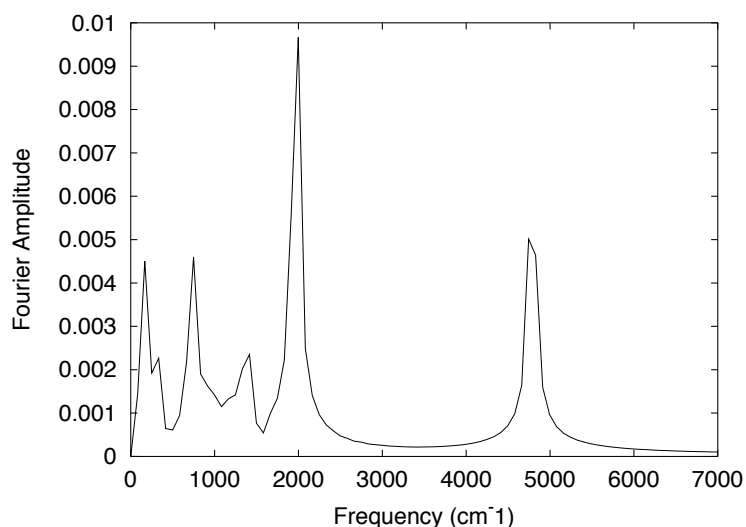


Fig. 47. Frequency measurements for the ethylene molecule from Fourier-Transform techniques. The C1=C2 bondlengths were measured over time and transformed to get vibrational frequencies. The graph represents the Fourier amplitudes plotted with respect to the corresponding frequencies. The time step $\Delta t = 0.005$ fs and the total time is 400 fs.

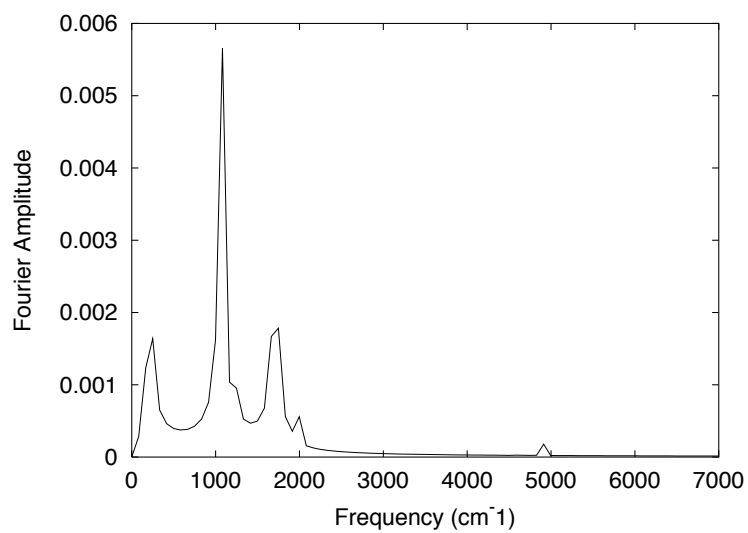


Fig. 48. Frequency measurements for the 2-butene molecule from Fourier-Transform techniques. The C2=C3 bondlengths were measured over time and transformed to get vibrational frequencies. The graph represents the fourier amplitudes plotted with respect to the corresponding frequencies. The time step $\Delta t = 0.005$ fs and the total time is 400 fs.

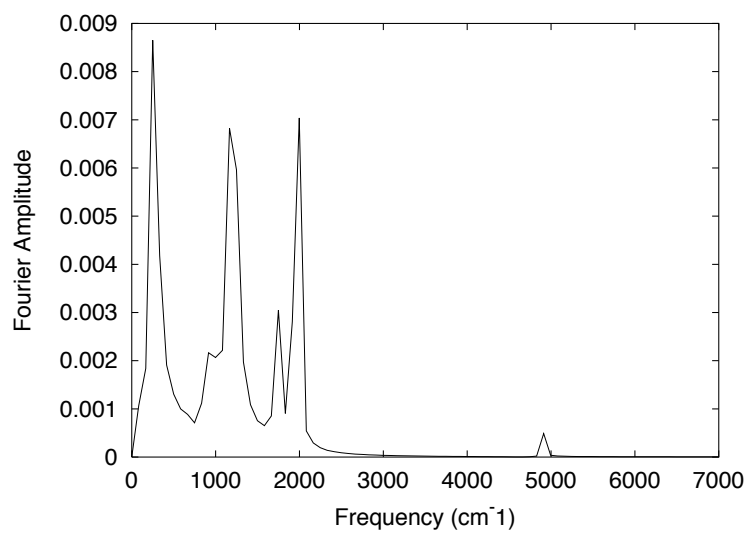


Fig. 49. Frequency measurements for the stilbene molecule from Fourier-Transform techniques. The C7=C8 bondlengths were measured over time and transformed to get vibrational frequencies. The graph represents the fourier amplitudes plotted with respect to the corresponding frequencies. The time step $\Delta t = 0.005$ fs and the total time is 400 fs.

CHAPTER V

RESULTS FOR THE MODEL MOLECULE RETINAL

The tight-binding model techniques were finally applied to the retinal molecule. Retinal is a large, 49-atom molecule which has heavy computation requirements and hence has not been investigated much in a theoretical sense. There are a number of reports based on experimental work and hence this was the molecule of choice for the current semi-empirical theoretical model. Figure 50 shows the retinal molecule in its *cis* form.

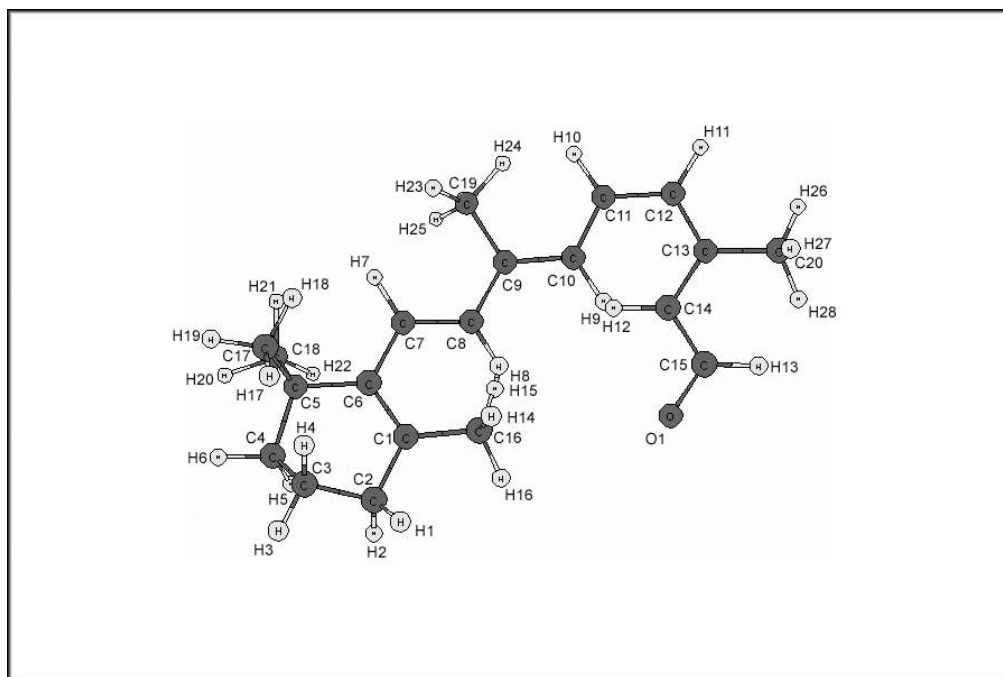


Fig. 50. The retinal molecule in its 11-*cis* form.

A. Results for the Retinal Molecule

1. Molecular dynamics study of *cis-trans* isomerization of retinal by switching the highest-occupied and lowest-unoccupied molecular orbitals

In this section we discuss the initial results obtained for the retinal molecule. We first investigated the dynamics of the molecule upon switching the π and the π^* orbitals. As we discussed in the last chapter, this was a straight-forward calculation and the molecule rotated by 180° from the *cis* to the *trans* form quite easily within a reasonable amount of time for all the test molecules. The π and the π^* molecular orbitals also coincided with the highest orbital coefficients in the population analysis scheme.

However, the calculations were far more complicated in the case of retinal. The true HOMO in this case is the 57^{th} molecular orbital and the true LUMO is the 58^{th} molecular orbital. Upon examination of the orbital coefficients of the C11=C12 bond, we found a reasonable estimate for the excitation states for the electrons. Initially, we did the calculations with the 52^{nd} and the 62^{nd} states respectively for the π - π^* excitation. The findings from this trial are reported in Figure 51.

From Figure 51 we find that the molecule rotates to almost 90° but doesn't rotate by 180° required for the *cis-trans* transformation. We then tried to use a different orbital, namely the 55^{th} orbital as the initial starting point for the electrons. This run did not yield satisfactory results, only rotating up to 40° as shown in Figure 52.

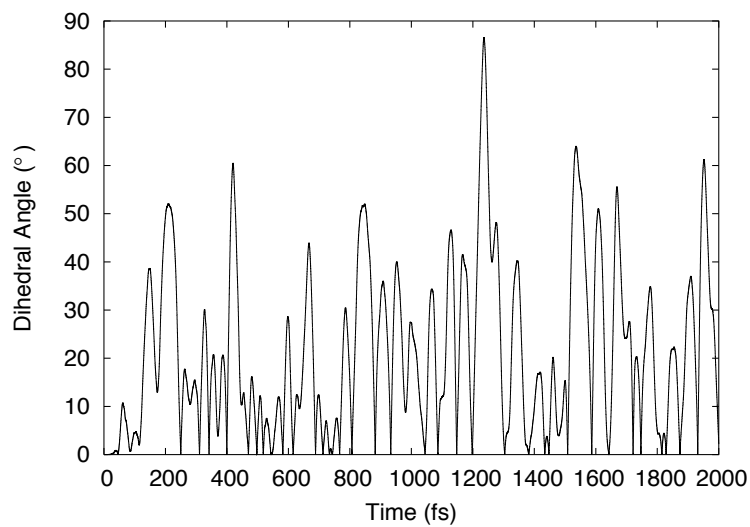


Fig. 51. Excited state-ground state simulation for retinal. The dihedral angle measurements are from H10-C11=C12-H11 plane. The 52nd and the 62nd are switched and the dynamics of the dihedral angle is measured with respect to time.

The conclusion from the study of the localized π - π^* orbitals on the C11=C12 bond is that for large molecules like retinal there is a lot of overlap between the s , p_x , p_y and the p_z orbitals. The population analysis study to find the π and the π^* from the large orbital coefficients in the eigenstates of the Hamiltonian proved to be beneficial in the test molecules. It helped determine the excitation states while also indicating the nature of the wave functions. This information was used to find the right direction for the propagation and the polarization of the light. However, in the case of retinal, due to the large size of the molecule, we weren't able to exactly determine the states for the electron population excitation.

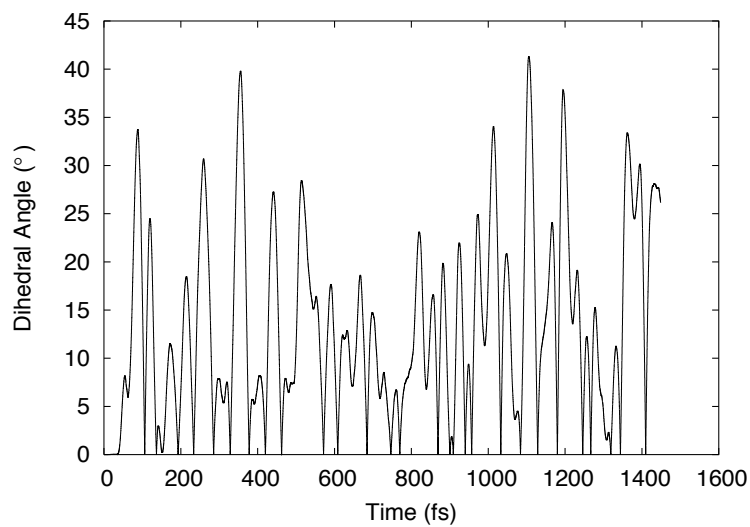


Fig. 52. Excited state-ground state simulation for retinal. The dihedral angle measurements are from H10-C11=C12-H11 plane. The 55th and the 62nd are switched and the dynamics of the dihedral angle is measured with respect to time.

2. Results for the dynamics of retinal without the application of an external field

In the absence of an external field, (amplitude $A_0 = 0.00$ gauss-cm), the eigenvalues are listed in the following histogram plot given in Figure 53. The actual values are listed later in Appendix B.

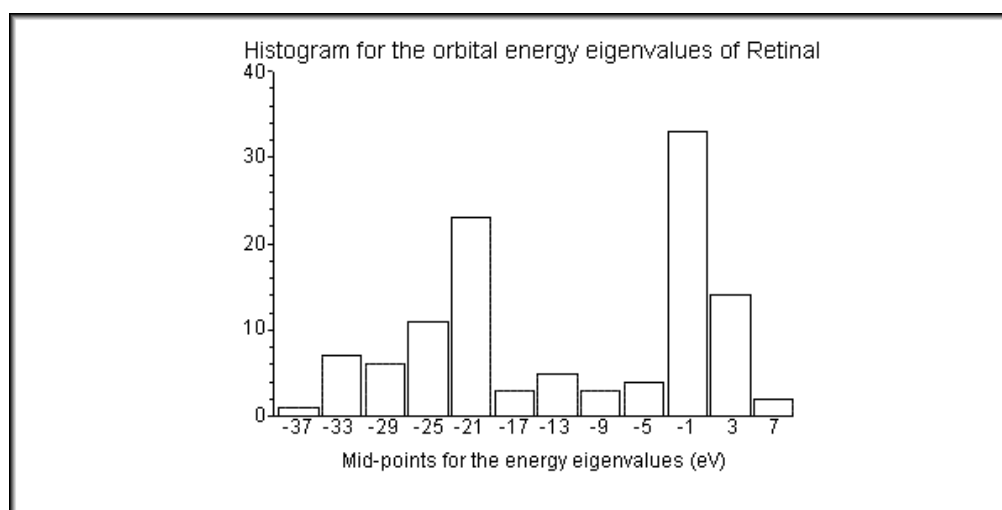


Fig. 53. The histogram shows a distribution of the molecular orbital energy eigenvalues of retinal without the application of an electro-magnetic field.

In Figure 54 we examined the bondlength of the C11=C12 bond and observed how the bond distance develops over time. Since there is no external applied field, we expect the bond distance to be unchanged. We use this information to find the vibrational frequencies within the molecule. The frequency calculations were also

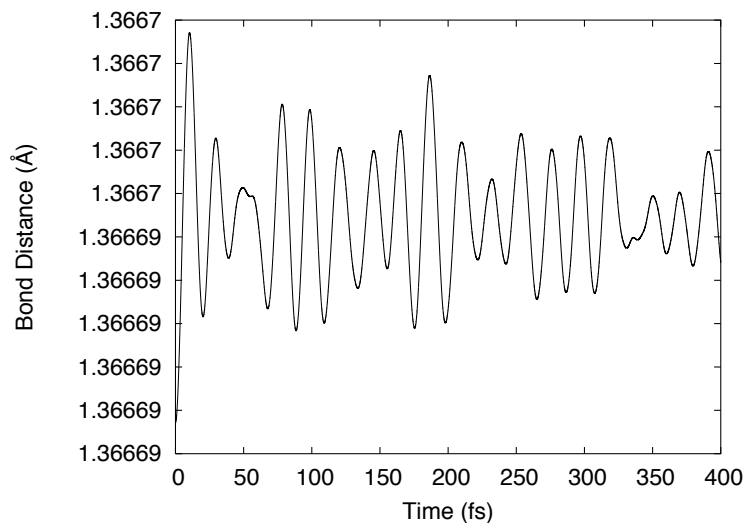


Fig. 54. The C11=C12 bond distance is plotted over time for the retinal molecule with no external field applied. The time step $\Delta t = 0.005$ fs.

performed using the force constant method described in Chapter III Section B. The values are listed in the following table VI.

Table VI.: Eigenvalues of the second-derivative matrix of the potential and the corresponding vibrational frequencies for retinal.

Vibrational Frequencies (cm^{-1}) Present Work	Vibrational Frequencies (cm^{-1}) Gaussian[37]
0.1238	0.0003
0.3233	0.0004
0.4016	0.0005
0.4826	0.2450
0.5805	0.3182
0.5988	0.4931
1.1785	13.4007
2.0521	26.8422
3.0822	34.2495
3.7857	42.5101
4.0012	58.4236
19.9017	76.1559
22.4711	101.6688
25.1161	111.5702
36.5588	135.4313
48.0770	149.3992
73.8360	159.5467
86.1949	173.3127

Table VI.: *continued*

Vibrational Frequencies (cm^{-1}) Present Work	Vibrational Frequencies (cm^{-1}) Gaussian[37]
112.7785	190.0867
116.1997	190.5780
129.6964	202.0929
148.6087	216.0811
160.2458	243.3058
182.6862	260.3334
193.4618	279.0154
196.0117	282.5417
224.8546	292.5493
233.0554	309.7879
247.2733	334.1847
259.7852	339.6012
273.1192	386.1681
293.3921	387.7216
315.1009	399.1435
337.4914	435.9402
348.9672	443.8838
376.2351	455.7820
403.1731	468.5877
414.0500	493.5405

Table VI.: *continued*

Vibrational Frequencies (cm^{-1}) Present Work	Vibrational Frequencies (cm^{-1}) Gaussian[37]
430.0880	509.4173
452.0192	521.6556
495.3010	556.6768
502.1657	584.3720
528.7515	602.6011
539.9679	620.1258
561.1109	629.8194
595.5320	709.8440
687.1943	731.0994
705.4014	803.8670
751.9145	841.7671
783.4661	859.5991
797.3491	894.2533
848.3770	921.5218
870.2239	930.4919
938.7707	945.4756
941.5768	953.4599
957.9477	978.6954
962.1402	997.6243
987.7823	1007.8629

Table VI.: *continued*

Vibrational Frequencies (cm^{-1}) Present Work	Vibrational Frequencies (cm^{-1}) Gaussian[37]
993.1843	1019.4034
1025.2982	1030.0714
1048.9166	1062.3731
1107.7717	1064.2982
1115.7848	1078.2428
1139.8317	1101.7605
1152.2627	1105.0780
1156.9110	1110.1810
1162.6268	1116.9059
1164.8616	1124.7209
1178.4879	1127.4214
1198.4842	1144.0298
1205.8800	1144.7409
1207.3750	1147.1252
1214.0963	1155.9784
1216.8125	1170.4545
1248.9031	1216.3547
1269.1584	1235.4778
1303.3282	1247.4397
1306.9416	1292.2147

Table VI.: *continued*

Vibrational Frequencies (cm^{-1}) Present Work	Vibrational Frequencies (cm^{-1}) Gaussian[37]
1318.7913	1295.4341
1328.6001	1298.4135
1336.1081	1323.2068
1376.1865	1330.4031
1398.9818	1340.6729
1440.7336	1374.9655
1449.1585	1385.9650
1465.8954	1405.1227
1500.2716	1419.9371
1518.5164	1429.9302
1542.8513	1443.4777
1615.5391	1473.7040
1625.8481	1481.9395
1640.1920	1505.9550
1674.0756	1511.4652
1695.7229	1513.9895
1704.2711	1522.9183
1722.0369	1527.2493
1735.9443	1529.7533
1737.7993	1538.5237

Table VI.: *continued*

Vibrational Frequencies (cm^{-1}) Present Work	Vibrational Frequencies (cm^{-1}) Gaussian[37]
1740.8153	1542.3739
1741.7506	1565.4933
1746.9494	1577.6124
1747.8797	1581.4378
1749.3628	1582.3402
1750.6415	1584.7820
1754.4872	1585.6389
1755.7697	1586.8080
1761.8598	1587.8276
1762.6448	1592.5664
1763.7475	1594.8634
1767.1184	1600.2232
1768.1056	1604.0295
1785.0213	1607.8020
1797.8758	1615.2630
1820.7230	1790.3511
1854.8513	1839.1753
1881.8452	1851.1310
1934.8297	1863.8458
1948.6723	1866.0064

Table VI.: *continued*

Vibrational Frequencies (cm^{-1}) Present Work	Vibrational Frequencies (cm^{-1}) Gaussian[37]
1969.7913	1979.2446
4534.3791	3146.2794
4557.3728	3160.2314
4565.5357	3162.3013
4578.1997	3167.0351
4595.2686	3170.3526
4596.1280	3176.5751
4654.5572	3180.4795
4658.9859	3187.8888
4667.3272	3188.3034
4681.2361	3191.7463
4696.4988	3206.4650
4703.2403	3215.4106
4732.4728	3224.2820
4744.0567	3238.9042
4744.3207	3244.8304
4748.0267	3245.7675
4748.5344	3248.7344
4749.7971	3254.4597
4750.0894	3267.0125

Table VI.: *continued*

Vibrational Frequencies (cm^{-1}) Present Work	Vibrational Frequencies (cm^{-1}) Gaussian[37]
4770.3386	3300.3353
4776.3890	3307.3103
4805.1951	3309.5954
4917.1431	3316.2628
4917.6306	3321.3162
4919.1523	3333.5182
4920.3983	3352.5565
4920.9824	3357.7821
4923.4978	3363.4998

The following Figure 55 shows the vibrational frequencies obtained using the fourier transform analysis of the C11=C12 double bond about which the molecule rotates from the *cis* to the *trans* form. The results are comparable to the ones listed in the table above obtained from the current model.

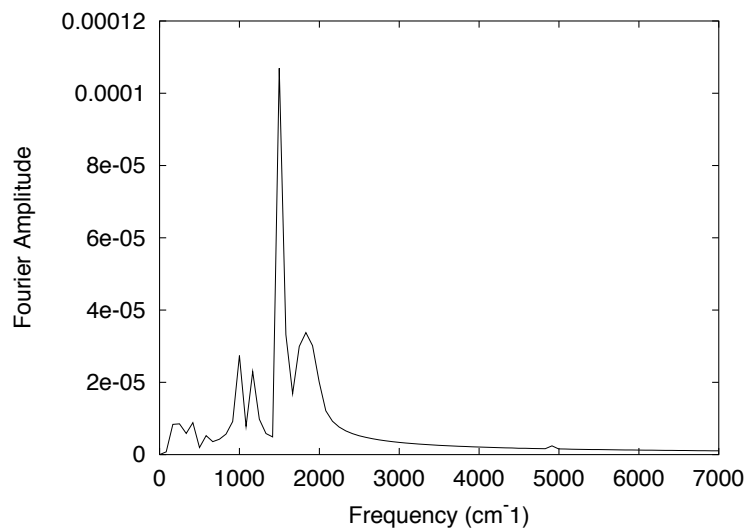


Fig. 55. Frequency measurements for the retinal molecule from Fourier-Transform techniques. The C11=C12 bondlengths were measured over time and transformed to get vibrational frequencies. The graph represents the fourier amplitudes plotted with respect to the corresponding frequencies. The time step $\Delta t = 0.005$ fs and the total time is 400 fs.

3. Results for the photo-isomerization of retinal with the application of an electro-magnetic field

In this section, we study the photo-isomerization of the retinal molecule. Due to the uncertainty of the excitation states for the electrons, we were unable to do the wavelength calculations from the energy difference of the excitation states. We look at different experimental studies which indicated that the wavelength of the light used for most of these studies was between 560-570 nm[53]. We selected a value of 568.0 nm[54], well within the visible range of 400-700 nm.

From earlier studies with the test molecules, we found that for the ethylene and the 2-butene molecule a time step of 0.010 fs was sufficient to do the simulations. However from the study of stilbene dynamics we concluded that a time step larger than 0.005 fs was not appropriate for accuracy purposes. Therefore, we decided to use a time step of $\Delta t = 0.005$ fs for all further retinal dynamics calculations.

In the following Figure 56 we plot the energy eigenvalues around the true HOMO-LUMO as a function of time. Here also we see the avoided crossing which occurs at ~ 120.0 fs between the HOMO (57^{th}) orbital corresponding to an energy of ~ -10.0 eV and the LUMO (58^{th}) orbital corresponding to an energy of ~ -8.8 eV, although it is not as apparent as was for the test molecules. We next study the dynamics of the total energy and the dihedral angle over time. In the energy plot in Figure 57 we find that the system continues to absorb energy in order to rotate by 180° from the *cis* to the *trans* configuration. Figure 58 shows the dihedral angle rotates by 180° in 217.91 fs. We shall see later that the action of the 180° -rotation and the time required largely depend on the strength of the vector potential. In this case, it agrees with reports from experimental studies which suggest that the isomerization is complete within 200 fs[3].

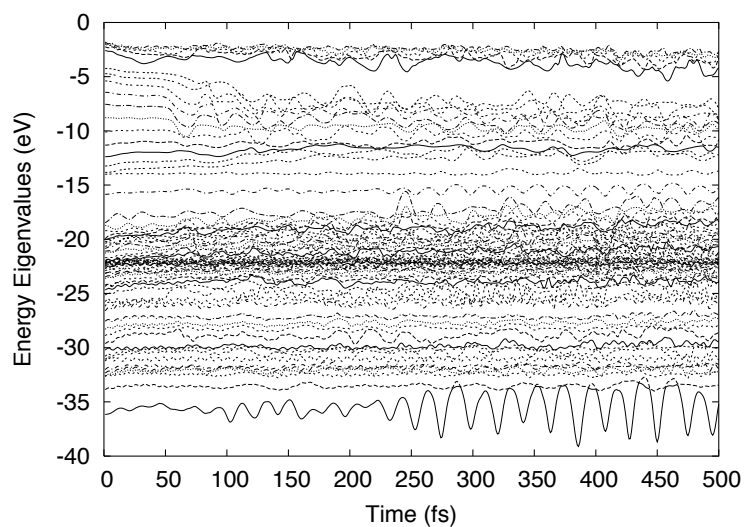


Fig. 56. The energy eigenvalues for the retinal molecule are plotted over time. The time step is $\Delta t = 0.005$ fs, amplitude of the vector potential is $A = 1.0$ gauss-cm and the wavelength of the light is $\lambda = 568.0$ nm.

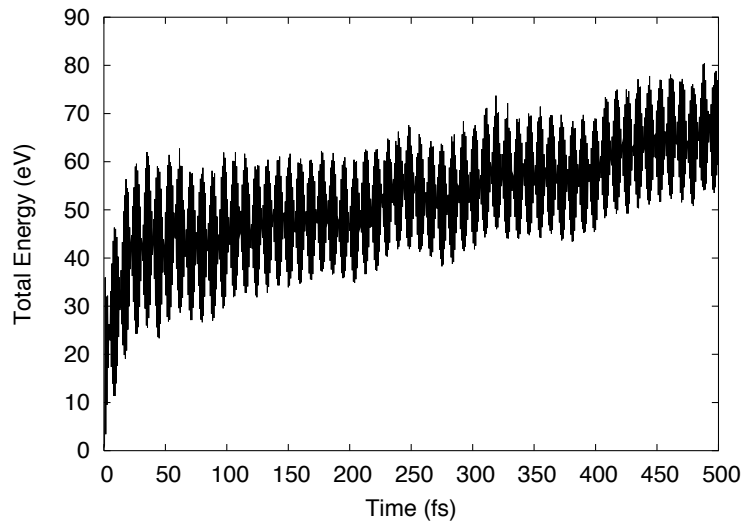


Fig. 57. The total energy for the retinal molecule is plotted over time. The time step is $\Delta t = 0.005$ fs, amplitude of the vector potential is $A = 1.0$ gauss-cm and the wavelength of the light is $\lambda = 568.0$ nm.

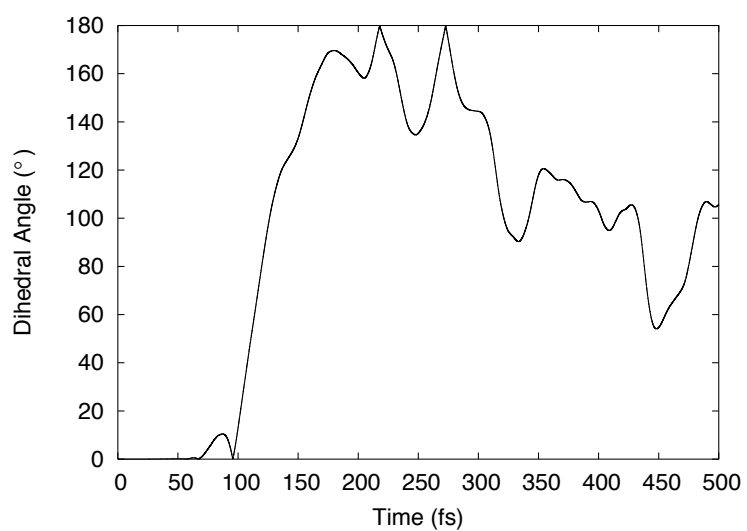


Fig. 58. The dihedral angle H10-C11=C12-H11 for the retinal molecule is plotted over time. The time step is $\Delta t = 0.005$ fs, amplitude of the vector potential is $A = 1.0$ gauss·cm and the wavelength of the light is $\lambda = 568.0$ nm.

In Figure 59, the C11=C12 bond distance is shown as a function of time. The bondlength initially vibrates slowly around the mean carbon-carbon bond length of 1.4 Å, but after about 400 fs, when the system keeps absorbing more energy, the bond length fluctuates more vigorously but still within the acceptable range of 1.2 - 1.9 Å.

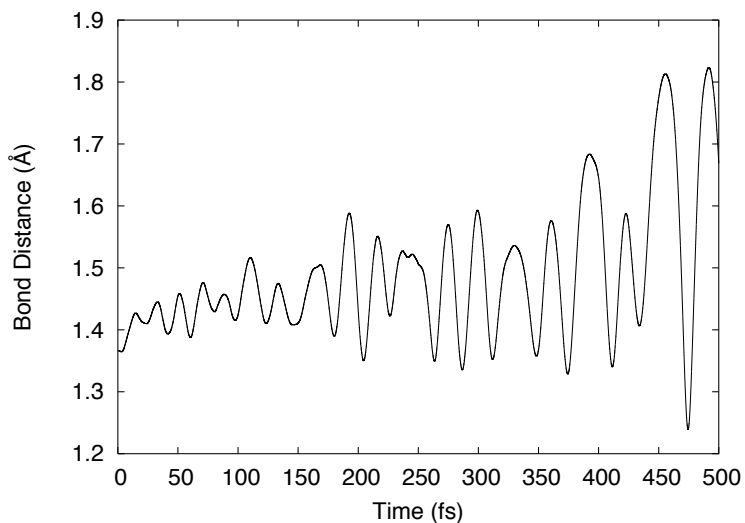


Fig. 59. The C11=C12 bond distance is plotted over time for the retinal molecule with amplitude of the vector potential is $A = 1.0$ gauss-cm and the wavelength of the light is $\lambda = 568.0$ nm. The time step $\Delta t = 0.005$ fs.

In the following four figures, namely Figures 60, 61, 62 and 63, we again study the energy eigenvalues, the total energy, the dihedral angle and the C11=C12 bondlength for the retinal molecule with a slightly different value for the field strength $A = 0.8$ gauss·cm. In this case we allow the simulations to run for 2000 fs. There are no significant differences in the energy eigenvalues, the total energy and the bondlength dynamics from those reported in the previous study with $A = 1.0$ gauss·cm. The major difference is in the behavior of the dihedral angle, which now takes 1281.805 fs to complete the isomerization. This is within the range of 1-2 ps for the isomerization as reported by [55, 56, 57]. However, this simulation takes much longer than the one we previously reported for $A = 1.0$ gauss·cm. This shows the simulation largely depends on the field strength, even when the wavelength stays the same.

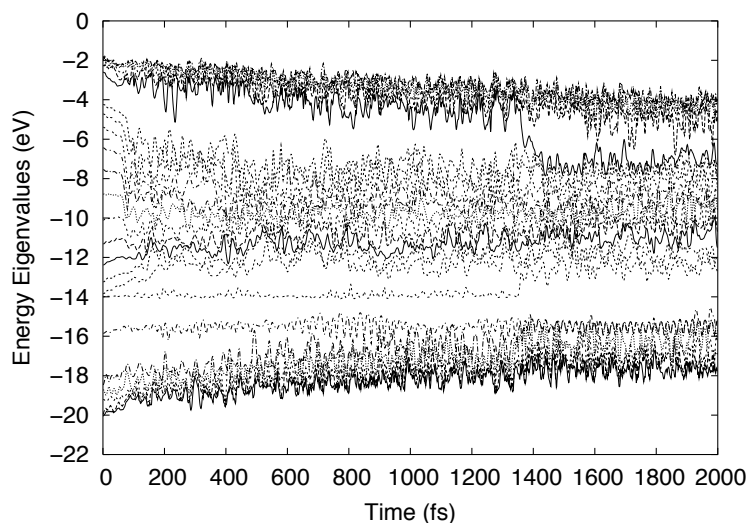


Fig. 60. The energy eigenvalues for the retinal molecule are plotted over time. The time step is $\Delta t = 0.005$ fs, amplitude of the vector potential is $A = 0.8$ gauss·cm and the wavelength of the light is $\lambda = 568.0$ nm.

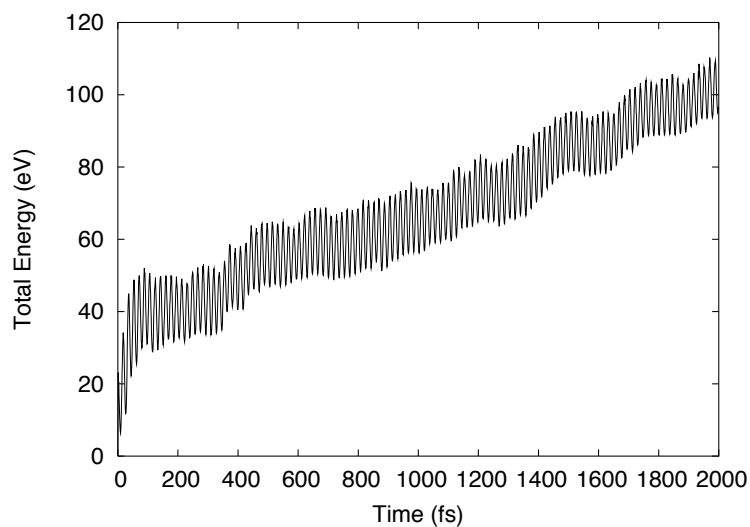


Fig. 61. The total energy for the retinal molecule is plotted over time. The time step is $\Delta t = 0.005$ fs, amplitude of the vector potential is $A = 0.8$ gauss-cm and the wavelength of the light is $\lambda = 568.0$ nm.

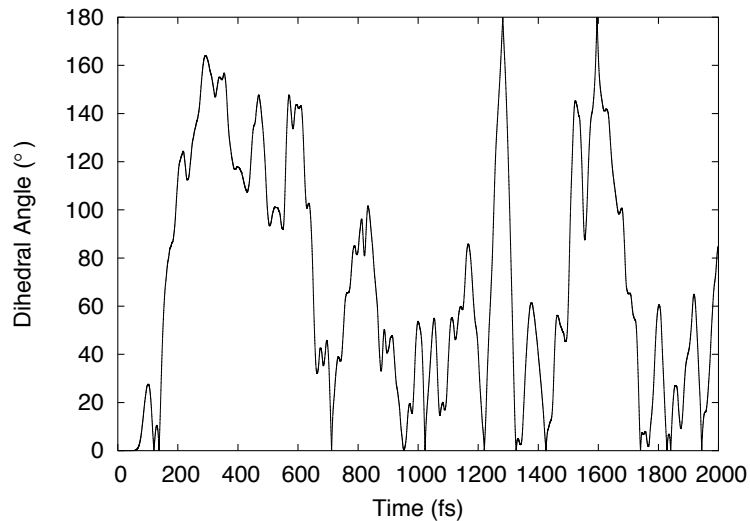


Fig. 62. The dihedral angle H10-C11=C12-H11 for the retinal molecule is plotted over time. The time step is $\Delta t = 0.005$ fs, amplitude of the vector potential is $A = 0.8$ gauss-cm and the wavelength of the light is $\lambda = 568.0$ nm.

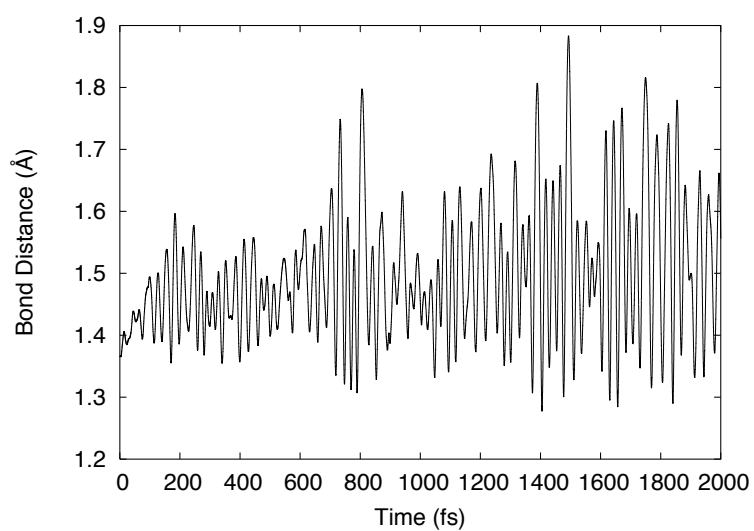


Fig. 63. The C11=C12 bond distance is plotted over time for the retinal molecule with amplitude of the vector potential is $A = 0.8$ gauss-cm and the wavelength of the light is $\lambda = 568.0$ nm. The time step $\Delta t = 0.005$ fs.

CHAPTER VI

CONCLUSIONS

The main objective of this work was to theoretically investigate the *cis-trans* photoisomerization scheme in the retinal molecule. We used the semi-empirical tight-binding technique which has proven to be a reliable method in computation of this kind of isomerization in semiconductors, biological molecules and also in the case of the test molecules from the current method, namely, ethylene and stilbene. We decided to test the technique for the 2-butene molecule since it is the third simplest molecule after ethylene and also has the typical C=C double bond structure that we wanted to investigate before embarking on the large retinal molecule.

The test molecules ethylene, 2-butene and stilbene all yielded satisfactory results when compared to experimental and other theoretical work. In the case of ethylene, the HOMO-LUMO study closely matched the full multiple spawning technique used by Ben-Nun *et al.*[43], as seen in the dihedral angle and the C=C bond length behavior. The photo-isomerization process in the ethylene molecule obtained from the current tight-binding method is also comparable to the studies done by Quenneville *et al.*[47] and Dou *et al.*[57], as discussed in Chapter IV.

The 2-butene molecule has been studied extensively via experiments. An exact comparison between the results of this work and those from experiments cannot be made since in most cases the 2-butene molecule was not in gas phase. However, comparing the results from the study of 2-butene and ethylene, we can come to the conclusion that the dynamics of 2-butene gives reasonably expected results.

Stilbene, on the other hand, has been the focus of numerous studies both from theoretical and experimental points of view. The results of photo-isomerization in stilbene from the present work closely match the ones from Ben-Nun *et al.*[43] and

Dou *et al.*[57] thereby confirming the validity of the model the results obtained from using the model.

Finally, we investigated the photo-isomerization in the retinal molecule, which is the main focus of this work. As has been reported in Chapter V, there were difficulties in determining the π and the π^* about the C=C bond, primarily because the molecule is very complex and there is a lot of overlap between the s , p_x , p_y and the p_z non-local versus local orbitals. Due to this overlap, it was not possible to correctly determine the excitation states. On the other hand, the isomerization of the retinal molecule under the influence of the electro-magnetic field yielded quite satisfactory results as discussed in the last chapter. One major drawback for this isomerization study was the computational restrictions which made each calculation for retinal very slow (~ 4 -5 days). This made it impossible to try several runs with slightly different parameters.

An important aspect of molecular dynamics study which was not investigated in this current work is the effect of pulse shape control. While the present research was conducted with the light turned on continuously, it could have also been controlled by switching on and off, thereby applying a pulse. This would have affected the dynamics considerably. Also different pulse shapes, e. g., Gaussian, square etc. shapes would have also resulted in different dynamical behavior.

The current scope of work also didn't include the thermal effect on molecular dynamics. We considered the dynamics at absolute zero, whereas a change of temperature to 300 K (room temperature) would have yielded many more initial states and therefore altered the molecular dynamics. In this case the initial velocities instead of being zero would have satisfied the equipartition theorem:

$$\frac{1}{2} \sum_{i=1}^N M_i \dot{R}_i^2 = \frac{(3N - 6)}{2} kT. \quad (6.1)$$

In the above equation N is the number of ions, k is the Boltzmann's constant and T is the absolute temperature in K. There are $3N - 6$ degrees of freedom, since the center of mass is unchanged under translation or rotation.

Overall, the conclusion is that the primary goal of the current work of using the semi-empirical tight-binding method in order to simulate the photo-isomerization of retinal has been achieved. The results are comparable to those from experimental studies. There are certain restrictions in the tight-binding concept, one of which is that the electrons always have to be doubly excited which leads to limitations to the types of molecules that can be studied with the current model. However, by using this model we were able to study a large molecule like retinal with 49 atoms, which has previously not been studied computationally.

REFERENCES

- [1] G. G. Kochendoerfer, P. J. E. Verdegem, I. van der Hoef, J. Lugtenburg, and R. A. Mathies, *Biochemistry*, **35**, 16230 (1996).
- [2] G. G. Kochendoerfer, and R. A. Mathies, *Journal of Physical Chemistry*, **100**, 14526 (1996).
- [3] R. A. Mathies, S. O. Smith and J. Lugtenburg, *Biophysical Studies of Retinal Proteins*, edited by T.G. Ebrey, H. Frauenfelder, B. Honig, and K. Nakanishi, (University of Illinois, Champaign, 1987).
- [4] V. Vachev, J. Frederick, B. Grishanin, V. Zadkov, and N. Koroteev, *Chem. Phys. Lett.* **215**, 306 (1993).
- [5] J. Quenneville, Ph.D. Dissertation, Univ. of Illinois at Urbana, Champaign (2003).
- [6] M. Du, and G. Fleming, *Biophysical Chemistry* **48**, 101 (1993).
- [7] S. Futterman, and M. Rollins, *The Journal of Biological Chemistry* **248**, 7773 (1973).
- [8] S. W. Lin, M. Groesbeek, I. van der Hoef, P. Verdegem, J. Lugtenburg, and R. A. Mathies, *Journal of Physical Chemistry*, **102**, 2787 (1998).
- [9] R. A. Mathies, S. O. Smith, G. S. Harbison, J. M. L. Courtin, J. Herzfeld, R. G. Griffin, and J. Lugtenburg, *Retinal Proteins* edited by U. Ovchinnikov, (VNU Press, Utrecht, The Netherlands, 1987).
- [10] F. Boll, *On the anatomy and physiology of the retina* (Acad Wiss, Berlin, 1876).

- [11] Y. Shichida in *The Retinal Basis of Vision*, edited by Jun-Ichi Toyoda, Motohiko Murakami, Akimichi Kaneko and Takehiko Saito (Elsevier, 1999).
- [12] R. W. Schoenlein, L. A. Peteanu, R. A. Mathies, and C. V. Shank, *Science*, **254**, 412 (1991).
- [13] Y. Shichida, S. Mantuoka, and T. Yoshizawa, *Photobiochem. Photobiophys.*, **7**, 221 (1984).
- [14] Q. Wang, R. W. Schoenlein, L. A. Peteanu, R. A. Mathies, and C. V. Shank, *Science*, **266**, 422 (1994).
- [15] G. G. Kochendoerfer, and R. A. Mathies, *Israeli Journal of Chemistry*, **35**, 211-226 (1995).
- [16] Y. Shichida, T. Ono, T. Yoshizawa, H. Matsumoto, A. E. Asato, J. P. Zingoni, and R. S. H. Liu, *Biochemistry*, **26**, 4422 (1987).
- [17] R. R. Birge, C. M. Einterz, H. M. Knapp, L. P. Murray, *Biophys. J.* **53**, 367 (1988).
- [18] J. Baskin, L. Bañares, S. Pedersen, and A. Zewail, *J. Phys. Chem.* **100**, 11920 (1996).
- [19] F. Gai, K. Hasson, J. McDonald, and P. Anfinrud, *Science* **279**, 1886 (1998).
- [20] J. S. Graves, Ph.D. Dissertation, Texas A&M Univ. (1997).
- [21] R. Hamilton, Ph.D. Dissertation, Texas A&M Univ. (1999).
- [22] J. S. Graves, and R. E. Allen, *Phys. Rev.* **B58**,13627 (1998).
- [23] R. E. Allen, *Phys. Rev. B* **50**, 18629 (1994).

- [24] M. Menon, and R. E. Allen, Phys. Rev. B **33**, 7099 (1986).
- [25] J. C. Slater, and G. F. Koster, Phys. Rev. **94**, 1498 (1954).
- [26] W. A. Harrison, *Solid State Theory* (Dover, New York, 1980).
- [27] M. Graf, and P. Vogl, Phys. Rev. B **51**, 4940 (1995).
- [28] J. D. Jackson, *Classical Electrodynamics* (John Wiley & Sons, New York, 1962).
- [29] H. Hellmann, *Einführung in die Quantumchemie* (Deuticke, Leipzig, 1937).
- [30] R. P. Feynman, Phys. Rev. **56**, 340 (1939).
- [31] W. A. Harrison, Phys. Rev. Letters **34**, 1198 (1975).
- [32] W. A. Harrison, and S. Ciraci, Phys. Rev. **B10**, 1516 (1974).
- [33] O. F. Sankey, Phys. Rev. **B33**, 7164 (1986).
- [34] J. J. Sakurai, *Modern Quantum Mechanics* (Addison-Wesley, New York, 1985).
- [35] NIST Chemistry WebBook, NIST Standard Reference Database Number 69, June 2005 Release, (<http://webbook.nist.gov/chemistry/>).
- [36] I. Levine, *Quantum Chemistry* (Prentice Hall, Upper Saddle River, NJ, 2000).
- [37] Gaussian 03, Revision C.02, M. J. Frisch, G. W. Trucks, H. B. Schlegel, G. E. Scuseria, M. A. Robb, J. R. Cheeseman, J. A. Montgomery, Jr., T. Vreven, K. N. Kudin, J. C. Burant, J. M. Millam, S. S. Iyengar, J. Tomasi, V. Barone, B. Mennucci, M. Cossi, G. Scalmani, N. Rega, G. A. Petersson, H. Nakatsuji, M. Hada, M. Ehara, K. Toyota, R. Fukuda, J. Hasegawa, M. Ishida, T. Nakajima, Y. Honda, O. Kitao, H. Nakai, M. Klene, X. Li, J. E. Knox, H. P. Hratchian, J. B. Cross, V. Bakken, C. Adamo, J. Jaramillo, R. Gomperts, R. E. Stratmann,

- O. Yazyev, A. J. Austin, R. Cammi, C. Pomelli, J. W. Ochterski, P. Y. Ayala, K. Morokuma, G. A. Voth, P. Salvador, J. J. Dannenberg, V. G. Zakrzewski, S. Dapprich, A. D. Daniels, M. C. Strain, O. Farkas, D. K. Malick, A. D. Rabuck, K. Raghavachari, J. B. Foresman, J. V. Ortiz, Q. Cui, A. G. Baboul, S. Clifford, J. Cioslowski, B. B. Stefanov, G. Liu, A. Liashenko, P. Piskorz, I. Komaromi, R. L. Martin, D. J. Fox, T. Keith, M. A. Al-Laham, C. Y. Peng, A. Nanayakkara, M. Challacombe, P. M. W. Gill, B. Johnson, W. Chen, M. W. Wong, C. Gonzalez, and J. A. Pople, Gaussian, Inc., Wallingford CT, (2004).
- [38] W. Press, B. Flannery, S. Teukolsky, and W. Vetterling, *Numerical Recipes in C: The Art of Scientific Computing* (Cambridge Univ. Press, New York, 2002).
- [39] H. Gould, and J. Tobochnik, *An Introduction to Computer Simulation Methods* (Addison-Wesley, New York, 1988).
- [40] W. A. Harrison, *Electronic Structure and the Properties of Solids* (Freeman, San Francisco, 1980).
- [41] R. M. Martin, Phys. Rev. **186**, 871 (1969).
- [42] M. Menon, and R. Allen, Phys. Rev. B **38**, 6196 (1988).
- [43] M. Ben-Nun, and T. Martínez, Chem. Phys. Lett. **298**, 57 (1998).
- [44] E. N. Glezer, Y. Siegal, L. Huang, and E. Mazur, Phys. Rev. B **51**, 6959 (1995).
- [45] E. N. Glezer, Y. Siegal, L. Huang, and E. Mazur, Phys. Rev. B **51**, 9589 (1995).
- [46] K. Sokolowski-Tinten, J. Bialkowski, and D. von der Linde, Phys. Rev. B **51**, 14186 (1995).
- [47] J. Quenneville, and T. Martínez, J. Phys. Chem. A **107**, 829 (2003).

- [48] J. Saltiel, S. Ganapathy, and C. Werking, *J. Phys. Chem* **91**, 2755 (1987).
- [49] H. Morrision, J. Pajak, and R. Peiffer, *J. Amer. Chem. Soc.* **93**, 3978 (1971).
- [50] D. Todd, J. Jean, S. Rosenthal, A. Ruggiero, D. Yang, and G. Fleming, *J. Chem. Phys.* **93**, 8658 (1990).
- [51] D. Todd, and G. Fleming, *J. Chem. Phys.* **97**, 8915 (1992).
- [52] G. Gershinsky, and E. Pollak, *J. Chem. Phys.* **107**, 812 (1997).
- [53] D. Oesterhelt, P. Hegemann, P. Tavan, and K. Schulten, *Eur. Biophys. J.* **14**, 123 (1986).
- [54] A. Hermone, and K. Kuczera, *Biochemistry* **37**, 2843 (1998).
- [55] F. Peters, J. Herbst, J. Tittor, D. Oesterhelt, and R. Diller, *Chem. Phys.* **323**, 109 (2006).
- [56] R. Diller, R. Jakober, C. Schumann, F. Peters, J. Klare, and M. Engelhard, *Biopolymers* **82**, 358 (2006).
- [57] Y. Dou and R. Allen, (Unpublished Result 2003).

APPENDIX A

CALCULATING THE HAMILTONIAN MATRIX ELEMENTS

In our calculations for the force on the individual atoms, we find that for the electronic part, we need to find the derivative of the Hamiltonian. In order to calculate the values of the Hamiltonian and its derivatives, we use the formulation of Slater and Kostev[25]. We code the equations in our program as follows:

```
double ss(double Ess_sig, double d){
return (Ess_sig*(hh/(d*d)));
}

double sp(double Esp_sig, double dir, double d){
return ((Esp_sig*dir)*(hh/(d*d)));
}

double pp(double Epp_sig,double Epp_pi,double Tdiadic,\
           double kdelta,double d){
return ((Tdiadic*(Epp_sig-Epp_pi) + kdelta*Epp_pi)*(hh/(d*d)));
}

vector dss(double Ess_sig,double d, vector dircos){
return (((-2.0)*dircos*Ess_sig)*(hh/(d*d*d)));
}

vector dsp(double Esp_sig,matrix &Tdiadic,\
```

```

        matrix &kdelta,int l,double d){
int m;
vector matrix_element(3);

for (m=0;m<3;m++){
    matrix_element(m)=(Tdiadic(1,m)*(-3.0) +\
        kdelta(1,m))*Esp_sig*((hh)/(d*d*d));
}
return matrix_element;
}

cvector dpp(double Epp_sig,double Epp_pi,matrix &Tdiadic,\
    matrix &kdelta,vector dircos,int i, int j, double d){
int k;
vector matrix_element(3);

for (k=0;k<3;k++){
matrix_element(k)=((kdelta(i,k)*dircos(j)+kdelta(j,k)*dircos(i)\
    -4*Tdiadic(i,j)*dircos(k))*(Epp_sig-Epp_pi)\
    -2*(\kdelta(i,j)*dircos(k)*Epp_pi))*((hh)/(d*d*d));
}
return matrix_element;
}

```

In the above numerical code, the first three routines show how to get the tight-

binding matrix elements of the Hamiltonian. The next three routines represent the derivatives of the Hamiltonian matrix elements. The parameter hh represents $\hbar^2/m_e = 7.62eV \cdot \text{\AA}^2$ where $\hbar = h/2\pi$ and h is the Planck's constant. m_e is the electronic mass and d is the interatomic distance. The constants $E_{ss_{sig}}$, $E_{sp_{sig}}$, $E_{pp_{sig}}$ and $E_{pp_{pi}}$ are represented as follows: $E_{ss_{sig}}$ is described in equation (2.40) as $\eta_{ss\sigma}$ as the constant involving the overlap between two neighboring s -orbitals; $E_{sp_{sigma}}$ is described in equation (2.41) as $\eta_{sp\sigma}$ for overlap between s and p orbitals and similarly $E_{pp_{sig}}$ and $E_{pp_{pi}}$ come from equation (2.42) where they represent overlap between two p orbitals and are denoted by σ or π depending on their orientations. The values of the constants used in the present calculations are: In the code *dir* denotes

Table VII. Tight-binding parameters for an s - p model according to Harrison[40].

$$(\eta_{ps\sigma} = -\eta_{sp\sigma}).$$

Tight-Binding parameter	Value (eV)
$\eta_{ss\sigma}$	-1.32
$\eta_{sp\sigma}$	1.42
$\eta_{ps\sigma}$	-1.42
$\eta_{pp\sigma}$	2.22
$\eta_{pp\pi}$	-0.63

the specific direction x , y or z and *dircos* stands for the directional cosines which is described earlier in this section. *Tdiadic* is a matrix representing the product of the directional cosines between the two orbitals participating in the overlap and *kdelta* is the kronecker delta.

APPENDIX B

**MOLECULAR ORBITAL ENERGY EIGENVALUES OF ETHYLENE,
2-BUTENE, STILBENE AND RETINAL**

Table VIII.: Molecular orbital energy eigenvalues of ethylene without an external field.

	Energy Eigenvalues (<i>eV</i>)
Ethylene	-31.687407159584
	-27.575895296481
	-24.142736616655
	-22.565335609074
	-21.959666638033
	-11.687796386013
	-6.2522037064692
	-1.1450597580212
	-1.108684405121
	-0.57013048764484
	2.1074629922656
	3.3274530708302

Table IX.: Molecular orbital energy eigenvalues of 2-butene without an external field.

	Energy Eigenvalues (<i>eV</i>)
2-butene	-32.842303113638
	-31.846661974936
	-28.959515578436
	-25.694452417834
	-24.07128433236
	-22.182504020853
	-22.141340178116
	-22.113845470885
	-21.801301607675
	-21.057091570099
	-19.806429453064
	-11.750036445955
	-6.6753592796011
	-1.8723938338005
	-1.322491941072
	-1.0735312245784
	-0.30063974499861
-0.098718200083541	
-0.0576129892669	
0.42925288003828	

Table IX.: *continued*

	Energy Eigenvalues (<i>eV</i>)
	0.7270695242499
	0.76826078504462
	3.1087087436795
	4.1142214442405

Table X.: Molecular orbital energy eigenvalues of stilbene without an external field.

	Energy Eigenvalues (<i>eV</i>)
Stilbene	-32.468462621824
	-32.234929628248
	-31.046997190369
	-30.022788996823
	-30.018737669369
	-29.726515587345
	-28.857745152255
	-27.071727003426
	-26.798427398814
	-26.698970049336
	-25.964248858478
	-25.490977193793
	-24.810578335633
	-24.6799233138
	-24.410209856998
	-23.823354806637
	-23.749771685498
	-23.26483329077
	-22.913739327508
-22.594683712739	

Table X.: *continued*

	Energy Eigenvalues (<i>eV</i>)
	-22.57720760401
	-22.262877091293
	-21.931873511869
	-20.829570916181
	-20.826610517254
	-20.434904612542
	-20.256972558553
	-14.551430989243
	-14.202558554146
	-12.794270780755
	-11.860398322899
	-11.532283406164
	-11.532084023925
	-10.321880237601
	-7.6181353125286
	-6.4079278331466
	-6.4077268822323
	-6.0796432076158
	-5.1457965037606
	-3.7374903361125

Table X.: *continued*

	Energy Eigenvalues (<i>eV</i>)
	-3.3887475892898
	-2.0488926817415
	-1.9500396550307
	-1.8024039424741
	-1.6151920511393
	-1.5615376735648
	-1.3989302027174
	-1.2616906337504
	-1.1189904384903
	-1.0892864117491
	-1.084112692844
	-1.0552451051408
	-1.0281410011706
	-0.72182520269004
	0.49842047009608
	1.4114932653417
	2.0008614423894
	2.00198769591
	2.1886019750241
	2.3018540913806

Table X.: *continued*

	Energy Eigenvalues (<i>eV</i>)
	2.3112214420824
	2.5561262188594
	3.115418795041
	3.8515681227751
	4.5280292358613
	5.1850217586465
	5.8199342647069
	6.0937613851714

Table XI.: Molecular orbital energy eigenvalues of retinal without an external field.

	Energy Eigenvalues (eV)
Retinal	-36.164518525526
	-33.888936853043
	-32.699814205361
	-32.602822370666
	-32.382543240644
	-32.07404761703
	-31.265485278855
	-31.098736009247
	-30.82424101408
	-30.280334291892
	-29.647041593898
	-28.919037283668
	-28.341816057995
	-27.612046307625
	-26.621365172512
	-26.259261896881
	-25.82805364721
	-25.147734268541
	-24.703770329975
	-24.421902054813

Table XI.: *continued*

	Energy Eigenvalues (<i>eV</i>)
	-24.243146120929
	-23.631485735457
	-23.486648044573
	-23.204778768492
	-23.142377356586
	-22.906736461431
	-22.766373382291
	-22.706359018857
	-22.542293775325
	-22.493696736998
	-22.360586965128
	-22.272921780796
	-22.196768923577
	-22.180664961464
	-22.174005910759
	-22.12523342711
	-22.105153280911
	-22.014006029905
	-21.703524890461
	-21.323632288348

Table XI.: *continued*

	Energy Eigenvalues (<i>eV</i>)
	-21.103599436569
	-20.853843740885
	-20.662501152093
	-20.389107324794
	-20.196108820047
	-20.058853690464
	-19.994113465652
	-19.219386038151
	-18.696347363898
	-18.492232449578
	-15.849411392651
	-14.001926055998
	-13.821422096168
	-13.23732040544
	-12.379970181169
	-11.313538768829
	-10.1045818278
	-8.7873595268466
	-7.5369077918926
	-6.4358502262841

Table XI.: *continued*

	Energy Eigenvalues (<i>eV</i>)
	-5.3941036014833
	-4.7210546449012
	-4.2465314067491
	-2.5860573429018
	-2.2270479575567
	-1.9000244140348
	-1.8179074575341
	-1.7734428648182
	-1.5884988672076
	-1.5410067961647
	-1.5112014951296
	-1.4478965971875
	-1.3214613605446
	-1.2988207447042
	-1.2269624638106
	-0.9667768254985
	-0.83136531260257
	-0.7194948876125
	-0.70731608045921
	-0.64686698506258

Table XI.: *continued*

	Energy Eigenvalues (<i>eV</i>)
	-0.46483225347683
	-0.44285802189755
	-0.3964010734813
	-0.3451273609201
	-0.20080315539937
	-0.11420579093162
	-0.097918858450444
	0.03502322617891
	0.31933344573331
	0.52216568728267
	0.53842167376619
	0.63503487481856
	0.68815647155235
	0.74698678596678
	0.8512732298877
	0.99264040829551
	1.0957145613595
	1.2732724342139
	1.4270294345496
	1.8023747754539

Table XI.: *continued*

	Energy Eigenvalues (<i>eV</i>)
	2.1504141612293
	2.3488234579308
	2.5746695639043
	2.7555358872378
	2.7810200238861
	3.2652542480036
	4.0895432439872
	4.1638527425093
	4.6460876270634
	4.8645555109893
	5.1525991881842
	5.3844855906026

VITA

Indrani Sinha was born in Calcutta, India and is the daughter of Justice Sujit Kumar Sinha and Mrs. Lina Sinha. She has an elder brother Dr. Indrajit Sinha who is a Professor of Marketing at Temple University in Philadelphia. She is the grand-daughter of the late Mr. Dibyendu Sundar Sinha, of whom she has very fond memories.

She is married to Mr. Darren Joseph Herhold whom she met during her studies at the University of Kansas.

Indrani received her Master's in physics and computational physics from the University of Kansas in Lawrence, Kansas. Prior to attending the University of Kansas, she achieved her B.Sc. in physics from Jadavpur University, Calcutta, India.

Indrani can be contacted via her permanent address at 5220 Sagecircle Street North, Houston, Texas 77056, USA or her email address at indrani_sinha@yahoo.com.

The typist for this thesis was Indrani Sinha.